10-12-2018

Genome-Wide Screening Identifies Genes and Biological Processes Implicated in Chemoresistance and Oncogene-Induced Apoptosis

Tengyu Ko
Louisiana State University and Agricultural and Mechanical College, tko1@lsu.edu

GENOME-WIDE SCREENING IDENTIFIES GENES AND BIOLOGICAL PROCESSES IMPLICATED IN CHEMORESISTANCE AND ONCOGENE-INDUCED APOPTOSIS

A Dissertation

Submitted to the Graduate Faculty of the
Louisiana State University and
Agricultural and Mechanical College
in partial fulfillment of the
requirements for the degree of
Doctor of Philosophy

in

Biomedical and Veterinary Medical Sciences through the
Department of Comparative Biomedical Sciences

by
Tengyu Ko
B.S., University of California, Santa Barbara 2010
December 2018

ACKNOWLEDGEMENTS

I would like to express my sincerest gratitude to my major supervisor Dr. Shisheng Li for giving me the opportunity to join his team and the freedom to pursue projects. I appreciate all of his thoughts and efforts. Truly, none of these findings would be possible without his supervisions, supports, insightful discussions, and patience.

I am deeply indebted to the members of my committee Dr. Yoshimura, Dr. Yao, Dr. Larkin, and Dr. Marzilli. Without Dr. Yoshimura's encouragements, Dr. Yao's useful equipment, Dr. Larkin's constructive suggestions, and Dr. Marzilli's willingness to help out, I would not be able to finish this dissertation.

Special thanks to Dr. Penn for letting me go rampage on his sophisticated pathway analysis software, and for encouraging me, calming me down, and trying not to shoot me in the face when I make bad presentations.

I would also like to thank my colleagues Dr. Wentao Li, Dr. Kathiresan Selvam, Dr. Mingyang Li, and Mr. Wenzhi Gong for their helpful discussions and unwavering friendships even though I always puzzled them in lab meetings.

Last but not the least, I would like to extend my gratitude to my Father in Heaven, my family, Ms. Fuqi Sun, Mr. Shane Chang, Ms. Laura Yen, Ms. Zora Yo, Ms. Iris Chen, Dr. Zhong Li, Ms. Mary Price, Ms. Sue, Mr. Finch, Dr. John Fu, and many more that I don't have the time to mention. Thanks for putting up with me all these years.

TABLE OF CONTENTS

LIST OF TABLES

LIST OF FIGURES

LIST OF ABBREVIATIONS

BCAA……..……..branched-chain amino acid

BCKD……..……..branched-chain ketoacid dehydrogenase

Cas9……..……CRISPR-associated protein 9

cDNA…….……complementary DNA

CRISPR…….……..clustered regularly interspaced short palindromic repeats

crRNA…….……CRISPR RNA

DSB…….……...…double-strand break

ERK……...……extracellular signaling-regulated kinase

Etr……...……..……..early transduction

FACS……..……..……..fluorescent-activated cell sorting

FDR…….…..……..false discovery rate

gDNA…….……genomic DNA

GeCKO……..…...……..genome-scale CRISPR knockout-out

GFP…….……..……green fluorescent protein

GO……..……gene ontology

hTERT……...…….……..……human telomerase

IAP…….……..inhibitors of apoptosis proteins

Indel…….…..……insertion/deletion

MAPK.……...…….....…mitogen-activated protein kinase

OIA…….……..….oncogene-induced apoptosis

OIS…….……..…..oncogene-induced senescence

PAM……protospacer adjacent motif

PCR……..polymerase chain reaction

RB…….……..…….…….retinoblastoma protein

sgNTS…….…….non-targeting sgRNA sequence

sgRNA or gRNA……...…….……..single guide RNA

tracrRNA…….……..……..…….trans-activating CRISPR RNA

TRAIL…….……TNF-related apoptosis-inducing ligand

ABSTRACT

Anti-proliferative responses such as senescence and apoptosis are often used by normal cells to combat oncogenic insults and to prevent tumorigenesis. However, oncogenic mutations are frequently found in cancers, suggesting that additional mutations may occur to facilitate the bypass of these anti-proliferative responses. It is believed that some of these additional mutations may also contribute to the chemoresistance of cancers. This dissertation focused on identifying novel genes and biological processes implicated in chemoresistance and tumorigenesis.

Cisplatin-based chemotherapeutic regimens are frequently used for treatments of solid tumors. However, tumor cells may have inherent or acquired resistance to cisplatin, and the underlying mechanisms are largely unknown. We performed genome-wide knockout screening and found that protein translation, RNA catabolic process, and mitochondrial translational elongation and termination are the top biological processes responsible for cisplatin sensitivity in A375 human melanoma cells. In contrast, ubiquitin-dependent protein catabolic process, neddylation, and negative regulations of cellular catabolic process and canonical Wnt signaling are the top biological processes responsible for cisplatin resistance. ZNRF3, a ubiquitin ligase, enhances cisplatin resistance in normal and the melanoma cells by repressing β-Catenin, a key component of canonical Wnt signaling. ARIH1, another ubiquitin ligase, also enhances cisplatin resistance in normal and the melanoma cells. By regulating ARIH1, tumor suppressor NF2 enhances cisplatin resistance in the melanoma but not normal cells. ARIH1 is also upregulated in normal and the melanoma cells by YAP, an effector of Hippo signaling. However, the regulation of ARIH1 by NF2 is not via YAP-mediated transcription. These results shed new lights on cisplatin resistance mechanisms and may be useful for development of future treatment strategies.

By utilizing CRISPR/Cas9 genome-wide screening system, we identified 9 common genes that are involved in the bypass of anti-proliferative responses in human fibroblasts and melanocytes. Exclusively, DBT, an enzyme that involved in branched chain amino acid metabolism, and GPR4, a pH-sensing G-protein coupled receptor, are essential in mediating oncogene-induced apoptosis in human melanocytes only. These data were further confirmed by the single cell analysis of targeted populations that survived oncogenic selection. We also demonstrated that DBT deficient melanocytes suppressed oncogene-induced apoptosis comparing to the wild-type. In contrast, restoring DBT expression successfully recovered the apoptosis potential. Tumor suppressor p53 plays a key role in activating oncogene-induced apoptosis pathway. Previous studies had demonstrated that p53 is positively regulated by tumor suppressor p14ARF and negatively regulated by proto-oncogene AKT, and the oncogene activation can promote p14ARF activation and AKT inhibition. Our data suggested that DBT disruption suppresses oncogene-induced apoptosis by inactivating p53 via downregulation of p14ARF and upregulation of AKT. Collectively, these findings revealed a new understanding about the early stage development of tumorigenesis.

CHAPTER 1
LITERATURE REVIEW
TUMORIGENESIS AND MELANOMA TREATMENTS

1.1 Introduction

Melanoma is the most deadly form of skin cancer. Although it only accounts for less than 5% of all skin cancers, it is responsible for the most of the skin cancer related death (Ossio et al., 2017). In the past 3 decades, the risk of developing invasive melanoma has risen steadily (Glazer et al., 2016), and the 5-year survival rate still remains less than 20% (Siegel et al., 2016). DNA damaging agents such as chemotherapy and radiation are currently the preferred treatments for most late stage cancer patients; unfortunately, melanoma is extremely refractory to DNA damage-based therapeutic regimens (Shaffer et al., 2017). In the past decade, new methods, such as immunotherapies and targeted therapy, have been developed to combat melanoma; however, they were only able to prolong the life expectancy of patients, no sign of cure has been seen. Thus, obtaining a comprehensive understanding on how melanoma arises and the biological processes implicated in chemoresistance will be helpful for the development of novel treatments.

1.2 Oncogene

Unlike tumor suppressor genes, which induces anti-proliferative mechanisms such as senescence and apoptosis, proto-oncogenes are responsible for promoting cellular proliferation and differentiation. However, through certain point mutations, proto-oncogenes can be transformed to oncogenes and become constitutively active, resulting uncontrollable proliferation and genome instability. Genome instability is a hallmark of cancer and oncogene activation can cause such phenotype through at least 3 different mechanisms: DNA repair defects, replication

stress, and telomeric dysfunction (Kotsantis et al., 2018). First, overexpression of oncogenic RAS can cause DNA repair defects by inducing dissociation of the tumor suppressor protein BRAC1 from chromatin, which disables the DNA repair (Tu et al., 2011). Activated oncogene can also induce DNA replication stress, which is characterized by increased stalled/collapsed forks and decreased replication fork progression, leading to DNA double-strand breaks and mutations (Kotsantis et al., 2018). Lastly, telomere is a repetitive DNA sequence located at the ends of chromosomes functions to maintain genome integrity, and oncogenic HRAS has been shown to induce telomeric fork stalling and telomere depletion (Suram et al., 2012). Collectively, oncogene is considered as one of the major contributors to tumorigenesis and the root of cancers.

1.3 Oncogene-induced Senescence

To prevent cancer formation induced by oncogenes, cells could trigger the senescence program and permanently arrest the cell cycle at G1 phase in response to oncogene activation (Liu et al., 2018); this powerful defense mechanism is now known as the oncogene-induced senescence (OIS). OIS has been characterized as a collective phenotype of multiple effectors, and most of these effectors belong to the p53 and $p16^{INK4A}$ pathways (van Deursen, 2014). These two pathways ultimately converge to activate a tumor suppressor protein retinoblastoma protein (RB), which inhibits transcription factor E2F and promotes cell cycle exist. (McHugh and Gil, 2018; van Deursen, 2014).

Mechanistically, oncogenic pressure can cause replicative stress and DNA damages, inducing a DNA damage response in the early phase of tumorigenesis (Di Micco et al., 2006; Hills and Diffley, 2014). The DNA damage response involves the activation of protein kinases, including ATM, ATR, CHK1, and CHK2, which eventually leads to the phosphorylation of p53

(Salama et al., 2014). The phosphorylated p53 in turn induces transcription of the cyclin-dependent kinase inhibitor $p21^{CIP1}$, which represses CDK2 and CDK4/6 activity (He et al., 2005), resulting in RB activation (Fig. 1.1). Besides the p53 pathway, RB can also become active through the direct repression of CDK4/6 by tumor suppressor protein $p16^{INK4A}$ (Serrano et al., 1993). Indeed, dysregulation in p53 and $p16^{INK4A}$ pathways are frequently found in cancers, highlighting the importance of OIS in tumor suppression (Muller and Vousden, 2013; Zhao et al., 2016).

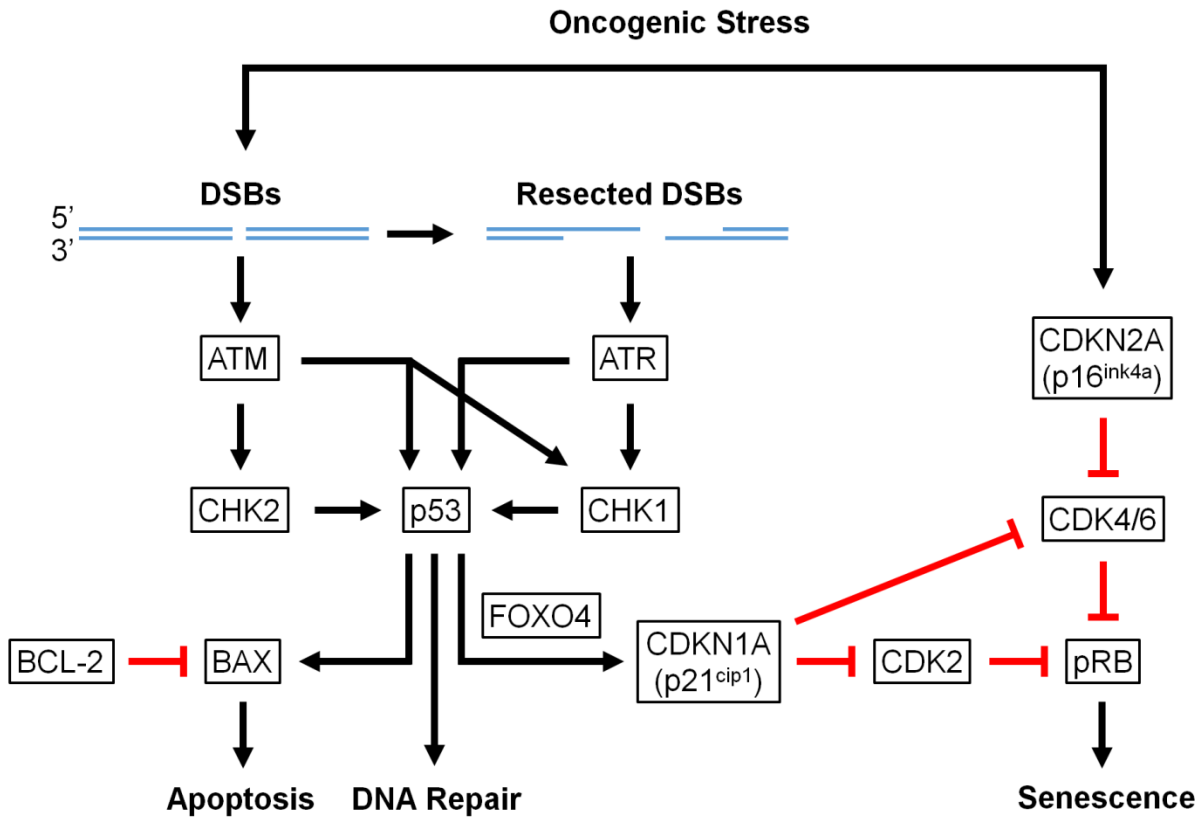

Figure 1.1. Oncogene-induced apoptosis and senescence through p53- and p16-mediated pathways. Black arrows represent activation and red lines represent inhibition.

1.4 Oncogene-induced Apoptosis

In addition to senescence, cells can also turn on the programmed cell death (apoptosis) program, which activates a caspase cascade and degrades the cellular content in a controlled

manner (Baig et al., 2016). In general, there are two pathways that regulate the caspase activity: extrinsic and intrinsic pathways. The extrinsic pathway is stimulated by external factors, such as TNF-related apoptosis-inducing ligand (TRAIL). When TRAILs bind to death receptors at the plasma membrane, caspases are activated and lead to cell death(Baig et al., 2016). The intrinsic pathway, which is often dysregulated in cancers, is stimulated by intracellular factors, such as unrepairable DNA damage and oncogenic stress. This process is initiated by the activation of the pro-apoptotic protein BAX by p53, leading to the permeabilization of the outer mitochondrial membrane, which allows the release of cytochrome c from the inner mitochondrial membrane to the cytoplasm (Baig et al., 2016). In the cytoplasm, cytochrome c may bind to apoptotic protease activating factor 1 (Apaf-1) to form the apoptosome, resulting the activation of a caspase cascade and cell death (Ichim and Tait, 2016).

The oncogene c-Myc, a transcription factor, is one of the earliest evidences for oncogene-induced apoptosis (OIA). In nutrient deprived or quiescent cells, c-Myc expression can trigger proliferation; however, prolonged activation of c-Myc can also induce apoptosis (Evan et al., 1992). Meanwhile, another report demonstrated that c-Myc may cooperate with the anti-apoptotic factor Bcl-2 to transform rodent fibroblast (Bissonnette et al., 1992), supporting the idea that the abilities of c-Myc to drive cell proliferation and to induce apoptosis are coupled. Indeed, either the loss of tumor suppressor RB or the overexpression of oncogene E2F can result in OIA (Qin et al., 1994). This phenomenon was later explained by the discovery that E2F can transcriptionally activate tumor suppressor p14ARF, a positive regulator of p53 (Iaquinta et al., 2005), thus overactivation of E2F may result in p53-mediated apoptosis (Fig. 1.2). The fact that multiple cancer cells, including melanoma, contain high expression of either E2F or c-Myc (Li et al., 2018; Lin et al., 2017; Zhang et al., 2015) may suggest that cancers cells had evaded OIA

mechanism during tumorigenesis. Ironically, p53 is rarely mutated in melanoma and our knowledge about OIA is still limited. Further investigation on this subject may provide a more comprehensive understanding on tumorigenesis.

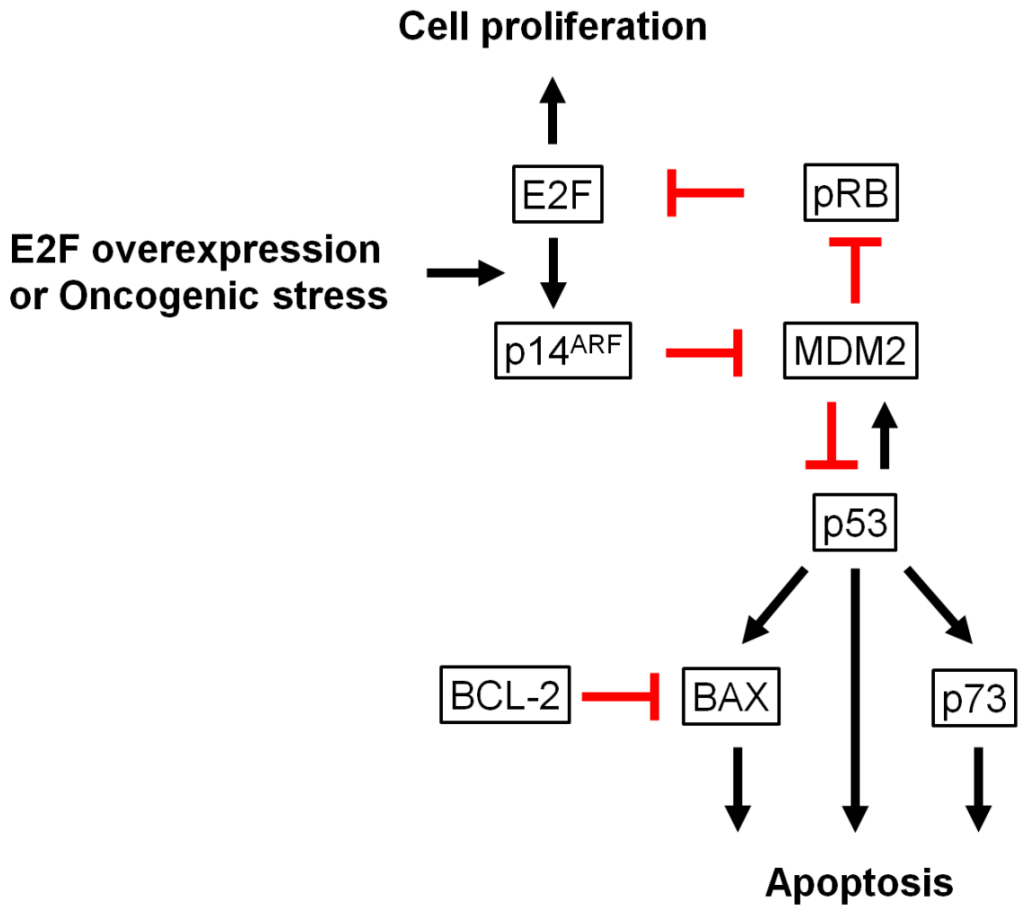

Figure 1.2. Coupling of cellular proliferation and apoptosis by oncogenic stress. Black arrows represent activation and red lines represent inhibition.

1.5 Melanoma treatments and resistance

A cisplatin-based chemotherapeutic regime is often the preferred treatment for many late-stage cancer patients. Cisplatin is an alkylating agent that induces intra-strand crosslinks between purine bases and causes DNA damages, which interfere with DNA repair mechanisms and lead to cancer cell death (Dasari and Tchounwou, 2014). For testicular cancer, combinational therapy

with cisplatin may increase the cure rate to as high as 80% (Winter and Albers, 2011). Unfortunately, the response rate for melanoma patients were only 23.3% and 16.3% when combined with other treatments or used as a single agent, respectively (Glover et al., 2003). There are several factors that may cause the cisplatin resistance, including enhanced drug efflux mechanism, altered drug-associated enzyme activity and DNA repair, and dysregulated apoptosis machinery; however, most of these mechanisms seem to be irrelevant to the chemoresistance of melanoma (Kalal et al., 2017). Despite years of intensive efforts, the genes and biological process implicated in cisplatin resistance are still largely unknown.

BRAF, a serine/threonine-protein kinase, belongs to the mitogen activated protein kinase (MAPK) pathway, which controls cellular proliferation, differentiation, and survival. About 50% of melanomas harbor activating mutations in the BRAF gene, among which ~80% is the resulting substitution of glutamic acid (E) for valine (V) at codon 600, BRAFV600E (Davies et al., 2002). This observation led to the development of specific inhibitors that target melanoma with BRAF mutations. Vemurafenib, one of the BRAFV600E inhibitors, initially showed a significant increase in drug response comparing to that of the traditional chemotherapy (Chapman et al., 2017). However, most patients treated with Vemurafenib developed resistance within 9 months (Solit and Rosen, 2010). Paradoxically, the mechanism of resistance involves re-activation of MAPK pathway, which causes cells to avoid apoptosis, proliferate, and invade (Pratilas et al., 2009).

Besides chemoresistance and the ability to adapt to selective pressure, melanoma can also evade immunosurveillance. Typically, melanoma can do so by expressing checkpoint proteins on their cell surface, thereby compromising T-cells' ability to attack the melanoma cells (Sharma et al., 2017). Furthermore, cancers can change their surroundings by recruiting seemingly normal

immune cells to generate an immunosuppressive and prometastatic microenvironment (Kitamura et al., 2015). Recently, researchers have developed several methods to improve the efficacy of immunotherapies, such as immune-checkpoint blockade and oncolytic viruses. Immune-checkpoint blockade utilizes inhibitors (e.g. chemical compound or antibody) to inactivate checkpoint proteins, such as PD-1 and CTLA-4, so $CD8^+$ Cytotoxic T lymphocytes and Natural Killer cells can be fully activated to kill cancer cells (Sadozai et al., 2017). Indeed, inhibitors such as Ipilimumab and Nivolumab have shown improved survival rate comparing to chemotherapy drugs (Ascierto et al., 2017; Robert et al., 2015; Topalian et al., 2014). Oncolytic viruses are genetically modified to specifically invade and lyse cancer cells. Upon lysis, the tumor antigens released stimulate immune cells, which further attack cancer cells (Choi et al., 2016). The recent FDA approved oncolytic virus, T-VEC, has shown improvement in response and survival rate during the phase III clinical trial (Bommareddy et al., 2017). Although immunotherapies have shown greater promise, the overall survival rate for metastatic melanoma patients is still unsatisfactory.

1.6 CRISPR/Cas9

Clustered Regularly Interspaced Short Palindromic Repeats (CRISPR) is a family of DNA sequences containing a short segment of virus DNA and is used to recognize and destroy similar DNA in viruses. It was originally discovered in bacteria and archaea and characterized as a defense mechanism against viruses (Barrangou, 2015). Type II, one of the simplest form of CRISPR systems, is composed of CRISPR RNA (crRNA) for DNA targeting, CRISPR-associated protein 9 (Cas9) for making DNA double-strand breaks, and trans-activating CRISPR RNA (tracrRNA) for recruiting Cas9. In 2012, Jennifer Doudna and Emmanuelle Charpentier re-engineered crRNA and tracrRNA to create a more concise and manageable sequence known as

single guide RNA (sgRNA) or guide RNA (gRNA), that when combined with Cas9 enzyme, can target specific regions of the genome by simply manipulating a short sequence in gRNA (Deltcheva et al., 2011; Jinek et al., 2012). One year after this discovery, Zhang's and Church's lab reported that they had successfully adapted CRISPR/Cas9 in the mammalian system, opening a new era for genome engineering (Cong et al., 2013; Mali et al., 2013).

Since then, many efforts have been invested in making CRIPSR/Cas9 technology a more efficient and elaborated tool for basic research and translational medicine communities. Today, the technology has evolved from creating the classical DNA double-strand break to creating single point mutations (Cox et al., 2017; Gaudelli et al., 2017), gene activation and silencing (La Russa and Qi, 2015; Qi et al., 2013), and engineering T-cells (Ren and Zhao, 2017). Researchers around the world are now using these technologies to explore difficult subjects, such as novel gene functions (Fogarty et al., 2017) and cancer formation (Hart et al., 2015), as well as to develop new treatments for a variety of diseases, such as genetic diseases (Cox et al., 2017; Gaudelli et al., 2017), HIV (Yin et al., 2017) and cancers (Cooper et al., 2018).

1.7 Statement of the Problem and Specific Aims

Melanoma is notoriously refractory to chemotherapy. Although recent advancement on therapeutic strategies has improved the response and survival rate, the overall efficacy treating melanoma is still unsatisfactory. To date, the underlying genes and biological process implicated in chemoresistance and melanomagenesis are still largely unknown. Therefore, understanding how melanoma was formed and why they are resistant to chemotherapy (e.g. cisplatin) may be helpful in developing novel treatment strategies. By utilizing genome-wide CRISPR/Cas9 knockout system, our aims are 1) to identify novel genes and biological processes responsible for

cisplatin resistance in A375 melanoma and 2) to identify novel genes responsible for anti-proliferative response in Hermes 4C human immortalized melanocytes.

1.8 References

Ascierto, P.A., Del Vecchio, M., Robert, C., Mackiewicz, A., Chiarion-Sileni, V., Arance, A., Lebbe, C., Bastholt, L., Hamid, O., Rutkowski, P., *et al.* (2017). Ipilimumab 10 mg/kg versus ipilimumab 3 mg/kg in patients with unresectable or metastatic melanoma: a randomised, double-blind, multicentre, phase 3 trial. The Lancet Oncology *18*, 611-622.

Baig, S., Seevasant, I., Mohamad, J., Mukheem, A., Huri, H.Z., and Kamarul, T. (2016). Potential of apoptotic pathway-targeted cancer therapeutic research: Where do we stand? Cell death & disease *7*, e2058.

Barrangou, R. (2015). The roles of CRISPR-Cas systems in adaptive immunity and beyond. Current opinion in immunology *32*, 36-41.

Bissonnette, R.P., Echeverri, F., Mahboubi, A., and Green, D.R. (1992). Apoptotic cell death induced by c-myc is inhibited by bcl-2. Nature *359*, 552-554.

Bommareddy, P.K., Patel, A., Hossain, S., and Kaufman, H.L. (2017). Talimogene Laherparepvec (T-VEC) and Other Oncolytic Viruses for the Treatment of Melanoma. American journal of clinical dermatology *18*, 1-15.

Chapman, P.B., Robert, C., Larkin, J., Haanen, J.B., Ribas, A., Hogg, D., Hamid, O., Ascierto, P.A., Testori, A., Lorigan, P.C., *et al.* (2017). Vemurafenib in patients with BRAFV600 mutation-positive metastatic melanoma: final overall survival results of the randomized BRIM-3 study. Annals of oncology : official journal of the European Society for Medical Oncology *28*, 2581-2587.

Choi, A.H., O'Leary, M.P., Fong, Y., and Chen, N.G. (2016). From Benchtop to Bedside: A Review of Oncolytic Virotherapy. Biomedicines *4*.

Cong, L., Ran, F.A., Cox, D., Lin, S., Barretto, R., Habib, N., Hsu, P.D., Wu, X., Jiang, W., Marraffini, L.A., *et al.* (2013). Multiplex genome engineering using CRISPR/Cas systems. Science *339*, 819-823.

Cooper, M.L., Choi, J., Staser, K., Ritchey, J.K., Devenport, J.M., Eckardt, K., Rettig, M.P., Wang, B., Eissenberg, L.G., Ghobadi, A., *et al.* (2018). An "off-the-shelf" fratricide-resistant CAR-T for the treatment of T cell hematologic malignancies. Leukemia.

Cox, D.B.T., Gootenberg, J.S., Abudayyeh, O.O., Franklin, B., Kellner, M.J., Joung, J., and Zhang, F. (2017). RNA editing with CRISPR-Cas13. Science *358*, 1019-1027.

Dasari, S., and Tchounwou, P.B. (2014). Cisplatin in cancer therapy: molecular mechanisms of action. Eur J Pharmacol *740*, 364-378.

Davies, H., Bignell, G.R., Cox, C., Stephens, P., Edkins, S., Clegg, S., Teague, J., Woffendin, H., Garnett, M.J., Bottomley, W., *et al.* (2002). Mutations of the BRAF gene in human cancer. Nature *417*, 949-954.

Deltcheva, E., Chylinski, K., Sharma, C.M., Gonzales, K., Chao, Y., Pirzada, Z.A., Eckert, M.R., Vogel, J., and Charpentier, E. (2011). CRISPR RNA maturation by trans-encoded small RNA and host factor RNase III. Nature *471*, 602-607.

Di Micco, R., Fumagalli, M., Cicalese, A., Piccinin, S., Gasparini, P., Luise, C., Schurra, C., Garre, M., Nuciforo, P.G., Bensimon, A., *et al.* (2006). Oncogene-induced senescence is a DNA damage response triggered by DNA hyper-replication. Nature *444*, 638-642.

Evan, G.I., Wyllie, A.H., Gilbert, C.S., Littlewood, T.D., Land, H., Brooks, M., Waters, C.M., Penn, L.Z., and Hancock, D.C. (1992). Induction of apoptosis in fibroblasts by c-myc protein. Cell *69*, 119-128.

Fogarty, N.M.E., McCarthy, A., Snijders, K.E., Powell, B.E., Kubikova, N., Blakeley, P., Lea, R., Elder, K., Wamaitha, S.E., Kim, D., *et al.* (2017). Genome editing reveals a role for OCT4 in human embryogenesis. Nature *550*, 67-73.

Gaudelli, N.M., Komor, A.C., Rees, H.A., Packer, M.S., Badran, A.H., Bryson, D.I., and Liu, D.R. (2017). Programmable base editing of A*T to G*C in genomic DNA without DNA cleavage. Nature *551*, 464-471.

Glazer, A.M., Winkelmann, R.R., Farberg, A.S., and Rigel, D.S. (2016). Analysis of Trends in US Melanoma Incidence and Mortality. JAMA dermatology.

Glover, D., Ibrahim, J., Kirkwood, J., Glick, J., Karp, D., Stewart, J., Ewell, M., Borden, E., and Eastern Cooperative Oncology, G. (2003). Phase II randomized trial of cisplatin and WR-2721 versus cisplatin alone for metastatic melanoma: an Eastern Cooperative Oncology Group Study (E1686). Melanoma Res *13*, 619-626.

Hart, T., Chandrashekhar, M., Aregger, M., Steinhart, Z., Brown, K.R., MacLeod, G., Mis, M., Zimmermann, M., Fradet-Turcotte, A., Sun, S., *et al.* (2015). High-Resolution CRISPR Screens Reveal Fitness Genes and Genotype-Specific Cancer Liabilities. Cell *163*, 1515-1526.

He, G., Siddik, Z.H., Huang, Z., Wang, R., Koomen, J., Kobayashi, R., Khokhar, A.R., and Kuang, J. (2005). Induction of p21 by p53 following DNA damage inhibits both Cdk4 and Cdk2 activities. Oncogene *24*, 2929-2943.

Hills, S.A., and Diffley, J.F. (2014). DNA replication and oncogene-induced replicative stress. Current biology : CB *24*, R435-444.

Iaquinta, P.J., Aslanian, A., and Lees, J.A. (2005). Regulation of the Arf/p53 tumor surveillance network by E2F. Cold Spring Harbor symposia on quantitative biology *70*, 309-316.

Ichim, G., and Tait, S.W. (2016). A fate worse than death: apoptosis as an oncogenic process. Nature reviews Cancer *16*, 539-548.

Jinek, M., Chylinski, K., Fonfara, I., Hauer, M., Doudna, J.A., and Charpentier, E. (2012). A programmable dual-RNA-guided DNA endonuclease in adaptive bacterial immunity. Science *337*, 816-821.

Kalal, B.S., Upadhya, D., and Pai, V.R. (2017). Chemotherapy Resistance Mechanisms in Advanced Skin Cancer. Oncology reviews *11*, 326.

Kitamura, T., Qian, B.Z., and Pollard, J.W. (2015). Immune cell promotion of metastasis. Nature reviews Immunology *15*, 73-86.

Kotsantis, P., Petermann, E., and Boulton, S.J. (2018). Mechanisms of Oncogene-Induced Replication Stress: Jigsaw Falling into Place. Cancer discovery *8*, 537-555.

La Russa, M.F., and Qi, L.S. (2015). The New State of the Art: Cas9 for Gene Activation and Repression. Molecular and cellular biology *35*, 3800-3809.

Li, Y., Huang, J., Yang, D., Xiang, S., Sun, J., Li, H., and Ren, G. (2018). Expression patterns of E2F transcription factors and their potential prognostic roles in breast cancer. Oncology letters *15*, 9216-9230.

Lin, X., Sun, R., Zhao, X., Zhu, D., Zhao, X., Gu, Q., Dong, X., Zhang, D., Zhang, Y., Li, Y., *et al.* (2017). C-myc overexpression drives melanoma metastasis by promoting vasculogenic mimicry via c-myc/snail/Bax signaling. Journal of molecular medicine *95*, 53-67.

Liu, X.L., Ding, J., and Meng, L.H. (2018). Oncogene-induced senescence: a double edged sword in cancer. Acta pharmacologica Sinica.

Mali, P., Yang, L., Esvelt, K.M., Aach, J., Guell, M., DiCarlo, J.E., Norville, J.E., and Church, G.M. (2013). RNA-guided human genome engineering via Cas9. Science *339*, 823-826.

McHugh, D., and Gil, J. (2018). Senescence and aging: Causes, consequences, and therapeutic avenues. The Journal of cell biology *217*, 65-77.

Muller, P.A., and Vousden, K.H. (2013). p53 mutations in cancer. Nature cell biology *15*, 2-8.

Ossio, R., Roldan-Marin, R., Martinez-Said, H., Adams, D.J., and Robles-Espinoza, C.D. (2017). Melanoma: a global perspective. Nature reviews Cancer *17*, 393-394.

Pratilas, C.A., Taylor, B.S., Ye, Q., Viale, A., Sander, C., Solit, D.B., and Rosen, N. (2009). (V600E)BRAF is associated with disabled feedback inhibition of RAF-MEK signaling and

elevated transcriptional output of the pathway. Proceedings of the National Academy of Sciences of the United States of America *106*, 4519-4524.

Qi, L.S., Larson, M.H., Gilbert, L.A., Doudna, J.A., Weissman, J.S., Arkin, A.P., and Lim, W.A. (2013). Repurposing CRISPR as an RNA-guided platform for sequence-specific control of gene expression. Cell *152*, 1173-1183.

Qin, X.Q., Livingston, D.M., Kaelin, W.G., Jr., and Adams, P.D. (1994). Deregulated transcription factor E2F-1 expression leads to S-phase entry and p53-mediated apoptosis. Proceedings of the National Academy of Sciences of the United States of America *91*, 10918-10922.

Ren, J., and Zhao, Y. (2017). Advancing chimeric antigen receptor T cell therapy with CRISPR/Cas9. Protein & cell *8*, 634-643.

Robert, C., Long, G.V., Brady, B., Dutriaux, C., Maio, M., Mortier, L., Hassel, J.C., Rutkowski, P., McNeil, C., Kalinka-Warzocha, E., *et al.* (2015). Nivolumab in previously untreated melanoma without BRAF mutation. The New England journal of medicine *372*, 320-330.

Sadozai, H., Gruber, T., Hunger, R.E., and Schenk, M. (2017). Recent Successes and Future Directions in Immunotherapy of Cutaneous Melanoma. Frontiers in immunology *8*, 1617.

Salama, R., Sadaie, M., Hoare, M., and Narita, M. (2014). Cellular senescence and its effector programs. Genes & development *28*, 99-114.

Serrano, M., Hannon, G.J., and Beach, D. (1993). A new regulatory motif in cell-cycle control causing specific inhibition of cyclin D/CDK4. Nature *366*, 704-707.

Serrano, M., Lin, A.W., McCurrach, M.E., Beach, D., and Lowe, S.W. (1997). Oncogenic ras provokes premature cell senescence associated with accumulation of p53 and p16INK4a. Cell *88*, 593-602.

Shaffer, S.M., Dunagin, M.C., Torborg, S.R., Torre, E.A., Emert, B., Krepler, C., Beqiri, M., Sproesser, K., Brafford, P.A., Xiao, M., *et al.* (2017). Rare cell variability and drug-induced reprogramming as a mode of cancer drug resistance. Nature *546*, 431-435.

Sharma, P., Hu-Lieskovan, S., Wargo, J.A., and Ribas, A. (2017). Primary, Adaptive, and Acquired Resistance to Cancer Immunotherapy. Cell *168*, 707-723.

Siegel, R.L., Miller, K.D., and Jemal, A. (2016). Cancer statistics, 2016. CA: a cancer journal for clinicians *66*, 7-30.

Solit, D., and Rosen, N. (2010). Oncogenic RAF: a brief history of time. Pigment cell & melanoma research *23*, 760-762.

Suram, A., Kaplunov, J., Patel, P.L., Ruan, H., Cerutti, A., Boccardi, V., Fumagalli, M., Di Micco, R., Mirani, N., Gurung, R.L., *et al.* (2012). Oncogene-induced telomere dysfunction enforces cellular senescence in human cancer precursor lesions. The EMBO journal *31*, 2839-2851.

Topalian, S.L., Sznol, M., McDermott, D.F., Kluger, H.M., Carvajal, R.D., Sharfman, W.H., Brahmer, J.R., Lawrence, D.P., Atkins, M.B., Powderly, J.D., *et al.* (2014). Survival, durable tumor remission, and long-term safety in patients with advanced melanoma receiving nivolumab. Journal of clinical oncology : official journal of the American Society of Clinical Oncology *32*, 1020-1030.

Tu, Z., Aird, K.M., Bitler, B.G., Nicodemus, J.P., Beeharry, N., Xia, B., Yen, T.J., and Zhang, R. (2011). Oncogenic RAS regulates BRIP1 expression to induce dissociation of BRCA1 from chromatin, inhibit DNA repair, and promote senescence. Developmental cell *21*, 1077-1091.

van Deursen, J.M. (2014). The role of senescent cells in ageing. Nature *509*, 439-446.

Winter, C., and Albers, P. (2011). Testicular germ cell tumors: pathogenesis, diagnosis and treatment. Nat Rev Endocrinol *7*, 43-53.

Yin, C., Zhang, T., Qu, X., Zhang, Y., Putatunda, R., Xiao, X., Li, F., Xiao, W., Zhao, H., Dai, S., *et al.* (2017). In Vivo Excision of HIV-1 Provirus by saCas9 and Multiplex Single-Guide RNAs in Animal Models. Molecular therapy : the journal of the American Society of Gene Therapy *25*, 1168-1186.

Zhang, X., Ni, Z., Duan, Z., Xin, Z., Wang, H., Tan, J., Wang, G., and Li, F. (2015). Overexpression of E2F mRNAs associated with gastric cancer progression identified by the transcription factor and miRNA co-regulatory network analysis. PloS one *10*, e0116979.

Zhao, R., Choi, B.Y., Lee, M.H., Bode, A.M., and Dong, Z. (2016). Implications of Genetic and Epigenetic Alterations of CDKN2A (p16(INK4a)) in Cancer. EBioMedicine *8*, 30-39.

CHAPTER 2
GENOME-WIDE SCREEN IDENTIFIES NOVEL GENES AND BIOLOGICAL PROCESSES IMPLICATED IN CISPLATIN RESISTANCE

2.1 Introduction

Cisplatin-based chemotherapeutic regimens are the most frequently used (neo)adjuvant treatments for the majority of solid tumors. After its cis-chloro groups are replaced by water molecules, cisplatin forms covalent bonds with methionine and a large panel of cysteine-containing peptides and polypeptides and reacts with DNA to produce intra- and inter-strand crosslinks (Galluzzi et al., 2014). Cisplatin treatment is highly efficient against testicular germ cell cancer, leading to a durable complete remission in >80% of the patients (Winter and Albers, 2011). However, clinical responses elicited by cisplatin-based therapeutic regimens in patients affected by other solid tumors are temporary and vanish as malignant cells become chemoresistant.

Cisplatin resistance is complex and may be caused by different mechanisms, including 1) decreased drug intake and/or increased drug extrusion by plasma membrane transporters, 2) increased nuclear and mitochondrial DNA repair, and preservation/turnover of cytoplasmic components, 3) altered checkpoints and safeguard mechanisms, and 4) molecular circuitries that deliver compensatory survival signals even though they are not directly activated by cisplatin (Ferreira et al., 2016; Galluzzi et al., 2014). However, despites decades of intensive effort, the genes and biological processes implicated in cisplatin resistance are still largely unknown.

Melanoma is the most aggressive skin cancer and notoriously resistant to chemotherapeutic agents including cisplatin (Mattia et al., 2018). Marked improvements in melanoma treatments, especially those with small-molecule targeted drugs and immunotherapies, have been achieved

over the past decade. However, due to its high heterogeneity and high genetic mutation rate, metastatic melanomas are still one of the toughest cancers to be treated. Insights into the mechanisms of cisplatin resistance will be invaluable for development of novel treatment strategies.

Here, we report the identifications of genes and biological processes implicated in cisplatin resistance by utilizing a genome-wide CRISPR/Cas9 gene knockout system. Interestingly, a large fraction of these genes and biological processes has not been previously recognized as the leading causes of cisplatin resistance.

2.2 Material and Methods

2.2.1 Cell lines

A375 human melanoma cells (ATCC® CRL-1619) were cultured in RPMI1640-GlutaMax medium supplemented with 10% of newborn calf serum. Human Hermes 4C melanocytes, which were immortalized by vectors expressing human telomerase (hTERT) and HPV16-E7 (Gray-Schopfer et al., 2006; Scott et al., 2002), were obtained from Wellcome Trust Functional Genomics Cell Bank and cultured in RPMI 1640-GlutaMax medium supplemented with 10% newborn calf serum, human stem cell factor (10 ng/ml), phorbal-12-myristate-13-acetate (200 nM), chlorotoxin (200 pM), and endothelin (10 nM). hTERT immortalized human fibroblast P1F/TERT was obtained from the Rheinwald Laboratory (Harvard Skin Disease Research Center) and cultured in DMEM/F12 medium supplemented with 15% newborn calf serum and 10 ng/ml of epidermal growth factor.

2.2.2 GeCKO library preparation and lentivirus production

Genome-scale CRISPR Knock-Out GeCKO libraries (Addgene, #1000000048) were transformed into Endura electrocompetent *E. coli* cells (Lucigen, #60242). After overnight

culturing in LB medium, plasmids were purified by using Qiagen Plasmid Maxi Kit**.** To prepare lentiviral particles expressing Cas9 and the GeCKO library sgRNAs, the plasmids were co-transfect with plasmids pCMV-VSV-G (Addgene #8454) and psPAX2 (Addgene #12260) into HEK293T cells (Clontech #632180) (Jordan et al., 1996). Lentivirus particles were harvested 48 hours after the transfection, concentrated by ultracentrifugation at 24,000 RPM for 2 hours at 4°C, and resuspended in RPIM1640 medium containing 10% fetus bovine serum by incubation at 4°C overnight.

2.2.3 GeCKO library transduction and cisplatin treatment of A375 human melanoma cells

The protocol is outlined in Fig. 2.1A. One hundred million melanoma A375 cells were transduced with lentiviral GeCKO libraries by using Spinfection (Berggren et al., 2008). Puromycin was added to the culture to a final concentration of 1 μg/ml 2 days after the transduction to eliminate untransduced cells. On day 7, cells were pooled and one third of the total population was harvested as early transduction (for estimation of distribution of transduced sgRNAs). The remaining cells were seeded back and cultured. On day 12, one half of the cultured cells were treated with 8 μM cisplatin for 16 hours, which killed ~ 50% of the cells, and the other half of the cells were left untreated. The cisplatin treated and untreated cells were passaged synchronously to ensure they underwent similar numbers of cell divisions. To maintain the coverage of the GeCKO libraries, the cells were pooled and > 2 million cells were seeded for each passage. Cisplatin-treated and untreated cells were harvested on Day 25.

2.2.4 Next-generation sequencing of GeCKO sgRNAs

The genomic DNA of the early transduction, and cisplatin-treated and untreated cells was purified by using Blood & Cell culture DNA midi Kit (Qiagen #13343). A total of 130 μg of

genomic DNA from each treatment group was used to create the sgRNA sequencing libraries. sgRNA sequences in the genomic DNA were amplified by PCR (24 cycles;10 μg/reaction) using Lenti-F1 and Lenti-R1 primers (Table 2-1) and Herculase II Fusion DNA polymerase (Agilent). All PCR products of 400-600 bp in the same group were combined and gel purified. Illumina sequencing adapters were attached to the purified DNA fragments by 21 cycle of PCR using GECKO1 and GECKO2 primers (Table 2-1). Finally, barcode sequences were attached to the fragments by 6 cycles of PCR using Tru-U (forward) and Tru-B1/2/3 (reverse) primers (Table 2-1). Sequencing was carried out on an Illumina Hi-Seq 2000 platform and the data was analyzed using MAGeCK (Li et al., 2014).

Table 2.1. Oligonucleotides used for creation of sequencing libraries of GeCKO gRNAs integrated in the genome of transduced cells

Lenti-F1	ATGGACTATCATATGCTTACCGTAACTTGAAAGTATTTCG
Lenti-R1	ACTTCTTGTCCATGGTGGCAGC
GECKO-1	ACACGACGCTCTTCCGATCTtcttGTGGAAAGGACGAAACACCG
GECKO-2	AGACGTGTGCTCTTCCGATCTACTTCTTGTCCATGGTGGCAGC
Tru-U	AATGATACGGCGACCACCGAGATCTACACTCTTTCCCTACACGACG CTCTTCCGATCT
Tru-B1	CAAGCAGAAGACGGCATACGAGATCGTGATGTGACTGGAGTTCAG ACGTGTGCTCTTCCGATCT
Tru-B2	CAAGCAGAAGACGGCATACGAGATACATCGGTGACTGGAGTTCAG ACGTGTGCTCTTCCGATCT
Tru-B3	CAAGCAGAAGACGGCATACGAGATGCCTAAGTGACTGGAGTTCAG ACGTGTGCTCTTCCGATCT

2.2.5 shRNA knockdown

shRNA sequences were determined based on the highest score ranked in The RNAi Consortium shRNA Library (https://www.broadinstitute.org/rnai-consortium/rnai-consortium-shrna-library). Several shRNA-encoding DNA sequences were tested for knocking down each of the genes of interest. The ones that are effective for gene knockdown are listed in Table 2-2. For knocking down genes in A375 melanoma and P1F/TERT cells, the shRNAs were expressed

by using the lentiviral vector TRC2-pLKO-Puro (Sigma). For knocking down genes in Hermes 4C cells, the shRNAs were expressed by using the lentiviral vector TRC2-pLKO-Hyg or TRC2-pLKO-Bst, which is identical to TRC2-pLKO-Puro except that the puromycin resistance gene was replaced by hygromycin or blasticidin resistance gene, respectively. Lentivirus particles were packaged as described above. Cells transduced with the viruses were selected with puromycin, hygromycin and blasticidine at 1, 100 and 10 μg/ml, respectively.

Table 2.2. shRNA-encoding DNA sequences that are effective for gene knockdown

ZNRF3	
shZNRF3	CCGGGTCTACCTAATGCACTATTATCTCGAGATAATAGTGCATTAGGTAGACTTTTTG
NF2	
shNF2-1	CCGGTACTTTGCAATCCGGAATAAACTCGAGTTTATTCCGGATTGCAAAGTATTTTTG
shNF2-2	CCGGTCGGGAACCATGATCTATTTACTCGAGTAAATAGATCATGGTTCCCGATTTTTG
UBE2F	
shUBE2F	CCGGGATGACTACATCAAACGTTATCTCGAGATAACGTTTGATGTAGTCATCTTTTTTG
shUBE2F-3	CCGGTTCTGCACAAGCGATGCTAATCTCGAGATTAGCATCGCTTGTGCAGAATTTTTTG
shUBE2F-4	CCGGTGATCCAAACAAGCTTCATTGCTCGAGCAATGAAGCTTGTTTGGATCATTTTTTG
RNF7	
shRNF7	CCGGTCAGAAATTCTCTGCGATTAACTCGAGTTAATCGCAGAGAATTTCTGATTTTTG
CTNNB1	
shCTNNB1	CCGGATCTGTCTGCTCTAGTAATAACTCGAGTTATTACTAGAGCAGACAGATTTTTTG
shCTNNB1-3	CCGGTCTAACCTCACTTGCAATAATCTCGAGATTATTGCAAGTGAGGTTAGATTTTTG
TP53	
shTP53	CCGGCACCATCCACTACAACTACATCTCGAGATGTAGTTGTAGTGGATGGTGTTTTTG
Scramble	
shScramble	CCGGTCCTAAGGTTAAGTCGCCCTCGCTCGAGCGAGGGCGACTTAACCTTAGGTTTTTG

2.2.6 Assay for cisplatin-induced apoptosis

Cells were seeded in 12-well plates (30% confluence for A375, 60% confluence for Hermes 4C and P1F/HTERT). After 24 hours of incubation, the cells were treated with different doses of cisplatin for 24 (A375 cells and derivatives) or 48 hours (Hermes 4C and P1F/TERT as well as their derivatives). Attached and floating cells from the same sample were harvested and pooled. After washing with PBS, the cells were stained with Alexa Fluor 488 conjugated Annexin V (ThermoFisher Scientific) and analyzed by using flow-cytometry. Standard errors and p-values (unpaired Student's *t*-test) were calculated from data generated from at least three independent experiments.

2.2.7 ARIH1 and EIF4E2 overexpression

Human ARIH1 (MHS6278-202802257) and EIF4E2 (MSH6278-202826512) sequence-verified cDNA plasmids were purchased from Dharmacon. To overexpress ARIH1, the Cas9 gene in the lentiviral vector lentiCRISPR v2 (Sanjana et al., 2014) were replaced with the ARIH1 cDNA. To overexpress EIF4E2, the Cas9 and puromycin genes in lentiCRISPR v2 were replaced with the EIF4E2 cDNA and the hygromycin gene respectively. Lentivirus particles expressing the cDNAs were packaged as described above. Cells transduced with the viruses were selected with 1 μg/ml puromycin or 100 μg/ml hygromycin.

2.2.8 Verteporfin treatment

Verteporfin was purchased from R&D Systems (#5305/10) and dissolved in DMSO. Cells at ~ 80% confluence were treated with different concentration of Verteporfin. After 24 - 48 hours of treatment, the cells were washed with PBS twice and whole cell proteins extracts were prepared.

2.2.9 Western blot

Cells (~$0.8x10^6$) in a well of a 6-well plate were washed with PBS, scraped off and pelleted. The cells were then lysed by vortexing in 100 µl of phenol, 5 µl of β-mercaptoethanol and 100 µl of PBS for 15min. Proteins in the lysate were precipitated by mixing with 1.2 ml methanol containing 0.1M ammonium acetate followed by centrifugation. Proteins were separated on SDS-PAGE gels, transferred onto PVDF membranes and probed with antibodies against ZNRF3 (Abiocode R2407-1), RNF7 (Proteintech 11905-1-AP), CTNNB1 (Proteintech 51067-2-AP), NF2 (Abclonal A13626), UBE2F (Santa Cruz Biotech sc-398668), p53 (Santa Cruz Biotech sc-126), phosphorylated p53 (Cell Signaling Tech 9284S), ARIH1 (Santa Cruz Biotech sc-514551) and EIF4E2 (Santa Cruz Biotech sc-100731).After overnight incubation at 4°C, membranes were washed with TBST (3X) followed by incubation with appropriate secondary antibody in 5% skimmed milk for 2 hours at room temperature.

2.2.10 Reverse transcription quantitative PCR

Total RNA was extracted from the cells using Quick-RNA Miniprep Plus Kit (Zymo Research, # R1057T). The mRNAs of ACTB (internal control), ARIH1 and EIF4E2 were hybridized to appropriated primers (Table 2-3) and reverse transcribed by using the ProtoScript II First Strand cDNA Synthesis Kit (New England Biolabs). The RNAs in the reverse transcribed samples were digested by using RNase I_f (New England Biolabs) and the cDNAs were purified by using DNA Clean & Concentrator (Zymo Research, #D4004). Real-time quantitative PCR of the cDNAs was performed by using the SYBR Select Master Mix (Thermo Scientific, #4472908) and appropriate primers (Table 2-3). The standard curves were generated by using plasmids bearing cDNAs of ACTB (MHS6278-202755711), EIF4E2 (MHS6278-202826512) and ARIH1 (MHS6278-202802257) (Dharmacon).

Table 2.3. Reverse transcription PCR primers

Primers for reverse transcription		
ACTB	AGCAATGATCTTGAT	
ARIH1	CTCACAGTATCTG	
EIF4E2	TGTCTTCCTGAAAGC	
Primers for real-time PCR of cDNAs		
ACTB	CTTCCTGGGCATGGAGTCC	AGCAATGATCTTGATCTTCATTGTGC TG
ARIH1	CCATTATCTTTGAGAATAACC AAGCAGATC	TCTCACAGTATCTGTACTTGTCTTGT ACTTTCTG
EIF4E2	CCCATGTGGGAGGATGATGC	TGTCTTCCTGAAAGCGGACAGAC

2.3 Results

2.3.1 Genome-wide CRISPR/Cas9 knockout screening of genes and biological processes implicated in cisplatin resistance

To identify novel genes implicated in cisplatin resistance, we performed a genome-wide gene knockout screening in A375 human melanoma cells by using the human Genome-Scale CRISPR Knock-Out (GeCKO, v2) lentiviral pooled libraries, which consist of ~ 1.2×10^5 unique single-guide RNAs (sgRNAs) targeting 99.4% of all human genes (6 sgRNAs per gene and up to 4 sgRNAs per miRNA) (Sanjana et al., 2014). After the sgRNA targeted gene knockout events had occurred, a fraction of the cells were treated with cisplatin to kills 50 – 60% of the cells. Total genomic DNA was isolated from the early transduction (Etr), and cisplatin-treated (Cis) and untreated (Ctrl) cells (Fig. 2.1A). The sgRNA sequences integrated into the genome were sequenced and analyzed by using MAGeCK-VISPR, which assesses positively and negatively selected genes by testing whether sgRNA abundance differs significantly between treated and untreated samples (Li et al., 2015; Li et al., 2014). Most of our sequencing reads are of high quality (Fig. 2.1B). Over 4 million reads from each treatment group were perfectly mapped to the sgRNAs contained in the GeCKO libraries (Fig. 2.1C) with reasonably good distribution and coverage (< 500 out of the 1.2×10^5 sgRNAs were missing in the Etr cells) (Fig. 2.1D-F). The top

10 genes positively (e.g., with their targeting sgRNAs enriched) and negatively (e.g., with their targeting sgRNAs diminished) selected by cisplatin treatment are shown in Fig. 2.1G and H, respectively. The top 1000 genes positively and negatively selected by cisplatin are shown in Table A1 and A2 of Appendix, respectively.

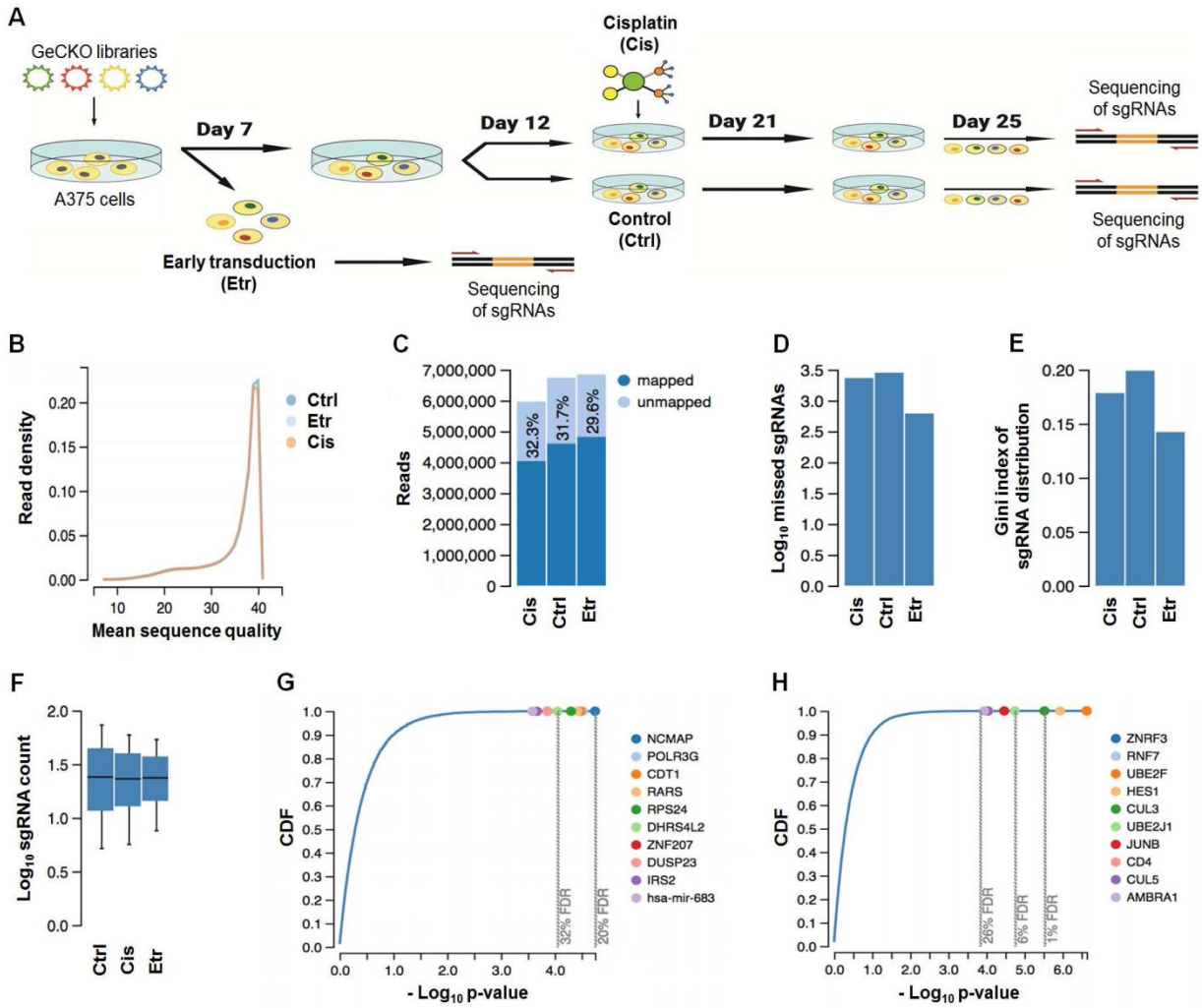

Figure 2.1. Genome-wide screening of genes implicated in cisplatin resistance/sensitivity in A375 human melanoma cells. (A) Flow-chart of the screening process. (B) Distribution of sequencing read quality (Phred score). (C) sgRNA reads perfectly mapped and unmapped (due to sequencing errors) to the GeCKO libraries. (D) Count of missing sgRNAs. (E) Gini-index of sgRNAs or the level of distribution of all sgRNA. (F) Count distribution of sgRNAs. (G) Top 10 genes positively selected by cisplatin when they were disrupted. (H) Top 10 genes negatively selected by cisplatin when they were disrupted. FDR, false discovery rate. CDF, cumulative distribution function.

To assess the biological processes that are implicated in cisplatin resistance we performed Gene Ontology (GO) enrichment analyses. Protein translation, RNA catabolic processes, and mitochondrial translational elongation and termination were the top biological processes positively selected by cisplatin (Table 2.4 and Fig. 2.2), indicating that these processes are responsible for cisplatin sensitivity and disruption of them leads to cisplatin resistance. In contrast, ubiquitin-dependent protein catabolic process, neddylation, and negative regulations of cellular catabolic process and canonical Wnt signaling were the top biological processes negatively selected by cisplatin (Table 2.5 and Fig. 2.3), indicating that these processes are responsible for cisplatin resistance and disruption of them leads to cisplatin sensitivity. The DNA damage checkpoint pathway was also negatively selected by cisplatin treatment to a moderate degree (p-value = 3.11×10^{-4}, Table 2.5). Neither DNA repair pathways nor drug transport systems were found to be among the top cisplatin-selected processes.

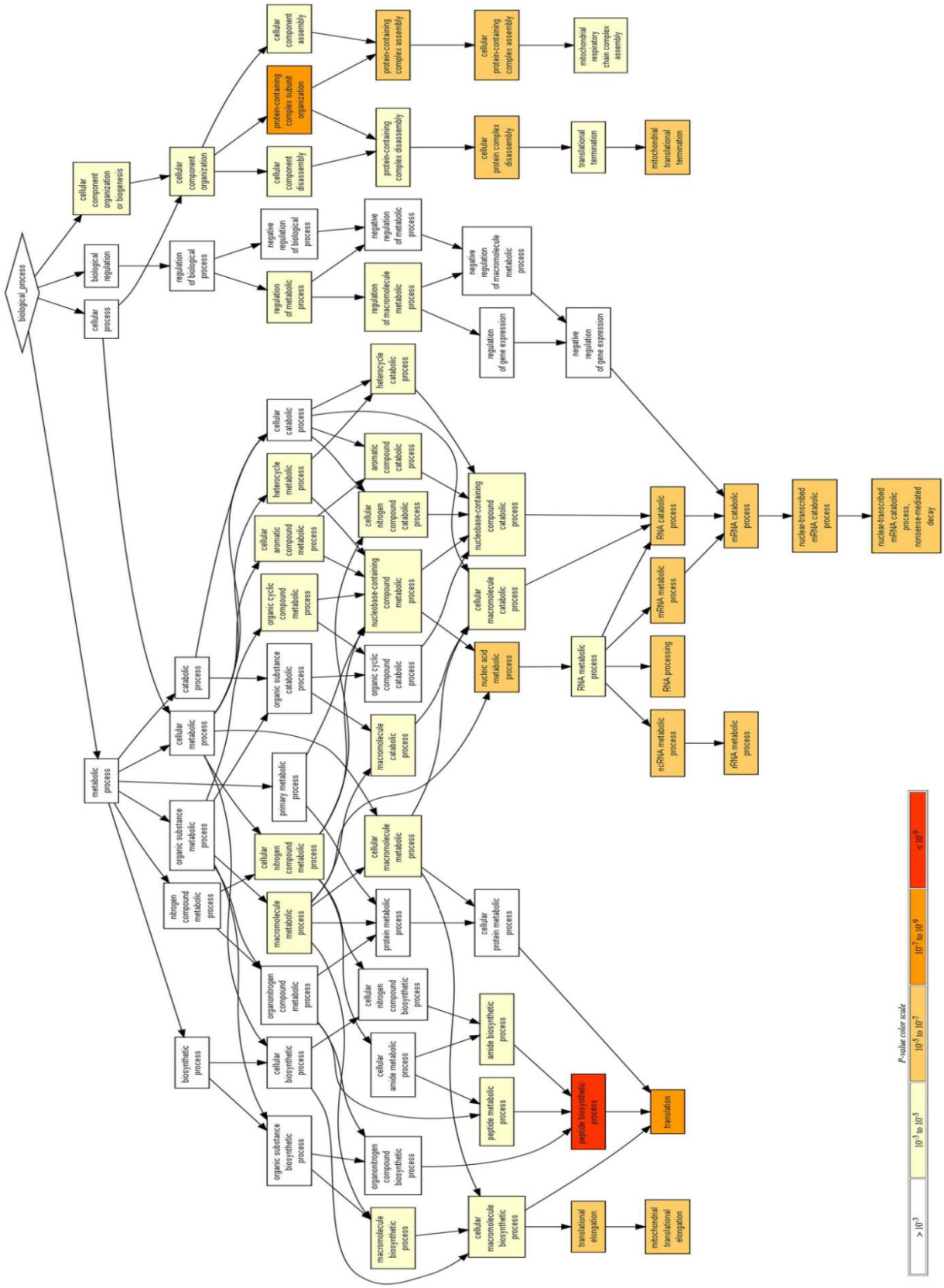

Figure 2.2. Top disrupted biological processes positively selected by cisplatin.

Table 2.4. Top 40 disrupted biological processes positively selected by cisplatin. N is the total number of genes. B is the total number of genes associated with a specific GO term.
n is the number of genes in the top of the user's input list or in the target set when appropriate. b is the number of genes in the intersection

GO term	Description	P-value	FDR q-value	Enrichment (N, B, n, b)
GO:0043043	peptide biosynthetic process	7.08E-10	1.09E-05	1.61 (18285,219,6398,123)
GO:0006412	translation	1.17E-09	8.98E-06	1.63 (18285,198,6398,113)
GO:0043933	protein-containing complex subunit organization	4.58E-08	2.34E-04	1.33 (18285,1742,2729,346)
GO:0034622	cellular protein-containing complex assembly	1.35E-07	5.18E-04	1.37 (18285,801,4159,250)
GO:0034660	ncRNA metabolic process	4.11E-07	1.26E-03	1.35 (18285,498,6087,223)
GO:0006396	RNA processing	4.39E-07	1.12E-03	1.36 (18285,786,4154,243)
GO:0000184	nuclear-transcribed mRNA catabolic process, nonsense-mediated decay	5.76E-07	1.26E-03	1.72 (18285,116,6398,70)
GO:0043624	cellular protein complex disassembly	7.85E-07	1.50E-03	1.66 (18285,133,6055,73)
GO:0070125	mitochondrial translational elongation	1.30E-06	2.21E-03	1.90 (18285,88,5695,52)
GO:0090304	nucleic acid metabolic process	1.33E-06	2.04E-03	1.14 (18285,3824,4275,1019)
GO:0016071	mRNA metabolic process	1.33E-06	1.86E-03	1.61 (18285,630,2073,115)
GO:0000956	nuclear-transcribed mRNA catabolic process	1.81E-06	2.30E-03	1.51 (18285,187,6398,99)
GO:0065003	protein-containing complex assembly	4.64E-06	5.46E-03	1.26 (18285,1474,3582,364)
GO:0006402	mRNA catabolic process	4.86E-06	5.32E-03	1.47 (18285,204,6398,105)
GO:0006414	translational elongation	5.51E-06	5.62E-03	2.27 (18285,119,2709,40)
GO:0016072	rRNA metabolic process	8.43E-06	8.07E-03	1.45 (18285,213,6392,108)
GO:0006401	RNA catabolic process	8.78E-06	7.91E-03	1.43 (18285,232,6398,116)
GO:0070126	mitochondrial translational termination	9.83E-06	8.36E-03	1.78 (18285,90,6055,53)

(Table Continued)

GO term	Description	P-value	FDR q-value	Enrichment (N, B, n, b)
GO:0006415	translational termination	1.21E-05	9.75E-03	1.79 (18285,95,5695,53)
GO:0032984	protein-containing complex disassembly	1.26E-05	9.62E-03	1.79 (18285,221,2873,62)
GO:0006614	SRP-dependent cotranslational protein targeting to membrane	1.44E-05	1.05E-02	1.73 (18285,89,6398,54)
GO:0016070	RNA metabolic process	1.45E-05	1.01E-02	1.14 (18285,3314,4442,914)
GO:0046483	heterocycle metabolic process	1.84E-05	1.22E-02	1.11 (18285,4523,4275,1177)
GO:0022607	cellular component assembly	1.84E-05	1.18E-02	1.23 (18285,2282,2647,407)
GO:0044260	cellular macromolecule metabolic process	1.98E-05	1.21E-02	1.07 (18285,5975,6108,2140)
GO:0006139	nucleobase-containing compound metabolic process	2.82E-05	1.66E-02	1.11 (18285,4360,4275,1135)
GO:0033108	mitochondrial respiratory chain complex assembly	3.47E-05	1.97E-02	2.28 (18285,90,2938,33)
GO:0006518	peptide metabolic process	3.54E-05	1.94E-02	1.33 (18285,334,6398,156)
GO:0070972	protein localization to endoplasmic reticulum	3.96E-05	2.09E-02	1.61 (18285,117,6404,66)
GO:0006260	DNA replication	4.05E-05	2.07E-02	5.20 (18285,146,265,11)
GO:0034641	cellular nitrogen compound metabolic process	4.63E-05	2.29E-02	1.10 (18285,4829,4275,1246)
GO:0006613	cotranslational protein targeting to membrane	5.48E-05	2.62E-02	1.67 (18285,94,6398,55)
GO:0072599	establishment of protein localization to endoplasmic reticulum	5.53E-05	2.57E-02	1.63 (18285,107,6398,61)
GO:0034645	cellular macromolecule biosynthetic process	5.88E-05	2.65E-02	1.11 (18285,2834,6400,1098)
GO:0071840	cellular component organization or biogenesis	5.97E-05	2.61E-02	1.13 (18285,4953,3032,924)
GO:0034250	positive regulation of cellular amide metabolic process	6.10E-05	2.59E-02	1.94 (18285,131,2883,40)
GO:0045047	protein targeting to ER	6.31E-05	2.61E-02	1.64 (18285,103,6398,59)
GO:0006413	translational initiation	6.52E-05	2.63E-02	2.26 (18285,138,1762,30)

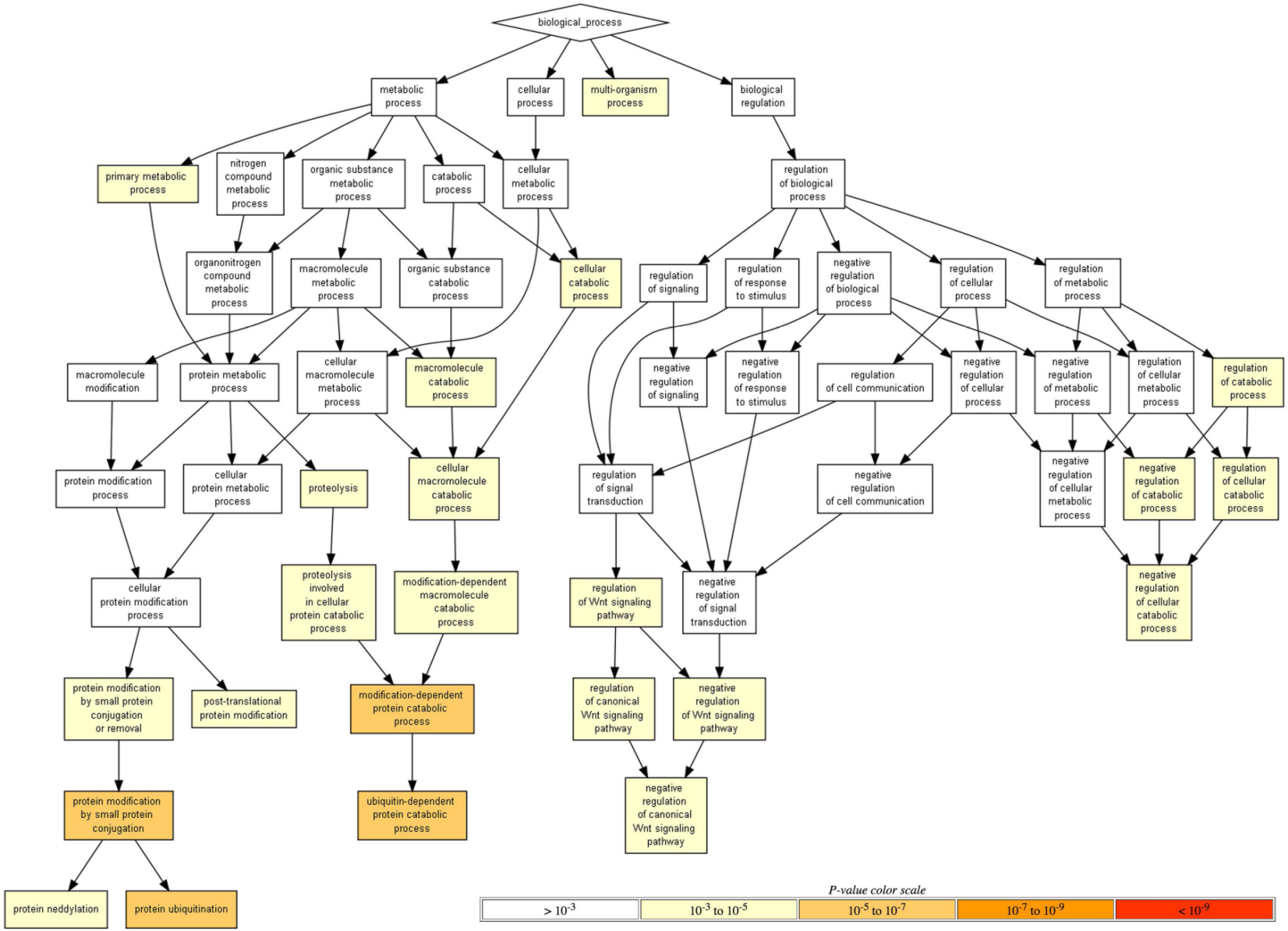

Figure 2.3. Top disrupted biological processes negatively selected by cisplatin.

Table 2.5. Top 40 disrupted biological processes negatively selected by cisplatin

GO term	Description	P-value	FDR q-value	Enrichment (N, B, n, b)
GO:0016567	protein ubiquitination	1.12E-06	1.72E-02	19.66 (18285,620,9,6)
GO:0032446	protein modification by small protein conjugation	1.76E-06	1.35E-02	18.44 (18285,661,9,6)
GO:0006511	ubiquitin-dependent protein catabolic process	7.84E-06	4.00E-02	22.78 (18285,446,9,5)
GO:0019941	modification-dependent protein catabolic process	8.31E-06	3.18E-02	22.52 (18285,451,9,5)
GO:0043632	modification-dependent macromolecule catabolic process	1.01E-05	3.09E-02	22.04 (18285,461,9,5)
GO:0070647	protein modification by small protein conjugation or removal	1.13E-05	2.89E-02	13.54 (18285,900,9,6)
GO:0045116	protein neddylation	1.31E-05	2.87E-02	937.69 (18285,13,3,2)
GO:0051603	proteolysis involved in cellular protein catabolic process	1.67E-05	3.20E-02	19.80 (18285,513,9,5)
GO:0031330	negative regulation of cellular catabolic process	1.88E-05	3.20E-02	2.99 (18285,229,614,23)
GO:0031329	regulation of cellular catabolic process	2.02E-05	3.09E-02	1.89 (18285,729,784,59)
GO:0009894	regulation of catabolic process	2.35E-05	3.28E-02	1.93 (18285,830,627,55)
GO:0043687	post-translational protein modification	3.34E-05	4.26E-02	18.19 (18285,359,14,5)
GO:0051704	multi-organism process	3.78E-05	4.46E-02	1.63 (18285,1247,801,89)
GO:0090090	negative regulation of canonical Wnt signaling pathway	7.91E-05	8.66E-02	10.77 (18285,129,79,6)
GO:0006508	proteolysis	1.00E-04	1.02E-01	7.88 (18285,1160,14,7)
GO:0044265	cellular macromolecule catabolic process	1.05E-04	1.01E-01	13.62 (18285,746,9,5)
GO:0060828	regulation of canonical Wnt signaling pathway	1.42E-04	1.28E-01	9.93 (18285,221,50,6)
GO:0051726	regulation of cell cycle	1.65E-04	1.41E-01	3.10 (18285,1128,94,18)
GO:1903358	regulation of Golgi organization	1.71E-04	1.37E-01	4.07 (18285,15,2995,10)
GO:0060341	regulation of cellular localization	1.81E-04	1.39E-01	1.86 (18285,786,626,50)

(Table Continued)

GO term	Description	P-value	FDR q-value	Enrichment (N, B, n, b)
GO:0044419	interspecies interaction between organisms	1.86E-04	1.36E-01	1.25 (18285,677,5380,248)
GO:0038018	Wnt receptor catabolic process	2.17E-04	1.51E-01	9,142.50 (18285,2,1,1)
GO:0045977	positive regulation of mitotic cell cycle, embryonic	2.19E-04	1.46E-01	4,571.25 (18285,1,4,1)
GO:2000227	negative regulation of pancreatic A cell differentiation	2.19E-04	1.40E-01	4,571.25 (18285,1,4,1)
GO:2000226	regulation of pancreatic A cell differentiation	2.19E-04	1.34E-01	4,571.25 (18285,1,4,1)
GO:0061106	negative regulation of stomach neuroendocrine cell differentiation	2.19E-04	1.29E-01	4,571.25 (18285,1,4,1)
GO:0061105	regulation of stomach neuroendocrine cell differentiation	2.19E-04	1.24E-01	4,571.25 (18285,1,4,1)
GO:0018963	phthalate metabolic process	2.22E-04	1.21E-01	20.61 (18285,3,887,3)
GO:0009895	negative regulation of catabolic process	2.29E-04	1.21E-01	2.55 (18285,269,614,23)
GO:0042127	regulation of cell proliferation	2.38E-04	1.22E-01	5.80 (18285,1577,16,8)
GO:0060716	labyrinthine layer blood vessel development	2.49E-04	1.23E-01	261.21 (18285,20,7,2)
GO:0030178	negative regulation of Wnt signaling pathway	2.71E-04	1.30E-01	8.57 (18285,162,79,6)
GO:0072576	liver morphogenesis	2.73E-04	1.27E-01	3,657.00 (18285,1,5,1)
GO:0009057	macromolecule catabolic process	2.97E-04	1.34E-01	11.35 (18285,895,9,5)
GO:0070417	cellular response to cold	3.06E-04	1.34E-01	16.71 (18285,8,547,4)
GO:0000077	DNA damage checkpoint	3.11E-04	1.32E-01	3.97 (18285,68,880,13)
GO:0043161	proteasome-mediated ubiquitin-dependent protein catabolic process	3.66E-04	1.51E-01	32.19 (18285,284,6,3)
GO:0045786	negative regulation of cell cycle	4.03E-04	1.62E-01	3.46 (18285,518,143,14)
GO:0033032	regulation of myeloid cell apoptotic process	4.17E-04	1.64E-01	9.23 (18285,27,440,6)
GO:0008283	cell proliferation	4.35E-04	1.67E-01	2.51 (18285,646,259,23)

2.3.2 Knockdown of the top negatively selected genes also sensitizes A375 melanoma and melanocyte cells to cisplatin

ZNRF3 is an E3 ubiquitin ligase that acts as a negative regulator of the Wnt signaling pathway (Hao et al., 2012). UBE2F is an E2 NEDD8-conjugase involved in neddylation of CUL5, the core component of multiple SCF-like ECS E3 ubiquitin-protein ligase complexes (Huang et al., 2009). RNF7 is a probable component of the SCF E3 ubiquitin ligase complex that

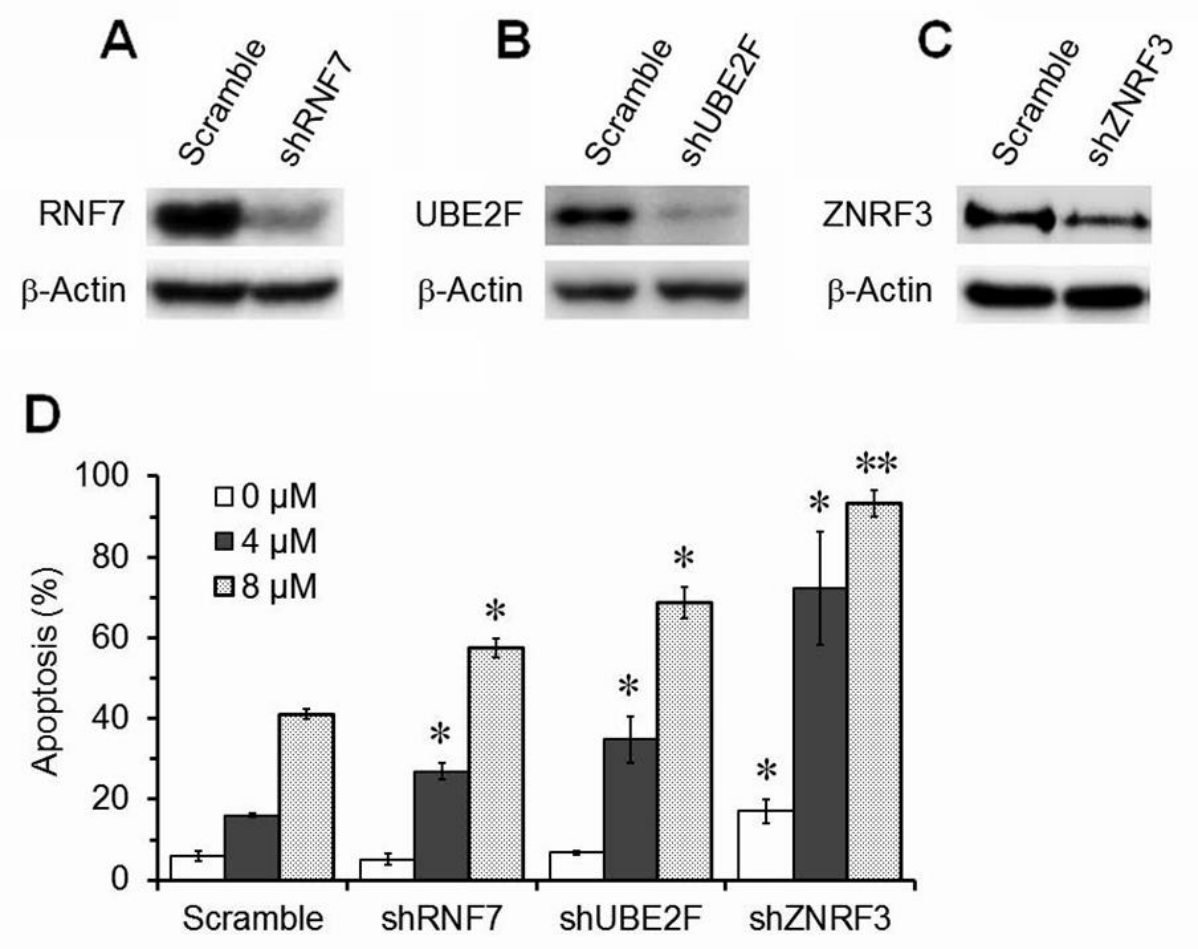

Figure 2.4. Confirmation of the top 3 genes negatively selected by cisplatin in A375 melanoma cells. (A-C) Western blot showing knockdown of the genes by shRNAs. β-Actin serves as loading control. (D) Cisplatin (0, 4, and 8 μM) induced apoptosis. Error bars stand for standard errors of 3 independent experiments. Single and double asterisks denote p values < 0.05 and < 0.001, respectively (Student's t-test), by comparing different knockdown cell lines to scramble at the same cisplatin dosage.

also promotes neddylation of CUL5 via its interaction with UBE2F (Huang et al., 2009). Our genome-wide knockout screening indicates that ZNRF3, RNF7 and UBE2F are the top 3 genes negatively selected by cisplatin (Fig. 2.1H). To determine if the screening results are valid, we knocked down these genes by using lentivirus-based shRNAs (Fig. 2.4A-C). Indeed, knockdown any of these genes, especially ZNRF3, caused significant increase of cell apoptosis upon cisplatin treatment (Fig. 2.4D). To determine if the implications of ZNRF3, RNF7, and UBE2F in cisplatin resistance are limited to melanoma, we knocked down these genes in the Hermes 4C human immortalized melanocytes (Gray-Schopfer et al., 2006; Scott et al., 2002) (Fig. 2.5A-C). ZNRF3 or UBE2F knockdown significantly sensitized the melanocytes to cisplatin. However, RNF7 knockdown slightly (statistically insignificant) sensitized the melanocytes to cisplatin (Fig. 2.5D).

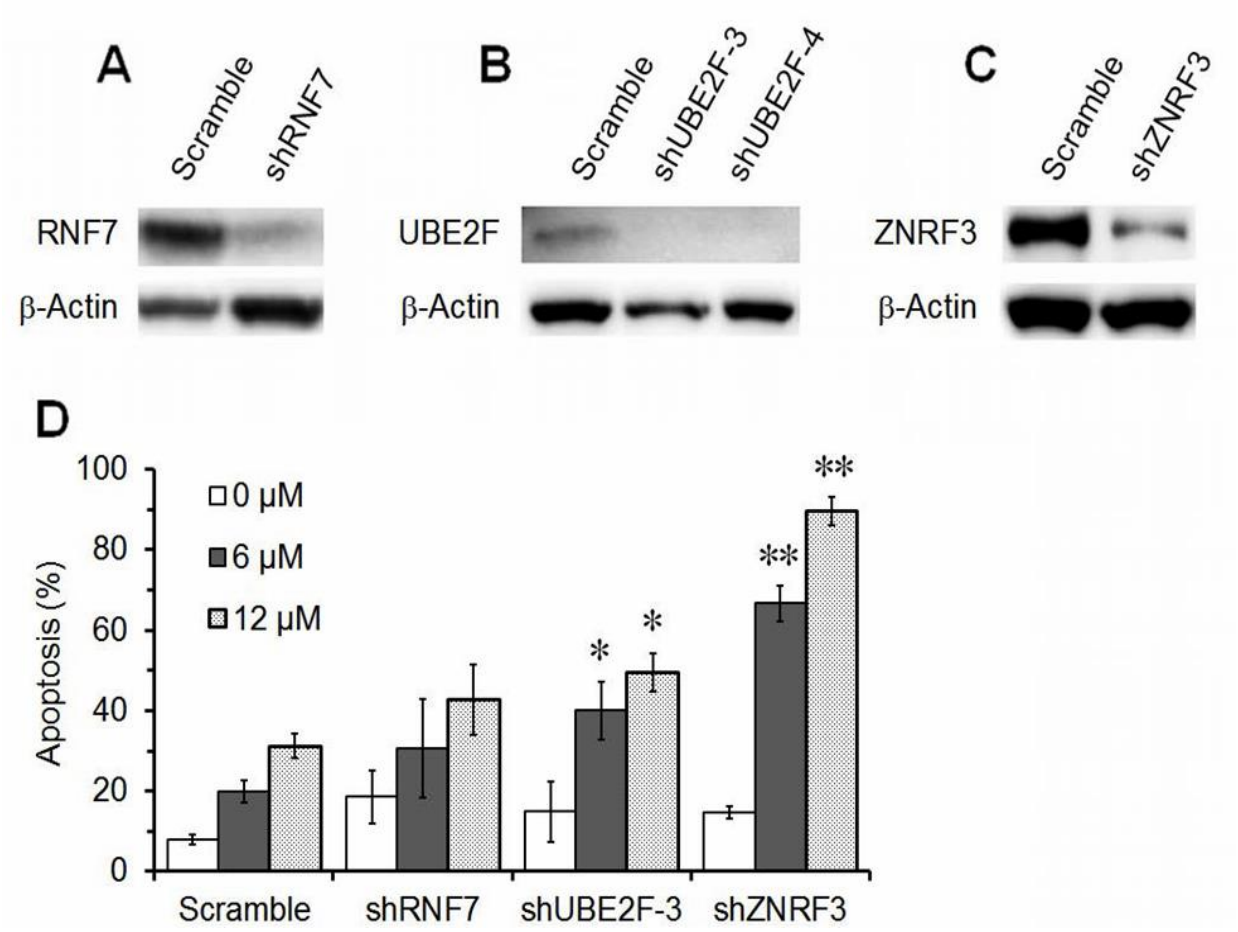

Figure 2.5. Knockdown of ZNRF3, RNF7 or UBE2F in Hermes 4C melanocytes also cause different degrees of cisplatin sensitivity. (A-C) Western blot showing knockdown of the genes by shRNAs. β-Actin serves as loading control. (D) Cisplatin induced apoptosis. Error bars stand for standard errors. Single and double asterisks denote p values < 0.05 and < 0.001, respectively (Student's t-test).

2.3.3 Knockdown of ZNRF3 sensitizes melanoma and melanocyte cells to cisplatin by derepressing the Wnt/β-Catenin signaling

ZNRF3 has been known to negatively regulate the Wnt signaling pathway by mediating the ubiquitination and subsequent degradation of Frizzled and LRP5/6, the receptor and co-receptor for Wnt (Fig. 2.6A) (Hao et al., 2012). The Wnt signaling is categorized into β-Catenin-dependent (canonical) and independent (non-canonical) pathways (Zhan et al., 2017). The canonical Wnt signaling pathway is activated upon binding of Wnt ligands to the Frizzled and LRP5/6, which causes translocation of the β-Catenin destruction complex to the plasma membrane thereby preventing phosphorylation and degradation of β-Catenin (Fig. 2.6A). Inhibition of ZNRF3 enhances the Wnt/β-Catenin signaling and disrupts the Wnt/planar cell polarity signaling (Hao et al., 2012). To determine if ZNRF3 modulates cisplatin resistance by regulating β-Catenin, we knocked down ZNRF3 and CTNNB1 (the β-Catenin gene) individually or simultaneously (Fig. 2.6B and C). The A375 melanoma and Hermes 4C melanocyte cells with ZRNF3 and CTNNB1 double knockdowns were more cisplatin-resistant than those with ZNRF3 single knockdown (Fig. 2.6D and E). As expected, the levels of total and phosphorylated p53, the key factor involved in cell apoptosis, were increased upon cisplatin treatment (Fig. 2.6F and G). ZNRF3 knockdown caused more dramatic increase of total and phosphorylated p53 upon cisplatin treatment (Fig. 2.6F and G). However, the p53 level was reduced in cells with ZNRF3 and CTNNB1 double knockdown compared to that in cells with ZNRF3 single knockdown (Fig. 2.6F and G). Taken together, our data suggests that the sensitization of melanoma and melanocyte cells to cisplatin by ZNRF3 knockdown is due to derepression of Wnt/β-Catenin signaling, leading to increased p53 activities upon cisplatin treatment.

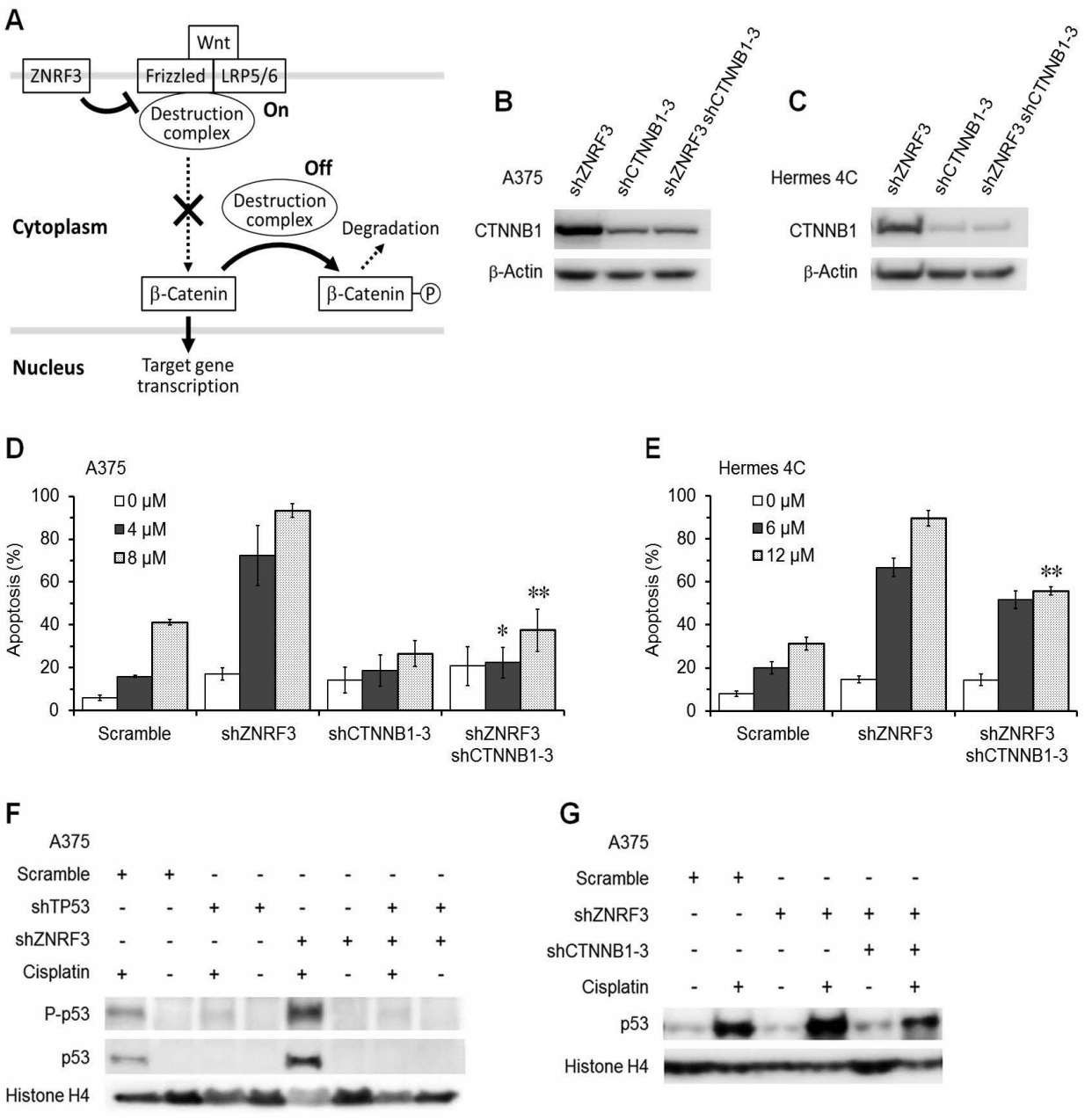

Figure 2.6. ZNRF3 knockdown sensitizes cells to cisplatin via Wnt/β-Catenin signaling. (A) Simplistic schematic of canonical Wnt signaling. (B and C) Western blots showing CTNNB1 (encoding β-Catenin) in A375 (B) and Hermes 4C (C) cells with individual and double knockdowns of ZNRF3 and CTNNB1. (D and E) Cisplatin induced apoptosis of A375 (D) and Hermes 4C (E) cells with the indicated gene knockdowns. Error bars stand for standard errors. Single and double asterisks denote *p* values < 0.05 and < 0.001, respectively (Student's *t*-test). (F and G) Western blots showing total and phosphorylated p53 in A375 cells with the indicated gene knockdowns before and after cisplatin treatment. β-Actin or histone H4 serves as loading control.

2.3.4 Knockdown of NF2 sensitizes A375 melanoma but not normal cells to cisplatin

We noticed that NF2 (also known as Merlin) was ranked 36 among the negatively selected genes by cisplatin in A375 melanoma cells, with a p-value of 0.001 and an FDR (false discovery rate) of 0.6 (Table A2). However, 3 (A_31760, A_31761 and B_31719) out of 6 NF2-targeting sgRNAs were highly negatively selected, although the other 3 sgRNA were not significantly present in the cells (Fig. 2.7A). The assessment of positively or negatively selected genes by using the MAGeCK-VISPR software is affected by the presence and/or cutting efficiency of different sgRNAs present in the GeCKO libraries. If some of the 6 sgRNAs targeting a gene were absent or produced low cutting efficiency, a high p-value or FDR would be assigned to the gene. We therefore tested if NF2 was negatively selected by cisplatin. Indeed, NF2 knockdown sensitized A375 melanoma cells to the drug (Fig. 2.7B and E).

To determine if the implication of NF2 in cisplatin resistance is limited to melanoma, we knocked down this gene in the Hermes 4C melanocytes (Fig. 2.7C) and telomerase immortalized human fibroblast (P1F/TERT) (Fig. 2.7D) cells. In contrast to the A375 melanoma cells (Fig. 2.7E), the Hermes 4C cells (Fig. 2.7F) became slightly more resistant to cisplatin whereas the P1F/TERT cells (Fig. 2.7G) became significantly more resistant to cisplatin. The levels of total or phosphorylated p53 were not significantly affected by NF2 knockdown (Fig. 2.7H), indicating that the modulation of cisplatin sensitivity by NF2 is independent of p53.

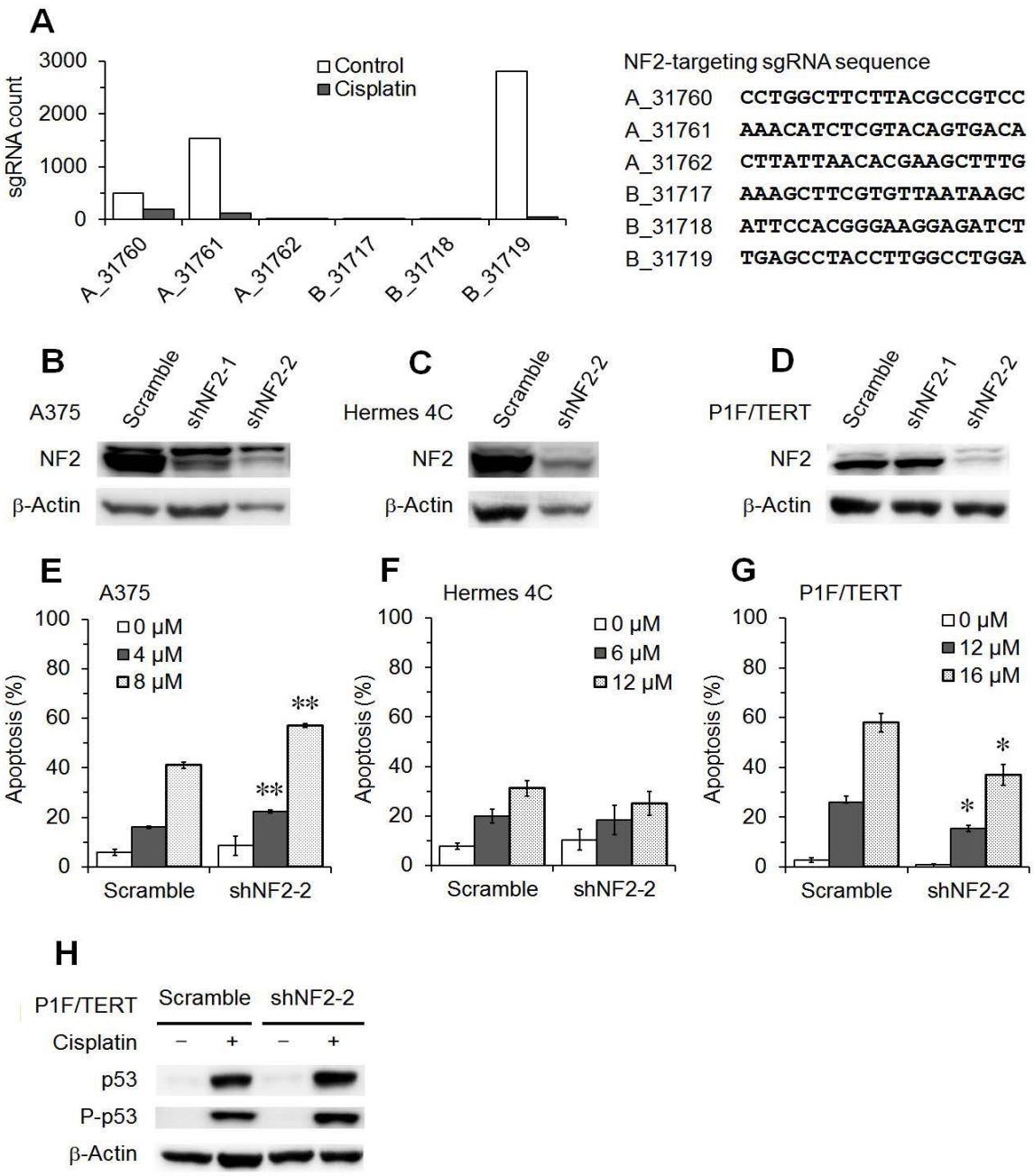

Figure 2.7. NF2 knockdown sensitizes the A375 melanoma cells but not Hermes 4C melanocyte and P1F/TERT fibroblast cells to cisplatin. (A) Counts of the 6 sgRNAs targeting NF2 in the control and cisplatin treated A375 melanoma cells. The sequences of the 6 sgRNAs are shown on the right. (B-D) Western blots showing NF2 knockdown in the A375 (B), Hermes 4C (C) and P1F/TERT (D) cells. (E-G) Cisplatin induced apoptosis of A375 (E), Hermes 4C (F) and P1F/TERT (G) cells with NF2 knockdown. Error bars stand for standard errors. Single and double asterisks denote p values < 0.05 and < 0.001, respectively (Student's t-test). (H) Western blots showing total and phosphorylated p53 in P1F/TERT cells with the indicated gene knockdowns before and after cisplatin treatment. β-Actin serves as loading control.

2.3.5 NF2 and YAP regulate the levels of ARIH1 and EIF4E2

NF2 regulates multiple signaling pathways including the Hippo pathway (Fig 2.8A) (Ehmer and Sage, 2016; Petrilli and Fernandez-Valle, 2016). YAP is a potent transcription coactivator and the main downstream target of the Hippo pathway, acting via binding to the TEAD transcription factor. YAP can be phosphorylated by LATS1/2 and then degraded in the cytoplasm. In certain cell types, NF2 may downregulate YAP by promoting its phosphorylation and degradation. We searched for NF2-regulated factors that might be implicated in cisplatin resistance. We found that EIF4E2, a repressor for translation initiation (Morita et al., 2012), and ARIH1, an E3 ubiquitin ligase that promotes binding of EIF4E2 to the mRNA cap in response to DNA damage (von Stechow et al., 2015), were barely detectable in the Hermes 4C melanocyte and P1F/hTERT fibroblast cells but were highly expressed in A375 melanoma cells (Fig. 2.8B). Upon NF2 knockdown, both EIF4E2 and ARIH1 were upregulated in Hermes 4C and P1F/hTERT cells (Fig. 2.8B). The upregulations were not due to increased transcription as the mRNA levels of ARIH1 and EIF4E2 were not significantly changed upon NF2 knockdown (Fig. 2.8C). In contrast to the normal cells, the A375 melanoma cells showed decreased ARIH1, and unchanged EIF4E2 upon NF2 knockdown (Fig. 2.8B).

The levels of YAP correlated well with those of ARIH1 and EIF4E2, being high in A375 cells and low in Hermes 4C and P1F/TERT cells (Fig. 2.8, compare B and D). However, in contrast to those of ARIH1 and EIF4E2, the level of YAP was not significantly affected by NF2 knockdown (Fig. 2.8D), indicating NF2 does not regulate YAP in these cells. To examine if ARIH1 and EIF4E2 expressions are affected by YAP, we treated the cells with Verteporfin, a highly specific inhibitor of YAP-TEAD interaction (Liu-Chittenden et al., 2012). The levels of

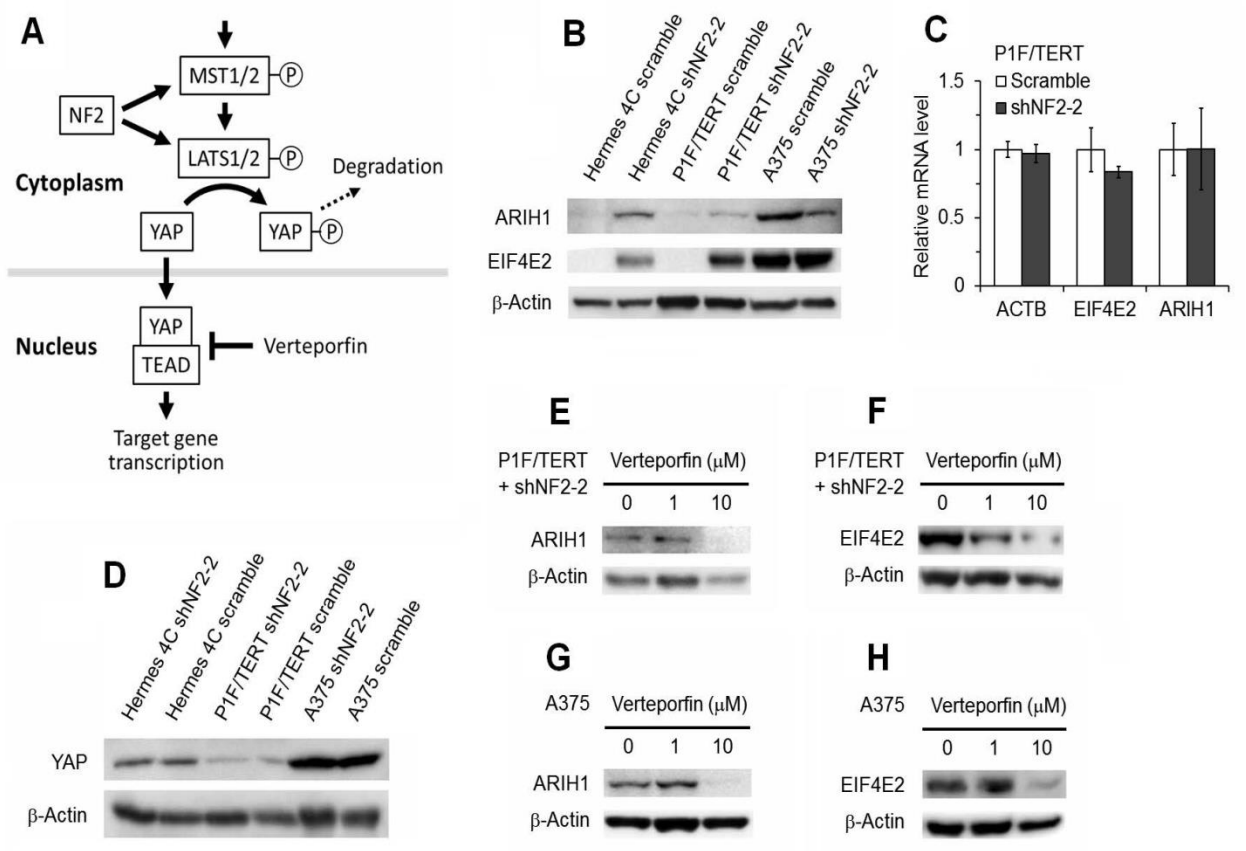

Figure 2.8. Regulation of ARIH1 and EIF4E2 by NF2 and YAP. (A) Simplistic schematic of Hippo signaling**.** (B) Western blots showing levels of ARIH1 and EIF4E2 in the indicated cells with or without NF2 knockdown. (C) Relative levels of the indicated mRNAs in P1F/TERT cells with or without NF2 knockdown. The data were obtained by reverse transcription quantitative PCR. Error bars stand for standard errors. (D) Western blot showing YAP levels in the indicated cells with or without NF2 knockdown. (E-H) Western blots showing ARIH1 and EIF4E2 in the indicated cells following treatment with Verteporfin, the inhibitor of YAP-TEAD interaction. β-Actin serves as loading control.

ARIH1 and EIF4E2 were greatly reduced in P1F/TERT (with NF2 knockdown) (Fig. 2.8E and F) and A375 cells (Fig. 2.8G and H) upon Verteporfin treatment, indicating that YAP upregulates ARIH1 and EIF4E2 in both the normal and melanoma cells.

Taken together, our results indicate that the levels of ARIH1 and EIF4E2 are regulated by both NF2 and YAP. However, the regulation of ARIH1 and EIF4E2 by NF2 is not via regulating YAP. While YAP upregulates ARIH1 and EIF4E2 in all the cells, NF2 regulates these factors differently between the normal and melanoma cells.

2.3.6 ARIH1 but not EIF4E2 is implicated in cisplatin resistance

To determine if upregulation of ARIH1 or EIF4E2 increase cisplatin resistance, we overexpressed these factors in P1F/TERT cells, which normally express very low levels of these factors (Fig. 2.9A). Neither EIF4E2 nor ARIH1 overexpression affected NF2 expression (Fig. 2.9A), indicating that the regulation of EIF4E2 and ARIH1 by NF2 is unidirectional (i.e., no feed-back regulation). Overexpression of ARIH1 but not EIF4E2 dramatically increased cellular resistance to cisplatin (Fig. 2.9B). Similar to NF2 knockdown, ARIH1 or EIF4E2 overexpression did not dramatically affect the levels of total p53 or the phosphorylated p53 (compare Fig. 2.7H and Fig. 2.9C). Collectively, these results indicate that the modulation of cisplatin sensitivity by NF2 may be via regulating ARIH1 and is largely independent of p53.

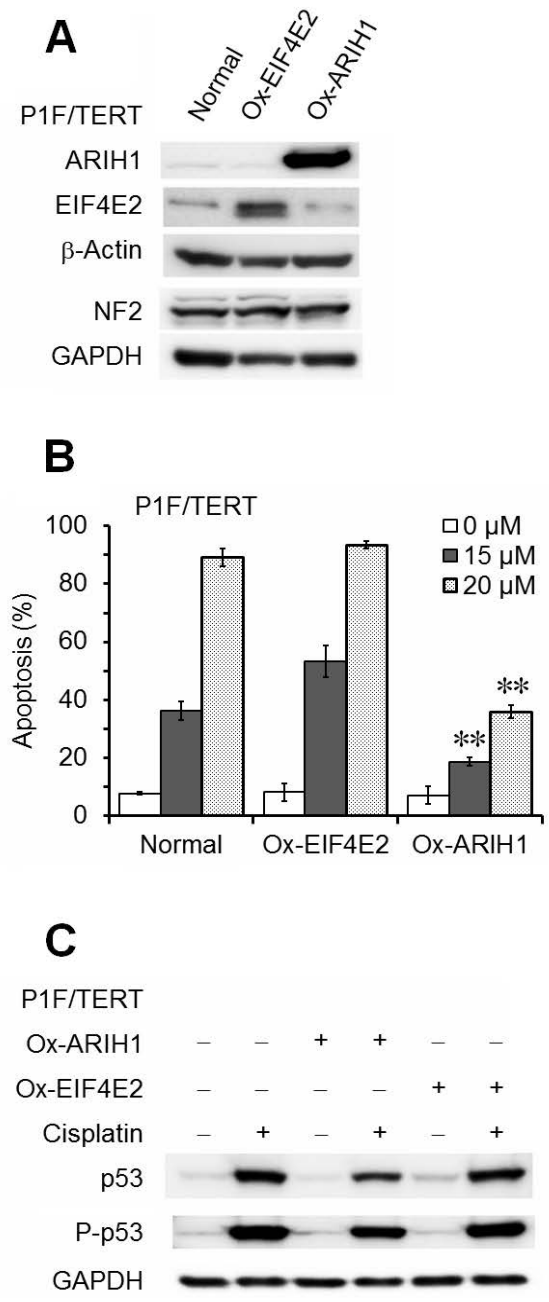

Figure 2.9. Overexpression of ARIH1 but not EIF4E2 causes cisplatin resistance. (A) Western blots showing ARIH1, EIF4E2 and NF2 in P1F/TERT cells normally expressing or overexpressing ARIH1 (Ox-ARIH1) or EIF4E2 (Ox-EIF4E2). (B) Cisplatin induced apoptosis of P1F/TERT cells normally expressing or overexpressing ARIH1 or EIF4E2. Error bars stand for standard errors. Single and double asterisks denote p values < 0.05 and < 0.001, respectively (Student's t-test). (C) Western blots showing total and phosphorylated p53 in P1F/TERT cells with the indicated gene overexpressions before and after cisplatin treatment. GAPDH serves as loading control.

2.4 Discussion

2.4.1 Biological processes responsible for cisplatin sensitivity and resistance

In this study, we screened for genes and biological processes positively and negatively selected by cisplatin when they are disrupted. Among the top positively selected biological processes are protein translation, RNA catabolic processes, and mitochondrial translational elongation and termination, indicating that these processes are normally responsible for cisplatin sensitivity. To the best of our knowledge, these biological processes have not been generally recognized as the leading contributors of cisplatin sensitivity. Protein synthesis consumes a lion's share of energy and cellular resources. When cells are under stress, protein translation is globally repressed except for certain stress proteins (Lasfargues et al., 2012; Liu and Qian, 2014). The so-called translational reprograming may lie at the heart of the stress response and is required for rapid cellular adaptation under stress (Liu and Qian, 2014). Therefore, disruption of genes that are not essential for cell viability but are involved in protein translation may allow the cell to better adapt cisplatin-induced cellular stress. Also, slow-cycling can be a common feature of melanoma cells to be drug resistant (Roesch et al., 2013). Disruption of protein translation may generally slowdown cell cycling, leading to cisplatin resistance. Global mRNA decay has been found in recent years to occur early in apoptosis, preceding membrane lipid scrambling, genomic DNA fragmentation, and apoptotic changes to translation initiation factors (Thomas et al., 2015). Therefore, disruption of RNA catabolism may impair the apoptosis process, leading to cisplatin resistance. Furthermore, mitochondrial dysfunction has been shown to enhance cisplatin resistance (Ma et al., 2015; Wang et al., 2016). Disruption of mitochondrial translational elongation and termination processes may impair mitochondrial function, leading to enhanced cisplatin resistance.

We found that the top negatively selected biological processes by cisplatin are ubiquitin-dependent protein catabolic process, neddylation, and negative regulations of cellular catabolic process and canonical Wnt signaling, indicating that these processes are normally responsible for cisplatin resistance. Neddylation most importantly is modifying the ubiquitin dependent protein degradation process by interacting with and activating cullin like E3 ubiquitin ligases, leading to a higher rate of poly-ubiquitination and subsequent proteasome-dependent degradation (Stintzing and Lenz, 2014). Therefore, neddylation appears to be in the same pathway as ubiquitination responsible for cisplatin resistance. Our findings are in line with the notion that inhibitors of apoptosis proteins (IAP) are E3 ubiquitin ligases regulating caspase activity which is required for apoptosis (Fulda, 2014; Gupta et al., 2018; Stintzing and Lenz, 2014). Also, in contrast to disruption of protein translation, disruption of ubiquitin-dependent protein catabolic process may impair cellular adaptation to stress leading to increased sensitivity to cisplatin.

Alteration of DNA repair pathways, including nucleotide excision repair, mismatch repair and homologous recombination, have been well known to be implicated in cisplatin resistance (Ferreira et al., 2016; Galluzzi et al., 2014). It is reasonable to believe that disruption of these pathways will result in at least a certain level of cisplatin sensitivity, because DNA intra- and inter-strand crosslinks are induced by cisplatin. However, none of these DNA repair pathways is near the top of biological processes negatively selected by cisplatin. This can be explained by the fact that only ~ 1% of intracellular cisplatin forms covalent bonds with nuclear DNA, and the majority of the drug molecules exert their cytotoxicity in the cytoplasm (Galluzzi et al., 2014). Therefore, compared to other biological processes, the DNA repair pathways may only contribute a small fraction to the cisplatin resistance.

2.4.2 ZNRF3 and Wnt/β-Catenin signaling in cisplatin resistance

Mutations ZNFR3, the negative regulator of Wnt signaling, are rare in cancers except for adrenocortical carcinoma (Assie et al., 2014). However, elevated Wnt/β-Catenin signaling is linked to a subset of human cancers including melanoma (Kaur et al., 2016; Xue et al., 2016). Small molecular inhibitors and antibodies of proteins involved in Wnt/β-Catenin signaling are currently in clinical testing (Zhan et al., 2017). However, we found that disruption of ZNRF3 sensitizes both melanoma and melanocyte cells to cisplatin. Our results are in agreement with previous findings that a reduced β-Catenin level in melanoma cell lines may contribute to invasiveness and cisplatin resistance, whereas an increased β-Catenin level may contribute to cellular proliferation and cisplatin sensitivity (Kovacs et al., 2016). Our results are also in line with previous findings that any increase in cytoplasmic concentrations of β-Catenin entails p53 activation (Pomerantz et al., 1998; Saegusa et al., 2004), and activation of Wnt/β-Catenin signaling increases apoptosis in melanoma cells treated with TRAIL (Zimmerman et al., 2013). Therefore, cisplatin and small molecule inhibitors (and antibodies) of the Wnt/β-Catenin signaling may be counterproductive for melanoma treatments. However, the implication of Wnt/β-Catenin signaling in cisplatin sensitivity may be cancer/cell type dependent. Activation of Wnt/β-Catenin signaling has been reported to enhance cisplatin resistance in oral squamous cell carcinoma (Li et al., 2016) and nasopharyngeal carcinoma cells (Liu et al., 2017).

2.4.3 Implications of NF2, YAP and ARIH1 in cisplatin resistance

NF2 is implicated in many signaling pathways including Hippo, EGFR, Ras, Rac, mTOR, FAK-Src, PI3K, and Lin28B (Ehmer and Sage, 2016; Petrilli and Fernandez-Valle, 2016). Mutations of NF2 are associated with nervous system tumors as well as several other malignant cancers including melanomas. To the best of our knowledge, if and/or how NF2 modulates

cisplatin sensitivity has not been documented. NF2 is required for proliferation arrest and apoptosis in developing imaginal discs (Hamaratoglu et al., 2006). Loss of NF2 has been shown to protect cardiac myocytes from apoptosis stimulated by β adrenergic receptor (Dalal et al., 2017), and pancreatic β cells from apoptosis associated with diabetes (Yuan et al., 2016). Therefore, NF2 appears to be a pro-apoptotic factor in normal (noncancer) cells, in line with its role as a tumor suppressor. However, we found that NF2 disruption sensitized the A375 melanoma cells but not normal cells to cisplatin (Fig. 2.7), indicating NF2 becomes an anti-apoptotic factor in the cancer cells. If the anti-apoptotic function of NF2 is common to cancers or limited to a subset of cancers remains to be determined. A better understanding of this issue may be very important for development of treatments that specifically kill cancer cells while minimizing toxicity to normal cells.

Upregulation of YAP, the downstream effector of the Hippo signaling, has been known to cause resistance of multiple types of cancer cells to cisplatin (Huang et al., 2013; Overholtzer et al., 2006; Xia et al., 2016; Zhang et al., 2011). Also, downregulation of MST1/2, the core components of the Hippo pathway that inhibits YAP, has been shown to cause resistance of prostate cancer cells to cisplatin (Ren et al., 2008). Interestingly, we found that the YAP level is not significantly regulated by NF2 in the melanocyte, fibroblast and melanoma cells we tested. The regulation of the Hippo signaling can be tissue specific (Ehmer and Sage, 2016). It is possible that NF2 does not significantly regulate the Hippo signaling in the cell types we tested.

ARIH1 has been shown recently to be widely overexpressed in cancer cells, notably in breast and lung adenocarcinomas, and protect against cisplatin induced cell death by promoting clearance of damaged mitochondria (mitophagy) (Villa et al., 2017). ARIH1 has also been shown to protect against cisplatin induced apoptosis by ubiquitinating EIF4E2 (also called 4EHP),

irrespective of the status of p53 or caspase-3 (von Stechow et al., 2015). The ubiquitinated EIF4E2 promotes translation arrest by competing with EIF4E for binding to the mRNA cap (von Stechow et al., 2015). In agreement with the previous reports, we found that ARIH1 is overexpressed in A375 melanoma cells and contributes to cisplatin resistance in a p53-independent manner. Interestingly, we also found that ARIH1 is regulated by both NF2 and YAP, and the roles of NF2 and YAP in modulating cisplatin resistance are at least partially achieved by regulating ARIH1. Furthermore, we found that the regulation of ARIH1 by NF2 is not at the transcription step and is independent of YAP. The molecular mechanisms as to how NF2 and YAP regulate ARIH1 remains to be elucidated. Insights into the mechanisms may be very informative for development of novel cancer treatment strategies.

2.5 References

Assie, G., Letouze, E., Fassnacht, M., Jouinot, A., Luscap, W., Barreau, O., Omeiri, H., Rodriguez, S., Perlemoine, K., Rene-Corail, F., *et al.* (2014). Integrated genomic characterization of adrenocortical carcinoma. Nat Genet *46*, 607-612.

Berggren, W.T., Lutz, M., and Modesto, V. (2008). General Spinfection Protocol. In StemBook (Cambridge (MA)).

Dalal, S., Connelly, B.A., Singh, M., and Singh, K. (2017). Involvement of NF2 Signaling Pathway in beta-Adrenergic Receptor-Stimulated Cardiac Myocyte Apoptosis. Faseb Journal *31*.
Ehmer, U., and Sage, J. (2016). Control of Proliferation and Cancer Growth by the Hippo Signaling Pathway. Mol Cancer Res *14*, 127-140.

Ferreira, J.A., Peixoto, A., Neves, M., Gaiteiro, C., Reis, C.A., Assaraf, Y.G., and Santos, L.L. (2016). Mechanisms of cisplatin resistance and targeting of cancer stem cells: Adding glycosylation to the equation. Drug Resist Updat *24*, 34-54.

Fulda, S. (2014). Molecular pathways: targeting inhibitor of apoptosis proteins in cancer--from molecular mechanism to therapeutic application. Clin Cancer Res *20*, 289-295.

Galluzzi, L., Vitale, I., Michels, J., Brenner, C., Szabadkai, G., Harel-Bellan, A., Castedo, M., and Kroemer, G. (2014). Systems biology of cisplatin resistance: past, present and future. Cell Death Dis *5*, e1257.

Gray-Schopfer, V.C., Cheong, S.C., Chong, H., Chow, J., Moss, T., Abdel-Malek, Z.A., Marais, R., Wynford-Thomas, D., and Bennett, D.C. (2006). Cellular senescence in naevi and immortalisation in melanoma: a role for p16? Br J Cancer *95*, 496-505.

Gupta, I., Singh, K., Varshney, N.K., and Khan, S. (2018). Delineating Crosstalk Mechanisms of the Ubiquitin Proteasome System That Regulate Apoptosis. Front Cell Dev Biol *6*, 11.

Hamaratoglu, F., Willecke, M., Kango-Singh, M., Nolo, R., Hyun, E., Tao, C.Y., Jafar-Nejad, H., and Halder, G. (2006). The tumour-suppressor genes NF2/Merlin and Expanded act through Hippo signalling to regulate cell proliferation and apoptosis. Nature Cell Biology *8*, 27-U29.

Hao, H.X., Xie, Y., Zhang, Y., Charlat, O., Oster, E., Avello, M., Lei, H., Mickanin, C., Liu, D., Ruffner, H., *et al.* (2012). ZNRF3 promotes Wnt receptor turnover in an R-spondin-sensitive manner. Nature *485*, 195-200.

Huang, D.T., Ayrault, O., Hunt, H.W., Taherbhoy, A.M., Duda, D.M., Scott, D.C., Borg, L.A., Neale, G., Murray, P.J., Roussel, M.F., *et al.* (2009). E2-RING expansion of the NEDD8 cascade confers specificity to cullin modification. Mol Cell *33*, 483-495.

Huang, J.M., Nagatomo, I., Suzuki, E., Mizuno, T., Kumagai, T., Berezov, A., Zhang, H., Karlan, B., Greene, M.I., and Wang, Q. (2013). YAP modifies cancer cell sensitivity to EGFR and survivin inhibitors and is negatively regulated by the non-receptor type protein tyrosine phosphatase 14. Oncogene *32*, 2220-2229.

Jordan, M., Schallhorn, A., and Wurm, F.M. (1996). Transfecting mammalian cells: optimization of critical parameters affecting calcium-phosphate precipitate formation. Nucleic Acids Res *24*, 596-601.

Kaur, A., Webster, M.R., and Weeraratna, A.T. (2016). In the Wnt-er of life: Wnt signalling in melanoma and ageing. Br J Cancer *115*, 1273-1279.

Kovacs, D., Migliano, E., Muscardin, L., Silipo, V., Catricala, C., Picardo, M., and Bellei, B. (2016). The role of Wnt/beta-catenin signaling pathway in melanoma epithelial-to-mesenchymal-like switching: evidences from patients-derived cell lines. Oncotarget *7*, 43295-43314.

Lasfargues, C., Martineau, Y., Bousquet, C., and Pyronnet, S. (2012). Changes in translational control after pro-apoptotic stress. Int J Mol Sci *14*, 177-190.

Li, L., Liu, H.C., Wang, C., Liu, X., Hu, F.C., Xie, N., Lu, L., Chen, X., and Huang, H.Z. (2016). Overexpression of beta-Catenin Induces Cisplatin Resistance in Oral Squamous Cell Carcinoma. Biomed Res Int *2016*, 5378567.

Li, W., Koster, J., Xu, H., Chen, C.H., Xiao, T., Liu, J.S., Brown, M., and Liu, X.S. (2015). Quality control, modeling, and visualization of CRISPR screens with MAGeCK-VISPR. Genome Biol *16*, 281.

Li, W., Xu, H., Xiao, T., Cong, L., Love, M.I., Zhang, F., Irizarry, R.A., Liu, J.S., Brown, M., and Liu, X.S. (2014). MAGeCK enables robust identification of essential genes from genome-scale CRISPR/Cas9 knockout screens. Genome Biol *15*, 554.

Liu-Chittenden, Y., Huang, B., Shim, J.S., Chen, Q., Lee, S.J., Anders, R.A., Liu, J.O., and Pan, D.J. (2012). Genetic and pharmacological disruption of the TEAD-YAP complex suppresses the oncogenic activity of YAP. Genes & Development *26*, 1300-1305.

Liu, B., and Qian, S.B. (2014). Translational reprogramming in cellular stress response. Wiley Interdiscip Rev RNA *5*, 301-315.

Liu, S.L., Lin, H.X., Lin, C.Y., Sun, X.Q., Ye, L.P., Qiu, F., Wen, W., Hua, X., Wu, X.Q., Li, J., *et al.* (2017). TIMELESS confers cisplatin resistance in nasopharyngeal carcinoma by activating the Wnt/beta-catenin signaling pathway and promoting the epithelial mesenchymal transition. Cancer Letters *402*, 117-130.

Ma, L.J., Wang, R.X., Duan, H.T., Nan, Y.D., Wang, Q.W., and Jin, F.G. (2015). Mitochondrial dysfunction rather than mtDNA sequence mutation is responsible for the multi-drug resistance of small cell lung cancer. Oncology Reports *34*, 3238-3246.

Mattia, G., Puglisi, R., Ascione, B., Malorni, W., Care, A., and Matarrese, P. (2018). Cell death-based treatments of melanoma:conventional treatments and new therapeutic strategies. Cell Death Dis *9*, 112.

Morita, M., Ler, L.W., Fabian, M.R., Siddiqui, N., Mullin, M., Henderson, V.C., Alain, T., Fonseca, B.D., Karashchuk, G., Bennett, C.F., *et al.* (2012). A Novel 4EHP-GIGYF2 Translational Repressor Complex Is Essential for Mammalian Development. Molecular and Cellular Biology *32*, 3585-3593.

Overholtzer, M., Zhang, J., Smolen, G.A., Muir, B., Li, W., Sgroi, D.C., Deng, C.X., Brugge, J.S., and Haber, D.A. (2006). Transforming properties of YAP, a candidate oncogene on the chromosome 11q22 amplicon. Proc Natl Acad Sci U S A *103*, 12405-12410.

Petrilli, A.M., and Fernandez-Valle, C. (2016). Role of Merlin/NF2 inactivation in tumor biology. Oncogene *35*, 537-548.

Pomerantz, J., Schreiber-Agus, N., Liegeois, N.J., Silverman, A., Alland, L., Chin, L., Potes, J., Chen, K., Orlow, I., Lee, H.W., *et al.* (1998). The Ink4a tumor suppressor gene product, p19Arf, interacts with MDM2 and neutralizes MDM2's inhibition of p53. Cell *92*, 713-723.

Ren, A., Yan, G., You, B., and Sun, J. (2008). Down-regulation of mammalian sterile 20-like kinase 1 by heat shock protein 70 mediates cisplatin resistance in prostate cancer cells. Cancer Res *68*, 2266-2274.

Roesch, A., Vultur, A., Bogeski, I., Wang, H., Zimmermann, K.M., Speicher, D., Korbel, C., Laschke, M.W., Gimotty, P.A., Philipp, S.E., *et al.* (2013). Overcoming Intrinsic Multidrug

Resistance in Melanoma by Blocking the Mitochondrial Respiratory Chain of Slow-Cycling JARID1B(high) Cells. Cancer Cell *23*, 811-825.

Saegusa, M., Hashimura, M., Kuwata, T., Hamano, M., and Okayasu, I. (2004). Beta-catenin simultaneously induces activation of the p53-p21WAF1 pathway and overexpression of cyclin D1 during squamous differentiation of endometrial carcinoma cells. Am J Pathol *164*, 1739-1749.

Sanjana, N.E., Shalem, O., and Zhang, F. (2014). Improved vectors and genome-wide libraries for CRISPR screening. Nat Methods *11*, 783-784.

Scott, M.C., Wakamatsu, K., Ito, S., Kadekaro, A.L., Kobayashi, N., Groden, J., Kavanagh, R., Takakuwa, T., Virador, V., Hearing, V.J., *et al.* (2002). Human melanocortin 1 receptor variants, receptor function and melanocyte response to UV radiation. J Cell Sci *115*, 2349-2355.

Stintzing, S., and Lenz, H.J. (2014). Molecular Pathways: Turning Proteasomal Protein Degradation into a Unique Treatment Approach. Clinical Cancer Research *20*, 3064-3070.

Thomas, M.P., Liu, X., Whangbo, J., McCrossan, G., Sanborn, K.B., Basar, E., Walch, M., and Lieberman, J. (2015). Apoptosis Triggers Specific, Rapid, and Global mRNA Decay with 3' Uridylated Intermediates Degraded by DIS3L2. Cell Rep *11*, 1079-1089.

Villa, E., Proics, E., Rubio-Patino, C., Obba, S., Zunino, B., Bossowski, J.P., Rozier, R.M., Chiche, J., Mondragon, L., Riley, J.S., *et al.* (2017). Parkin-Independent Mitophagy Controls Chemotherapeutic Response in Cancer Cells. Cell Rep *20*, 2846-2859.

von Stechow, L., Typas, D., Carreras Puigvert, J., Oort, L., Siddappa, R., Pines, A., Vrieling, H., van de Water, B., Mullenders, L.H., and Danen, E.H. (2015). The E3 ubiquitin ligase ARIH1 protects against genotoxic stress by initiating a 4EHP-mediated mRNA translation arrest. Mol Cell Biol *35*, 1254-1268.

Wang, S.F., Chen, M.S., Chou, Y.C., Ueng, Y.F., Yin, P.H., Yeh, T.S., and Lee, H.C. (2016). Mitochondrial dysfunction enhances cisplatin resistance in human gastric cancer cells via the ROS-activated GCN2-eIF2 alpha-ATF4-xCT pathway. Oncotarget *7*, 74132-74151.

Winter, C., and Albers, P. (2011). Testicular germ cell tumors: pathogenesis, diagnosis and treatment. Nat Rev Endocrinol *7*, 43-53.

Xia, Y., Chang, T., Wang, Y.M., Liu, Y.X., Li, W.H., Li, M., and Fan, H.Y. (2016). YAP Promotes Ovarian Cancer Cell Tumorigenesis and Is Indicative of a Poor Prognosis for Ovarian Cancer Patients (vol 9, e91770, 2014). Plos One *11*.

Xue, G.D., Romano, E., Massi, D., and Mandala, M. (2016). Wnt/beta-catenin signaling in melanoma: Preclinical rationale and novel therapeutic insights. Cancer Treatment Reviews *49*, 1-12.

Yuan, T., Gorrepati, K.D., Maedler, K., and Ardestani, A. (2016). Loss of Merlin/NF2 protects pancreatic beta-cells from apoptosis by inhibiting LATS2. Cell Death Dis *7*, e2107.

Zhan, T., Rindtorff, N., and Boutros, M. (2017). Wnt signaling in cancer. Oncogene *36*, 1461-1473.

Zhang, X., George, J., Deb, S., Degoutin, J.L., Takano, E.A., Fox, S.B., Bowtell, D.D.L., Harvey, K.F., and Grp, A.S. (2011). The Hippo pathway transcriptional co-activator, YAP, is an ovarian cancer oncogene. Oncogene *30*, 2810-2822.

Zimmerman, Z.F., Kulikauskas, R.M., Bomsztyk, K., Moon, R.T., and Chien, A.J. (2013). Activation of Wnt/beta-catenin signaling increases apoptosis in melanoma cells treated with trail. PLoS One *8*, e69593.

CHAPTER 3
GENOME-WIDE SCREEN IDENTIFIES NOVEL GENES IMPLICATED IN TUMORIGENESIS

3.1 Introduction

Oncogene-induced senescence (OIS) and apoptosis (OIA) are powerful anti-proliferative mechanisms that trigger stable proliferation arrest and programmed cell death under oncogenic stress (Childs et al., 2014). Since cancer cells proliferate uncontrollably, it is reasonable to believe that, in addition to oncogenic mutations, other mutations have been developed to facilitate the escape of anti-proliferative responses and tumorigenesis. For the past two decades, pathways involved in the bypass of OIS have been extensively studied (Bellelli et al., 2018; Gitenay et al., 2014; Kim et al., 2017; Liu et al., 2018; Patel et al., 2016). However, the evasion of OIA is less investigated.

Oncogenic stress can induce intrinsic apoptotic pathway through activating tumor suppressor p53 and pro-apoptotic factors (Aubrey et al., 2018; Kotsantis et al., 2018). Cancer cells may evade apoptosis response via 1) upregulating anti-apoptotic Bcl-2 members, 2) inactivating pro-apoptotic effectors, 3) disrupting p53, and 4) inhibiting cell death protease caspase (Lopez and Tait, 2015). Nevertheless, most of these findings were discovered in advanced stage cancer cells; factors that contribute to the early stage of cancer development are still largely unknown.

Proto-oncogene BRAF is mutated in about 50% of melanoma and 90% of these mutations contain substitution of valine to glutamic acid at codon 600 (V600E), granting a gain-of-function phenotype (Cheng et al., 2018). BrafV600E results in constitutive activation of

MEK-ERK pathway, which is believed to contribute to the constant proliferation of melanoma (Wang and Qi, 2013). In primary human melanocytes, BrafV600E expression preferentially leads to senescence instead of apoptosis (Bansal and Nikiforov, 2010). Intriguingly, recent studies have demonstrated that apoptosis can replace senescence program in senescence-deficient animals (Munoz-Espin et al., 2013; Storer et al., 2013), indicating that apoptosis and senescence programs are simultaneously engaged in stress response. Therefore, uncovering factors that contribute to OIA evasion will provide a more comprehensive understanding on tumorigenesis.

Here, by utilizing genome-wide CRISPR/Cas9 gene knockout system and senescence-deficient human melanocyte, we identified 20 candidates that facilitated the evasion of BrafV600E-induced apoptosis. To increase the confidence level, we also performed a genome-wide screening on telomere immortalized human fibroblasts, and identified 9 candidates that agree with the result of melanocyte. Notably, one of the most significant and exclusive candidates of melanocyte, DBT, plays a central role in altering the apoptosis threshold through regulating both AKT- and p14ARF-mediated p53 pathways. Together, our findings reveal a new insight on the early stage of melanomagenesis.

3.2 Materials and Methods

3.2.1 Cell Lines

Human Hermes 4C melanocytes (H4C) expressing human telomerase (hTERT) and HPV16-E7 were obtained from Wellcome Trust Functional Genomics Cell Bank and cultured in RPMI1640-GlutaMax medium supplemented with 10% newborn calf serum, 10 ng/ml human stem cell factor, 200nM Phorbol 12-myristate 13-acetate, 200pM Cholera Toxin, and 10nM Endothelin 1. hTERT immortalized human fibroblast (P1F/hTERT) was purchased from

Rheinwalk Lab of Harvard Skin Disease Research Center and cultured in DMEM/F12 medium supplemented with 15% newborn calf serum and 10 ng/ml of epidermal growth factor.

3.2.2 pLenti-BrafV600E-EGFP Plasmid and GeCKO Library Preparation

Plasmid pLenti-BrafV600E-EGFP was created using LentiCRISPR v2 plasmid (Addgene, #52961). First, puromycin selection marker was replaced with EGFP gene from pmaxGFP plasmid (Lonza). Next, the stuffer sequence was replaced by a 19 nucleotide long non-targeting sequence (sgNTS-1 & -2). Finally, Cas9 gene was replaced with BrafV600E cDNA sequence from pBABE-Puro-BRAF-V600E plasmid (Addgene, #15269). Genome-scale CRISPR Knockout-Out GeCKO libraries (Addgene, #1000000048) were transformed into Endura electrocompetent *E. coli* cells (Lucigen, #60242) and cultured in LB medium overnight. Plasmids were extracted and purified using EndoFree Plasmid Maxi Kit (Qiagen, #12362).

3.2.3 Lentivirus Packaging and Transduction

To package lentivirus, GeCKO libraries, pCMV-VSV-G (Addgene, #8454), and psPAX2 (Addgene, #12260) were co-transfected into HEK293T (Clontech, #632180) using calcium phosphate co-precipitation method. Lentivirus particles were harvested 48 hours after the transfection and concentrated by using ultracentrifugation at 24,000 RPM for 2 hours at 4°C. Ten million P1F/hTERT cells were transduced with lentivirus using Spinfection method (2,000RPM, 2 hours, room temperature) in medium containing 8 μg/ml polybrene. Puromycin selection began at 1 μg/ml two days after transduction. The transduction efficiency was determined to be ~80% by comparing the cell confluence between puromycin-treated and untreated groups when untransduced P1F/hTERT cells were completely killed off by puromycin. The same amount of lentivirus was used to transduce H4C cells. To determine the efficiency of

lenti-BrafV600E-EGFP transduction, flow cytometry analysis was used 4 days after transduction (Fig. 3.2A and E).

3.2.4 GeCKO and BrafV600E Screening

One week after transduction with GeCKO library, cells were pooled together and one half of the total population was stored as early transduction (ETr). This is used to determine sgRNA distribution and coverage. The other half was transduced with lenti-BrafV600E-EGFP. Green fluorescent cells were enriched by using fluorescent-activated cell sorting (FACS). When cells had grown to confluence, BrafV600E-GFP-positive cells (Braf) were enriched again by FACS followed by genomic DNA isolation.

3.2.5 Next-Generation Sequencing of GeCKO sgRNAs

Genomic DNA (gDNA) was isolated using Blood & Cell culture DNA midi Kit (Qiagen, #13343). A total of 130 μg of gDNA from ETr sample and 1 μg of gDNA from Braf sample were used to build the NGS library. sgRNA sequences were amplified by PCR (1-10 μg/reaction; 24 cycles), using Lenti-F1 and Lenti-R1 primers (Table 3.1) and Herculase II Fusion DNA polymerase (Agilent, #600675). PCR products of 400-600 bp in the same group were combined and gel purified. Illumina sequencing adapters were attached to the purified DNA fragments by 21 cycles of PCR using GECKO-1/GECKO-2 primers (Table 3-1). Finally, index sequences, were attached to the fragments by 6 cycles of PCR using Tru-U and Tru-B1/2/3/4 primers (Table 3.1). Next-generation sequencing was carried out on an Illumina Hi-Seq 2000 platform and the data was analyzed using MAGeCK-VISPR (Li et al., 2015).

3.2.6 Creating Indel Profiles for crGPR4-BrafV600E and crDBT-BrafV600E Cells

For obtaining the insertion/deletion (indel) sequences of GPR4 and DBT knockout cells

that have escaped BrafV600E-induced apoptosis, one hundred thousand H4C cells were first transduced with modified lentiCRISPRv2 (mCherry) (replacing purmycin with mcherry) with transduction efficiency of >80%. sgRNA sequences for GPR4 (GPR4-sgRNA-A & -B) and for DBT (DBT-sgRNA-A & -B) were listed in Table 3.1. One week after transduction, cells were transduced with lenti-BrafV600E-EGFP resulting 70~80% transduction efficiency. Thirty days after BrafV600E transduction, GFP-positive cells were enriched by FACS. Four weeks later, GFP-positive cells were sorted followed by deposition of single cell into 96-well plates by FACS. 250bp up- and down-stream of Cas9 cutting sites were amplified by PCR (31 cycles) using Herculase II and appropriate primers (DBT-F2 / DBT-R2 and GPR4-F2 / GPR4-R2) (Table 3.1). Illumina adapter sequences were attached to fragments by 35 cycles of PCR using DBT-Tru-U / DBT-Tru-Seq and GPR4-Tru-U / GPR4-Tru-Seq (Table 3.1). Lastly, index sequences were attached PCR product by 20 cycles using 8 different Tru-U primers (Tru-U1~8; Table 3.1) and 12 different Tru-B primers (Tru-B1~12; Table 3-1), resulting 96 different combinations. Pair-end sequencing was carried out on Illumina Miseq platform.

Table 3.1. Primers for Genome Screening and for creating indel profiles

Primer	Sequences
DBT-sgRNA-A	CACCGTCCATCATAACGACTAGTGA
DBT-sgRNA-B	AAACTCACTAGTCGTTATGATGGAC
GPR4-sgRNA-A	CACCGCGCCGATGACAAAGATGTAG
GPR4-sgRNA-B	AAACCTACATCTTTGTCATCGGCGC
sgNTS-1	AAACCCACGCCTGTTTGCCAGTTC
sgNTS-2	CACCGAACTGGCAAACAGGCGTGG
Lenti-F1	ATGGACTATCATATGCTTACCGTAACTTGAAAGTATTTCG
Lenti-R1	ACTTCTTGTCCATGGTGGCAGC
GeCKO-1	ACACGACGCTCTTCCGATCTTCTTGTGGAAAGGACGAAACACCG
GeCKO-2	AGACGTGTGCTCTTCCGATCTACTTCTTGTCCATGGTGGCAGC
DBT-F2	GAAGAAAGACTGGGAGAACTCCCATC
DBT-R2	CCTTTTCAATTTTCCTGATTTCGGCTTC

(Table Continued)

Primer	Sequences
GPR4-F2	GCTACACATACTTCCTAATTGCCCTGC
GPR4-R2	GGTACGACAGCAGCATGAGC
DBT-Tru-U	ACACGACGCTCTTCCGATCTGTACACCATCTGAAAGTAAATGCTGGG
DBT-Tru-Seq	AGACGTGTGCTCTTCCGATCTACGTTGAAAAGATTACATTTCCTCAAGAGC
GPR4-Tru-U	ACACGACGCTCTTCCGATCTTCTCTTCCCTGTAGACCACATCCC
GPR4-Tru-Seq	AGACGTGTGCTCTTCCGATCTCTGATGTAGATATTGGTGTAGAAGATGAACCC
Tru-U	AATGATACGGCGACCACCGAGATCTACACTCTTTCCCTACACGACGCTCTTCCGATCT
Tru-U1	AATGATACGGCGACCACCGAGATCTACACCTCTCTATACACTCTTTCCCTACACGACGCTCTTCCGATCT
Tru-U2	AATGATACGGCGACCACCGAGATCTACACTATCCTCTACACTCTTTCCCTACACGACGCTCTTCCGATCT
Tru-U3	AATGATACGGCGACCACCGAGATCTACACGTAAGGAGACACTCTTTCCCTACACGACGCTCTTCCGATCT
Tru-U4	AATGATACGGCGACCACCGAGATCTACACACTGCATAACACTCTTTCCCTACACGACGCTCTTCCGATCT
Tru-U5	AATGATACGGCGACCACCGAGATCTACACAAGGAGTAACACTCTTTCCCTACACGACGCTCTTCCGATCT
Tru-U6	AATGATACGGCGACCACCGAGATCTACACCTAAGCCTACACTCTTTCCCTACACGACGCTCTTCCGATCT
Tru-U7	AATGATACGGCGACCACCGAGATCTACACCGTCTAATACACTCTTTCCCTACACGACGCTCTTCCGATCT
Tru-U8	AATGATACGGCGACCACCGAGATCTACACTCTCTCCGACACTCTTTCCCTACACGACGCTCTTCCGATCT
Tru-B1	CAAGCAGAAGACGGCATACGAGATCGTGATGTGACTGGAGTTCAGACGTGTGCTCTTCCGATCT
Tru-B2	CAAGCAGAAGACGGCATACGAGATACATCGGTGACTGGAGTTCAGACGTGTGCTCTTCCGATCT
Tru-B3	CAAGCAGAAGACGGCATACGAGATGCCTAAGTGACTGGAGTTCAGACGTGTGCTCTTCCGATCT
Tru-B4	CAAGCAGAAGACGGCATACGAGATTGGTCAGTGACTGGAGTTCAGACGTGTGCTCTTCCGATCT
Tru-B5	CAAGCAGAAGACGGCATACGAGATCACTGTGTGACTGGAGTTCAGACGTGTGCTCTTCCGATCT
Tru-B6	CAAGCAGAAGACGGCATACGAGATATTGGCGTGACTGGAGTTCAGACGTGTGCTCTTCCGATCT
Tru-B7	CAAGCAGAAGACGGCATACGAGATGATCTGGTGACTGGAGTTCAGACGTGTGCTCTTCCGATCT
Tru-B8	CAAGCAGAAGACGGCATACGAGATTCAAGTGTGACTGGAGTTCAGACGTGTGCTCTTCCGATCT

(Table Continued)

Primer	Sequences
Tru-B9	CAAGCAGAAGACGGCATACGAGATCTGATCGTGACTGGAGTTCAGACGTGTGCTCTTCCGATCT
Tru-B10	CAAGCAGAAGACGGCATACGAGATAAGCTAGTGACTGGAGTTCAGACGTGTGCTCTTCCGATCT
Tru-B11	CAAGCAGAAGACGGCATACGAGATGTAGCCGTGACTGGAGTTCAGACGTGTGCTCTTCCGATCT
Tru-B12	CAAGCAGAAGACGGCATACGAGATTACAAGGTGACTGGAGTTCAGACGTGTGCTCTTCCGATCT

3.2.7 Creating DBT Knockout Hermes 4C melanocyte

DBT knockout H4C was created by using the lentiCRISPRv2 (mCherry) vector. Two-week after transduction, single cells were deposited into each well of two 96-well plates containing conditional medium by using FACS. 10 days after deposition, wells containing single cell colony were detached and re-seeded. When confluent, gDNA from each single cell clones was extracted for examining indel sequences using the same method and primers described in the previous selection.

3.2.8 Creating DBT Complemented Cells in DBT Knockout cells

To restore DBT function in DBT knockout cells, we first created a lentiviral vector by replacing CRISPR/Cas9 and puromycin cassette with DBT cDNA (Dharmacon, MGC3924492) and blasticidin resistance marker. To prevent the stably expressed Cas9 from cutting the cDNA in the knockout cells, 3 silent mutations were created at the PAM and subsequent codons. DBT knockout cells were transduced with lentivirus carrying DBT cDNA and blasticidin resistance gene and complemented cells were selected by Blasticidin (10 μg/ml) for 14 days.

3.2.9 Beta-Galactosidase Assay

One hundred thousand H4C cells were transduced with lenti-BrafV600E-EGFP with

~90% transduction efficiency. Nine days after transduction, transduced and untransduced cells were stained with ß-Galactosidase Staining Kit (Cell Signaling Technology, #9860) following the manufacture's instruction.

3.2.10 Apoptosis Assay

One hundred thousand wild-type, DBT knockout, DBT complemented H4C cells were transduced with lenti-BrafV600E-EGFP with >75% transduction efficiency. The same amount of lenti-BrafV600E (without GFP) virus was used to transduce WT, DBT knockout, and DBT complemented knockout cells. On day 3, day 6, and day 8 after transduction, the percentage of apoptotic cells was assessed in triplicate by using Annexin V staining (Thermo Sci, #A13201) and flow-cytometry analysis.

3.2.11 Western Blot

Cells (~$0.8x10^6$) were washed with PBS, scraped off, and pelleted. The cells were lysed by vortexing in 100 µl of phenol, 5 µl of β-mercaptoethanol and 100uL of PBS for 15min. Proteins were precipitated by mixing with 1.2 ml methanol containing 0.1M ammonium acetate followed by centrifugation. Proteins were separated on SDS-PAGE gels, transferred onto PVDF membranes, blocked by 5% skimmed milk, and probed with antibodies against p53 (SCBT, sc-126), AKT1 (SCBT, sc-55523), p14ARF (SCBT, sc-53639), GAPDH (SCBT, sc-47724), β-Actin (SCBT, sc-47778), and phosphorylated p53 (Cell Signaling, #9284). Membranes were washed with TBST (3X) followed by incubation with appropriate secondary antibodies in 5% skimmed milk for 2 hours at room temperature.

3.3 Results

3.3.1 RB inhibition enhances OIA in human immortalized melanocyte

It is well known that constitutive activation of BrafV600E could drive primary melanocytes to OIS via p16 and p53 pathways (Cisowski et al., 2016; van Deursen, 2014; Vredeveld et al., 2012). These two pathways ultimately converge to activate RB, which inhibits E2F transcription factor and arrests the cell at G1 phase of the cell cycle (McHugh and Gil, 2018; van Deursen, 2014). Therefore, to test whether melanocyte with senescence deficiency could undergo BrafV600E-induced apoptosis, we transduced RB-inhibited human immortalized melanocyte Hermes 4C (H4C) with lentivirus containing BrafV600E. As a result, apoptosis assay showed a constant increase in total number of apoptotic cells over the course of 8 days (Fig. 3.1B and C). Morphologically, a large portion of BrafV600E expressing cells, estimated by GFP signal (Fig. 3.1A and G), exhibited apoptosis phenotypes (round and floating cells) rather than senescence phenotypes (flatten and enlarged cells) (Joselow et al., 2017) 5 days after transduction (Fig. 3.1D-G). Senescence-associated β-galactosidase staining further confirmed that only a small portion of BrafV600E expressing cells went to senescence (Fig. 3.1H and I). This suggests that BrafV600E-induced apoptosis is significantly enhanced in the absence of functional RB.

3.3.2 Genome-wide CRISPR/Cas9 knockout screening identifies novel genes implicated in BrafV600E-induced apoptosis and senescence

To identify genes that facilitated the bypass of OIA, we performed a genome-wide loss-of-function screening by using lentivirus based GeCKO libraries, targeting ~99% of human genes (Sanjana et al., 2014). To increase the confidence level, we also included another cell line,

P1F/hTERT human fibroblast, in the screening. After gene editing events had occurred, we stably expressed BrafV600E-GFP cassette and enriched the transduced cells by using

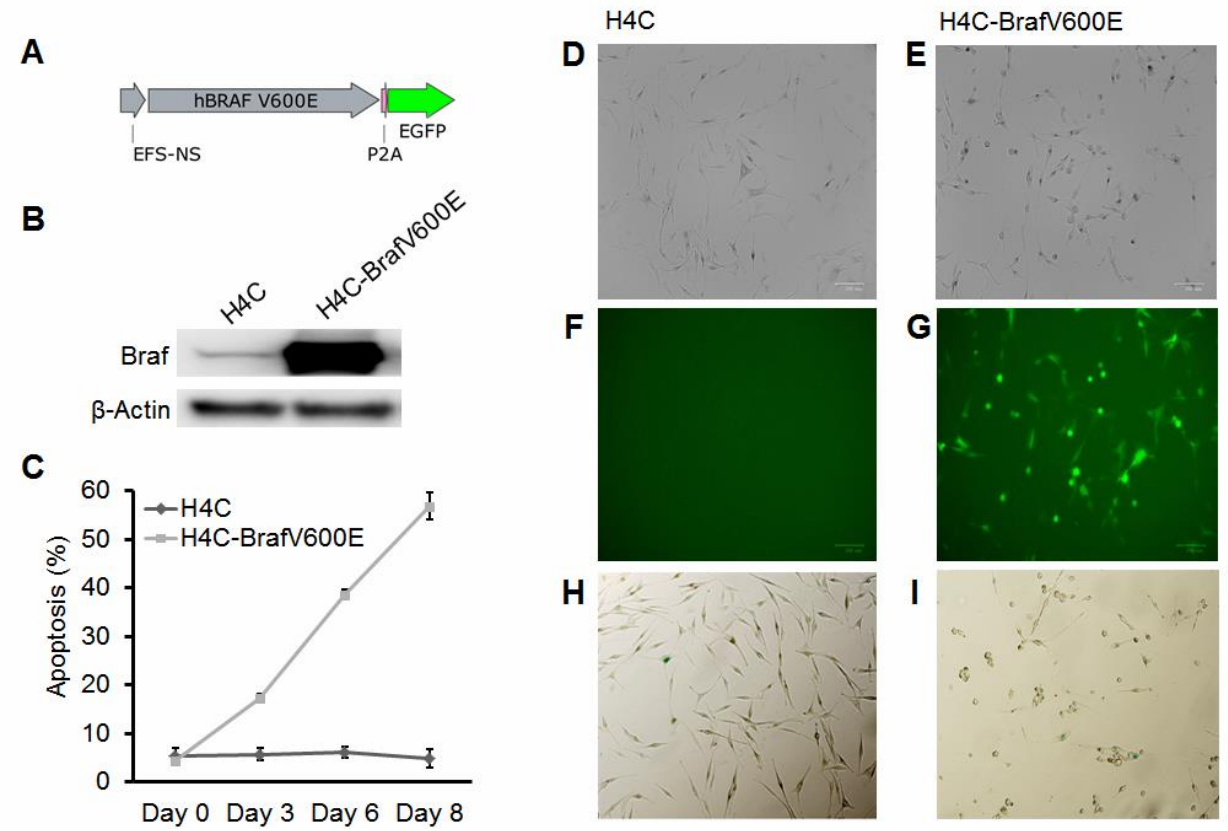

Figure 3.1.RB disruption enhances apoptosis response to BrafV600E expression. (A) BrafV600E-EGFP expression cassette. (B) Total Braf expression of H4C melanocytes with and without BrafV600E-EGFP transduction. (C) Apoptosis analysis of BrafV600E transduced H4C cells vs. no transduction control. Images of untransduced and BrafV600E transduced H4C melanocytes (D-E) in bright field. (F-G) under fluorescence microscope. (H-I) stained by senescence-associated β-galactosidase reagent, where cells that show blue color represent senescent cells.

fluorescent-activated cell sorting (FACS) (Fig. 3.2A and B). As expected, untransduced cells eventually out-populated BrafV600E expressing cells in the same pool due to oncogenic pressure (Fig. 3.2C and F). To enrich the GFP population, we performed another round of FACS. After weeks of culturing, we observed the growth of GFP cells (Fig. 3.2G), suggesting that some cells had survived the oncogenic selection. However, these surviving cells seem to contain lower

proliferative capacity comparing to the untransduced cells based on the fact that FACS typically yielded >80% GFP population but untransduced cells eventually out-numbered GFP cells after weeks of culturing. Finally, we performed one more FACS (Fig. 3.2D and H) followed by genomic DNA isolation of the sorted GFP cells (Braf) and the Etr cells. The sgRNAs integrated into the genome were sequenced and analyzed by using MAGeCK-VISPR to assess the positively selected genes (Li et al., 2015).

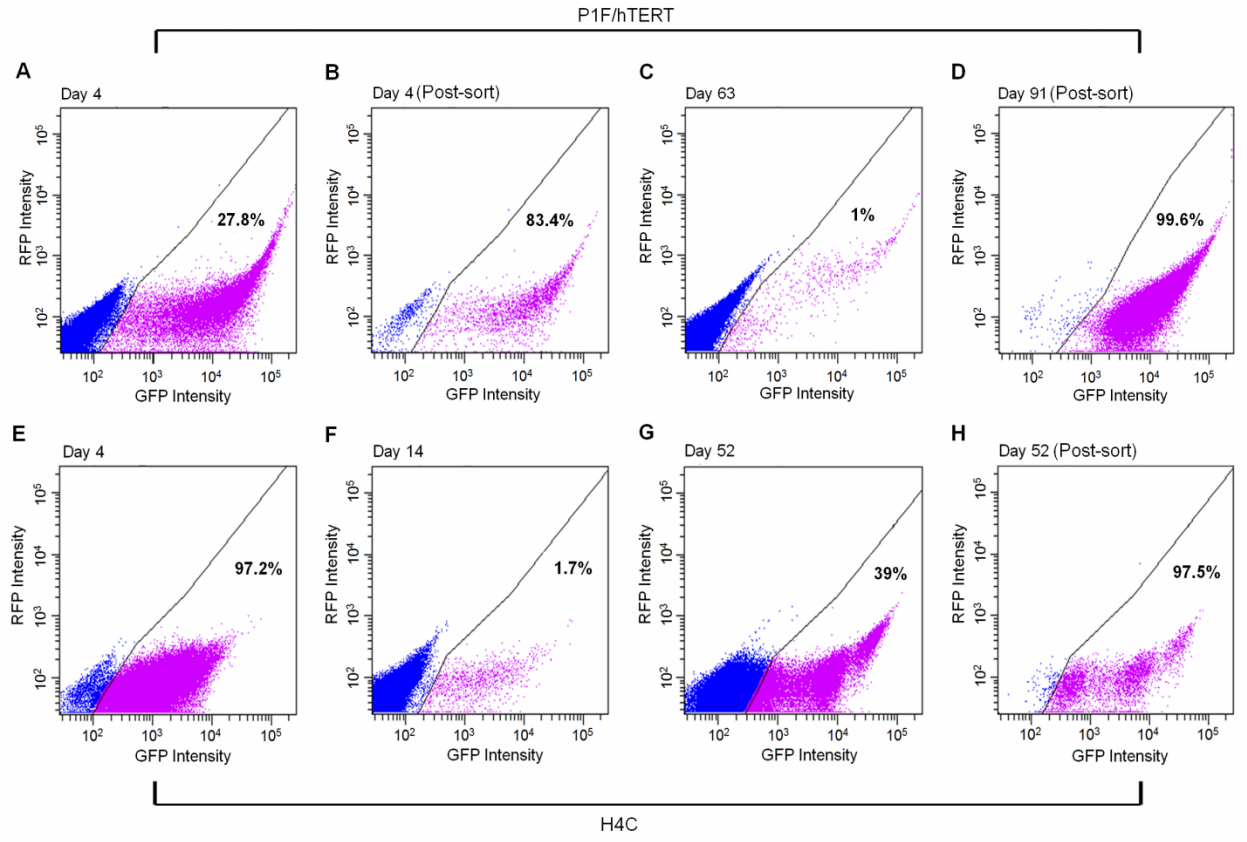

Figure 3.2. Flow-cytometry analysis of P1F/hTERT fibroblasts and H4C melanocytes expressing BrafV600E-EGFP cassette. (A) Percentage of GFP population of P1F/hTERT on Day 4. (B) Percentage of GFP population of P1F/hTERT after FACS. (C) Percentage of GFP population of P1F/hTERT on Day 63. (D) Percentage of GFP population of P1F/hTERT on Day 91 after FACS. (E) Percentage of GFP population of H4C on Day 4. (F) Percentage of GFP population of H4C on Day 14. (G) Percentage of GFP population of H4C on Day 52. (H) Percentage of GFP population of H4C on Day 52 after FACS.

The library contains mostly high quality sequencing reads (Fig. 3.3A). Over 3 million (≥70%) reads from each ETr group and about half million (≥79%) reads from each Braf group were mapped to the reference sgRNA sequences (Fig. 3.3B). ETr groups contain fairly good distribution and coverage while most sgRNAs in the Braf groups were lost due to oncogenic selection (Fig. 3.3C and D). Based on the degree of fold change and statistical significance, we identified a total of 54 and 20 candidates that are critical for bypassing oncogenic responses in human fibroblasts (Table A3) and melanocytes (Table A4), respectively.

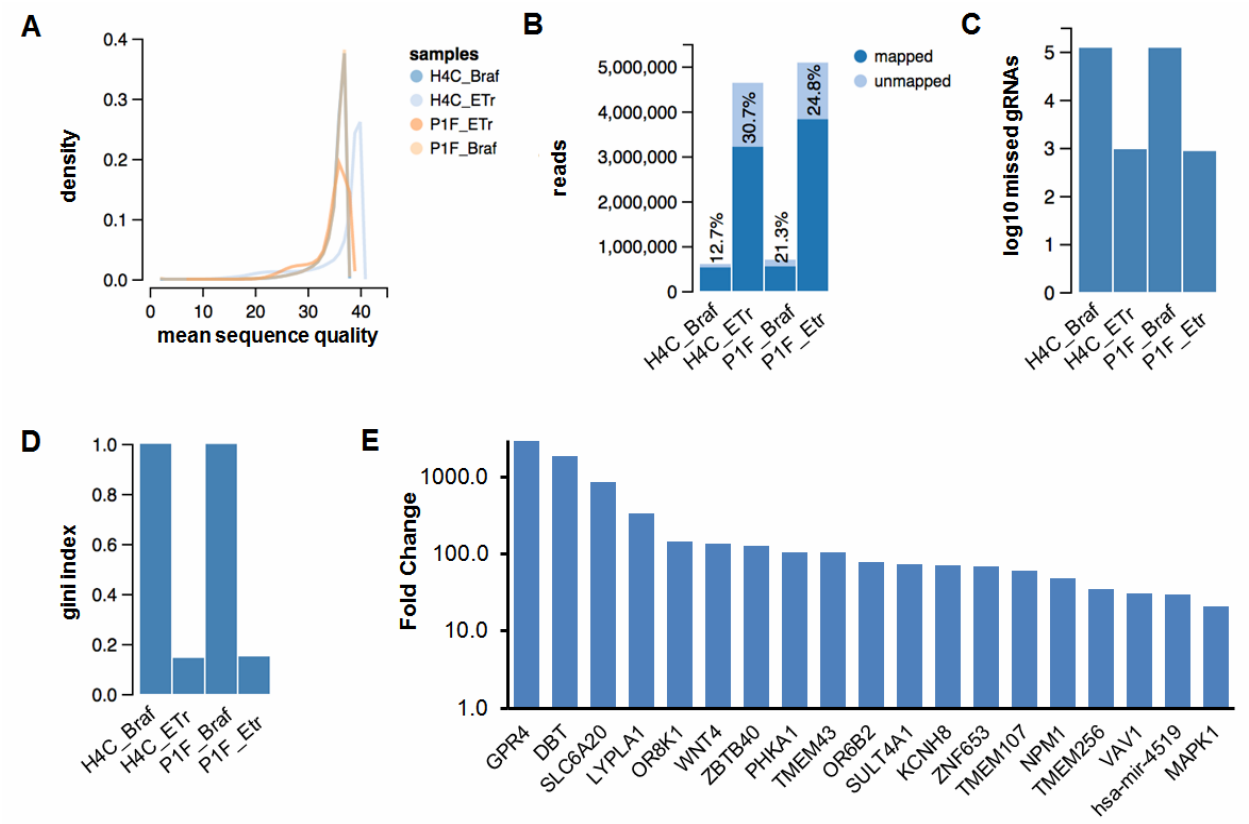

Figure 3.3. Genome-wide screening of genes implicated in OIS and OIA in P1F/hTERT fibroblasts and H4C melanocytes. (A) Distribution of sequencing read quality (Phred score). (B) sgRNA reads perfectly mapped and unmapped to the GeCKO libraries. (C) Count of missing sgRNAs. (D) Gini-index of sgRNAs (the level of distribution of all sgRNAs). (E) Top 20 candidates (19 genes and 1 microRNA) positively selected by BrafV600E when they were disrupted.

Because the immortalized fibroblasts possess senescence capacity (Gorbunova et al., 2002; Wei et al., 1999), the screening result may also reflect genes that are responsible for triggering OIS. By comparing the candidates from H4C and P1F/hTERT screenings, we identified 9 common candidates that may mediate BrafV600E-induced apoptosis (Table 3.2).

Table 3.2. Common candidates in P1F/hTERT and H4C cells.

sgRNA	Gene	Cell line	Fold increase	P-value	FDR
HGLibB_34499	OR8K1	H4C	146.7	0	0
HGLibB_54812	ZBTB40	H4C	126.6	0	0
HGLibB_36356	PHKA1	H4C	106.6	0	0
HGLibA_34377	OR6B2	H4C	79.9	0	0
HGLibA_24230	KCNH8	H4C	71.5	0	0
HGLibA_56463	ZNF653	H4C	69.9	0	0
HGLibA_50336	TMEM256	H4C	35.4	3.63E-157	5.10E-153
HGLibB_53483	VAV1	H4C	30.7	5.27E-123	6.99E-119
HGLibA_28248	MAPK1	H4C	21.3	3.13E-60	3.74E-56
HGLibB_34499	OR8K1	P1F/hTERT	17915.6	0	0
HGLibA_34377	OR6B2	P1F/hTERT	13277.1	0	0
HGLibA_24230	KCNH8	P1F/hTERT	9048.3	0	0
HGLibB_54812	ZBTB40	P1F/hTERT	8797.0	0	0
HGLibB_36356	PHKA1	P1F/hTERT	7530.7	0	0
HGLibA_56463	ZNF653	P1F/hTERT	5288.2	0	0
HGLibB_53483	VAV1	P1F/hTERT	2493.2	0	0
HGLibA_28248	MAPK1	P1F/hTERT	1472.0	0	0
HGLibA_50336	TMEM256	P1F/hTERT	1433.8	0	0

3.3.3 GPR4 and DBT are essential for the evasion of BrafV600E-induced apoptosis in melanocyte

The most striking candidates we found from screening H4Cs were GPR4 and DBT, each with almost 3000 and 2000 fold increase in read count, respectively (Fig 3.3E and Table A4). Off-targeting is one of the main concerns when using CRISPR/Cas9 system. To determine whether the evasion of OIA was due to off-targeting, we examined the targeted alleles of cells that have survived the oncogenic insult. We reason that if GPR4 and DBT deletion indeed facilitated the OIA evasion, then these cells should be bi-allelic frameshift knockouts. To do this, we first attempted the deletion of GPR4 and DBT by using lentivirus carrying GPR4 sgRNA (crGPR4)- or DBT sgRNA (crDBT)-Cas9-mCherry cassette (Fig. 3.4A) and allowed gene editing event to occur for a week before initiating BrafV600E selection. After 30 days of BrafV600E-GFP expression, GFP-positive cells were enriched by FACS (Fig. 3.4B-E). When cells reached confluence, 68 single cells from the crGPR4 pool (Fig. 3.4F) and 94 single cells from the crDBT pool (Fig. 3.4G) were sequenced around the Cas9 cutting site (Fig. 3.5). Based on the indel profiles, we determined that crGPR4 and crDBT pools were consisted of at least 13 and 8 different knockout cells, respectively, and ~99% of populations were bi-allelic frameshift knockouts (Table 3.3 and 3.4). In contrast, bi-allelic frameshift events only accounted for 33-44% of the populations in the absence of oncogenic pressure (Table 3.5 and 3.6), suggesting that GPR4 and DBT are essential in evading OIA for melanocytes.

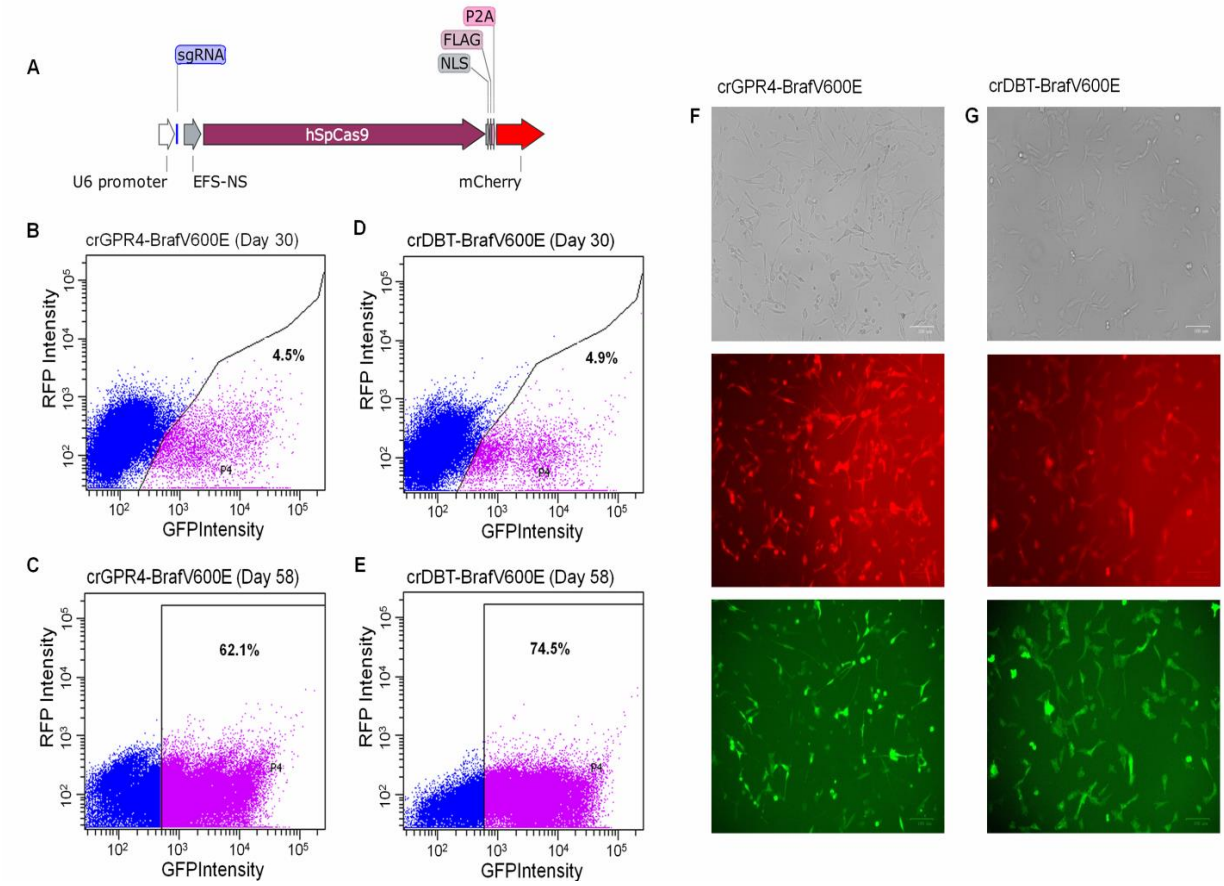

Figure 3.4. Ablation of GPR4 and DBT promotes proliferation under BrafV600E oncogenic pressure. (A) sgRNA-Cas9-mCherry expression cassette. Percentage of BrafV600E-positive GPR4-disrupted cells on (B) Day 30 and (C) Day 58. Percentage of BrafV600E-positive DBT-disrupted cells (D) on Day 30 and (E) on Day 58. (F-G) Images of OIA evaded cells.

Table 3.3. Distribution of GPR4 knockouts in cells survived BRAF-V600E expression[a]

Allele 1	Allele 2	Frame-shift knockout	Cell number
(-10) 9 del, 4 ins	(-7) 6 del, 1 ins	biallelic	41
(-6) 16 del	> 340 del	biallelic	8
(-6) 5 del	(-5) 5 del	biallelic	5
(-21) 43 del	> 340 del	biallelic	4
(-2) 26 ins	> 340 del	biallelic	2
(-2) 26 ins	(-7) 9 del, 4 ins	biallelic	1
(-2) 2 del	> 340 del	biallelic	1
(-21) 43 del	(-6) 5 del	biallelic	1
(-5) 5 del	(-5) 6 del, 1 ins	biallelic	1
(-6) 16 del	(-6) 5 del	biallelic	1
(-64) 123 del	> 340 del	biallelic	1
(-7) 6 del, 1 ins	(-6) 5 del	biallelic	1
(-5) 6 del	> 340 del	monoallelic	1
		Total	68

[a] numbers indicate nucleotides inserted (ins) or deleted (del); numbers in parentheses indicate ins and/or del start sites (relative to the CRISPR/Cas9 cutting site).

Table 3.4. Distribution of DBT knockouts in cells survived BRAF-V600E expression[a]

Allele 1	Allele 2	Frame-shift knockout	Cell number
(-1) 1 del	(+1) 2 del	biallelic	38
(+1) 2 del	> 340 del	biallelic	37
(-1) 1 del	> 340 del	biallelic	13
(-1) 10 del	(-1) 1 del	biallelic	2
(-1) 10 del	(+1) 4 ins	biallelic	1
(-1) 13 del	> 340 del	biallelic	1
(-11) 11 del	> 340 del	biallelic	1
(-11) 11 del	(-8) 15 del	monoallelic	1
		Total	94

[a] numbers indicate nucleotides inserted (ins) or deleted (del); numbers in parentheses indicate ins and/or del start sites (relative to the CRISPR/Cas9 cutting site).

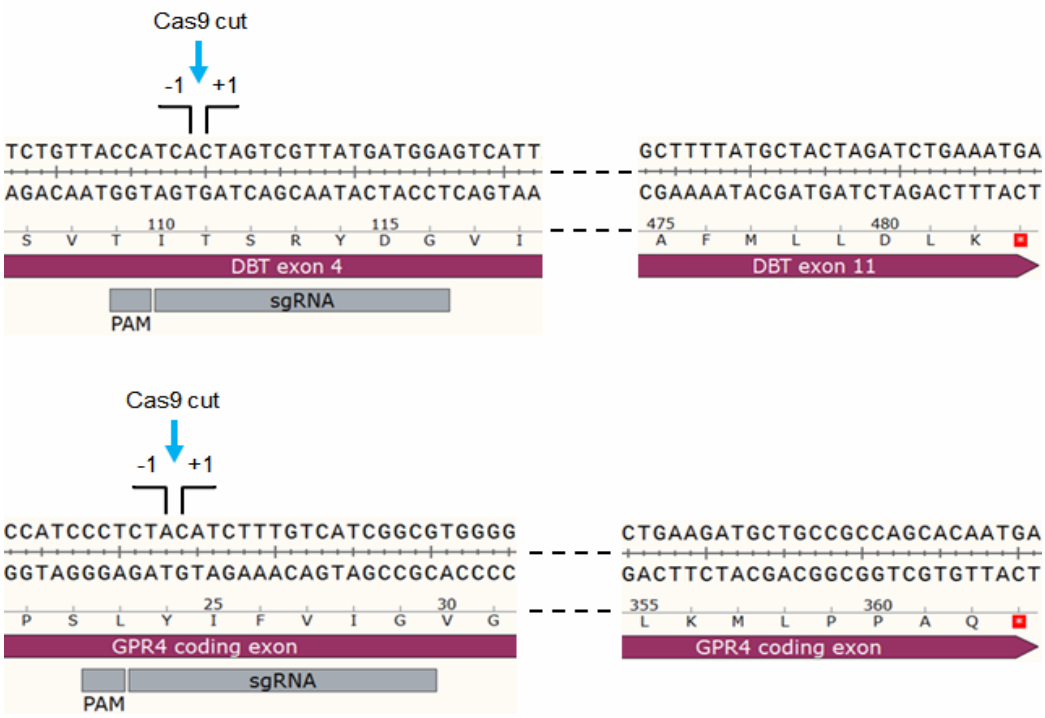

Figure 3.5. Cas9 cutting site on the DBT exon (top) and GPR4 exon (bottom).

Table 3.5. Distribution of GPR4 knockouts in cells without BRAF-V600E expression[a]

Allele 1	Allele 2	Frame-shift knockout	Cell number
(-1) 1 del	> 340 del	biallelic	1
(-13) 31 del	(-3) 19 del	biallelic	1
(-27) 26 del	> 340 del	biallelic	1
(-3) 2 del	(-1) 10 del	biallelic	1
(-1) 6 ins	> 340 del	monoallelic	1
(-27) 26 del	(-4) 3 del	monoallelic	1
(-27) 26 del	(-5) 6 del	monoallelic	1
(-4) 3 del	> 340 del	monoallelic	1
(-7) 6 del	(-5) 6 del	none	1
		Total	9

[a] numbers indicate nucleotides inserted (ins) or deleted (del); numbers in parentheses indicate ins and/or del start sites (relative to the CRISPR/Cas9 cutting site).

Table 3.6. Distribution of DBT knockouts in cells without BRAF-V600E expression[a]

Allele 1	Allele 2	Frame-shift knockout	Cell number
(-2) 3 del	(-1) 1 ins	monoallelic	3
(-2) 1 del	(-1) 2 del	biallelic	2
(-10) 11 del	(-2) 7 ins	biallelic	1
(-119) 118 del	(-2) 1 del	biallelic	1
(-2) 1 del	> 340 del	biallelic	1
(-2) 3 del	> 340 del	monoallelic	1
(-24) 33 del	> 340 del	monoallelic	1
(-34) 123 del	(-10) 10 del	monoallelic	1
(-5) 6 del	(-2) 1 del	monoallelic	1
(-5) 6 del	(-3) 5 del	monoallelic	1
(-5) 6 del	(-4) 4 del	monoallelic	1
(-8) 6 del	(-1) 1 del	monoallelic	1
		Total	15

[a] numbers indicate nucleotides inserted (ins) or deleted (del); numbers in parentheses indicate ins and/or del start sites (relative to the CRISPR/Cas9 cutting site).

3.3.4 DBT disruption alters apoptosis threshold through regulation of p53, AKT, and p14ARF

pH sensing receptor GPR4 is a G-protein coupled receptor that is activated in acidic condition (Dong et al., 2013). There have been multiple reports that demonstrated the significance of GPR4 in cancer developments and progression (Castellone et al., 2011; Justus and Yang, 2015; Tao et al., 2016). Yet, to the best of our knowledge, the effect of DBT on oncogenic response and tumorigenesis has not yet been described. To investigate, we first generated DBT-knockout (DBT-KO) cells by using H4C cell line and lentivirus carrying the crDBT-Cas9-mCherry cassette as mentioned above. Next, we restored the DBT expression in DBT-KO cells by using a lentiviral vector containing DBT cDNA. To prevent Cas9 from targeting the cDNA, 3 silent mutations were introduced in the protospacer adjacent motif (PAM) sequence and the two subsequent codons (Fig. 3.6A). The loss and the recovery of DBT expression in knockout and cDNA complemented (cDBT) cells was confirmed by using Western

blot (Fig. 3-6B). Upon BrafV600E activation, WT cells exhibited an increased apoptosis response, but the response was constantly, not completely, suppressed in DBT-KO cells (Fig. 3.6C). In contrast, the apoptosis potential was recovered to almost the same degree as that of the WT in cDBT cells (Fig. 3.6C).

Tumor suppressor p53 is a master regulator of the apoptosis and senescence programs. We found that DBT disruption suppresses OIA by downregulating p53 (Fig. 3.6E). Tumor suppressor p14ARF and proto-oncogene AKT are two important regulators of p53 (Fig. 3.6D). P14ARF is upregulated under oncogenic insult (Pauklin et al., 2005) and promotes cell cycle arrest and apoptosis by serving as an activator of p53 (Ozenne et al., 2010). AKT induces cellular proliferation and can negatively regulates p53 by enhancing MDM2-mediated degradation (Abraham and O'Neill, 2014). Our data suggest that, WT cells expresses AKT but not p14ARF under normal condition, but downregulates AKT and upregulates p14ARF during oncogenic stress (Fig. 3.6E). Interestingly, DBT disruption causes downregulation of AKT and has no effect on p14ARF under normal condition, but upregulates AKT and downregulates p14ARF when BrafV600E is expressed (Fig. 3.6E). Therefore, DBT deletion may suppress p53 and apoptosis through these collaborative efforts.

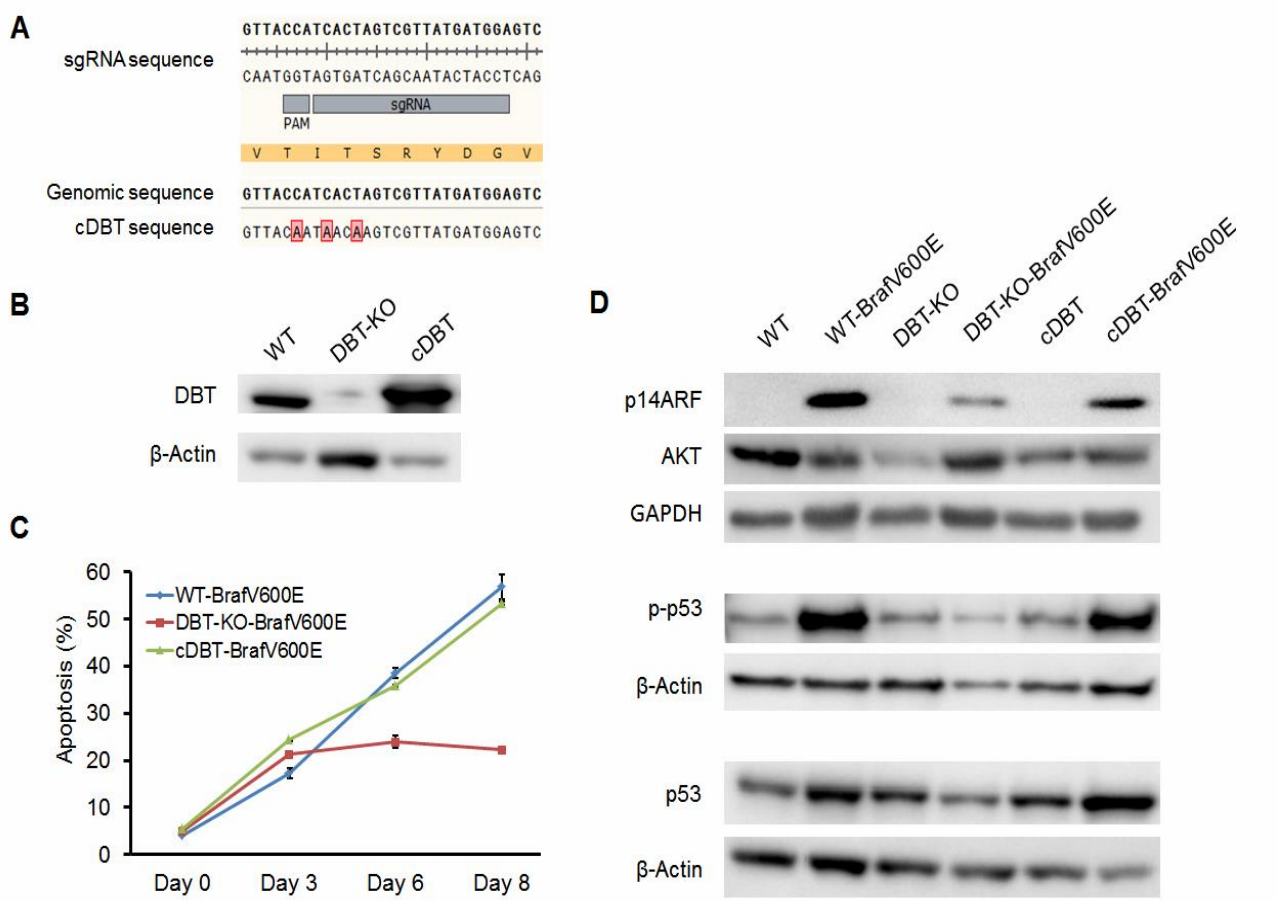

Figure 3.6. DBT knockout H4C suppresses OIA through regulating p53, p14ARF, and AKT. (A) DBT cDNA vector. (B) Western blot analysis of DBT expression in WT, DBT knockout, and DBT complemented H4C. (C) Apoptosis analysis of BrafV600E transduced WT, DBT knockout, and DBT complemented H4C. (D) Simplified schematics of BrafV600E-induced p53 activation. (D) Western blot analysis of p14ARF, AKT, p53, and phosphorylated p53 expression of WT, DBT knockout, and DBT complemented cells in normal condition and under oncogenic stress.

3.4 Discussion

3.4.1 Implication of GPR4 in cancers and OIA

Though conflicting, the relationship between GPR4 and cancers has been implicated in several studies. GPR4 was initially determined to be oncogenic based on the observation that its overexpression is sufficient to malignantly transform murine NIH3T3 fibroblasts (Sin et al., 2004). GPR4-deficient mice exhibit reduced angiogenesis and tumor growth, and the reduced angiogenic response was due to vascular endothelial growth factor, but not caused by basic fibroblast growth factor (Wyder et al., 2011). However, other studies have demonstrated that GPR4 overexpression can reduce mouse B16F10 melanoma and TRAMP-C1 prostate cancer cell migration and invasion (Castellone et al., 2011; Justus and Yang, 2015). Therefore, the contribution of GPR4 in cancer development seems to be dependent on the cell type and cellular context.

Recently, it is proposed that GPR4 is a suppressor of Yes-associated protein (YAP) (Tao et al., 2016). YAP is a major downstream effector of the Hippo pathway, and interacts with TEAD transcription factors to promote cellular proliferation, tumorigenesis, and to inhibit apoptosis (Felley-Bosco and Stahel, 2014; Zygulska et al., 2017). Indeed, overexpression of YAP is found in multiple cancers (Avruch et al., 2012; Wang et al., 2012; Zhang et al., 2015). Therefore, inactivation of GPR4 should, in theory, inactivates apoptosis machinery and promotes tumorigenesis. In addition, GPR4 activation has been suggested to activate ERK in 293T cells (Xu et al., 2013), thus GPR4 disruption could release some oncogenic pressure. Lastly, GPR4 has been found to activate p38 MAPK in immortalized human microvascular endothelial cells at pH 5.9 (Jing et al., 2016). P38 MAPK can be induced by oncogenic Ras and Braf and plays a

major role in activating p53, DNA damage response, and p16, thereby preventing tumorigenesis (Xu et al., 2014). Inactivating GPR4 may also bypass anti-tumor response in this context.

3.4.2 Implication of DBT in cancers and OIA

Lipoamide acyltransferase DBT is one of the three main components of Branched-chain ketoacid dehydrogenase (BCKD) complex found in the mitochondria (Ananieva and Wilkinson, 2018). BCKD complex catalyzes the rate-limiting step in the metabolism of branched-chain amino acids (BCAA) such as leucine, isoleucine, and valine (Nie et al., 2018). Dysfunctional BCKD complex results in the accumulation of BCAAs and their intermediates, and is believed to cause Maple Syrup Urine Disease (Imtiaz et al., 2017). In recent years, the role of BCAA metabolism in cancers has begun to receive attentions. BCAAs have shown to be the preferred amino acids for cancer growth, and overexpression of BCAT1, an enzyme that catalyzes the first and reversible reaction of BCAA catabolism, is found in multiple cancers (Ananieva and Wilkinson, 2018; Hattori et al., 2017). Increased level of BCAAs has also been recognized as an early event of pancreatic adenocarcinoma development (Mayers et al., 2014); however, the same oncogenic event can result in different BCAA metabolism due to tissue-of-origin (Mayers et al., 2016), suggesting that the contribution of BCAA to tumorigenesis is cell type specific.

Oncogenic stress is known to induce tumor suppressor p14ARF expression via E2F-mediated transcription (Pauklin et al., 2005). P14ARF contributes to apoptosis event by stabilizing p53 through p53 inhibitor MDM2 and ARF-binding protein1 inhibition (Ozenne et al., 2010). Consistent with previous reports, we observed a strong co-expression of phosphorylated p53 and p14ARF when expressing BrafV600E; however, these expressions are downregulated in the DBT-deficient melanocytes. Since p14ARF is a direct transcriptional target of E2F (Komori et al., 2005), it might be possible that DBT can somehow affect the E2F-

dependent transcription. On the other hand, recent evidence suggested that BCKD kinase, a negative regulator of BCKD complex, may enhance Ras/ERK pathway through direct phosphorylation of MEK (Xue et al., 2017). This opens up another possibility that DBT deficiency or BCKD dysfunction may cause alteration in oncogenic signals through BCDK kinase crosstalk, thus results in downregulated p14ARF expression.

Protein kinase AKT is well-known for promoting cell proliferation and survival (Manning and Toker, 2017); its aberrant activation has been implicated in many cancers (Mahajan and Mahajan, 2012; Manca et al., 2015). In addition, the activation of PI3K/AKT pathway has shown to abrogate BrafV600E-induced senescence in human fibroblast and melanocytes (Vredeveld et al., 2012). Mechanistically, AKT has been shown to degrade p53 by enhancing MDM2-mediated ubiquitination (Ogawara et al., 2002). In agreement, we observed the upregulation of p53 and downregulation of AKT in WT cells expressing BrafV600E. In contrast to the WT, AKT expression is elevated and p53 expression is repressed in DBT knockouts under oncogenic pressure. Moreover, we found that AKT expression is heavily dependent on DBT under normal condition. It is unclear whether there is crosstalk between p14ARF and AKT pathways; however, one report suggested that AKT may be involved in a negative feedback loop with E2F (Chaussepied and Ginsberg, 2004), suggesting that DBT may affect AKT expression via E2F-mediated transcription.

3.4.3 OIA/OIS evasion in human melanocyte and fibroblast

Our genome-wide loss-of-function screening identified 9 common candidates that may mediate BrafV600E-induced apoptosis in human fibroblast and melanocytes. Of these 9 genes, MAPK1 and VAV1 have been previously linked to tumorigenesis.

Mitogen-activated protein kinase 1 (MAPK1), also known as extracellular signal-regulated kinase 2 (ERK2), is a downstream effector of Ras/Raf/ERK pathway and partners with ERK1 to function as an integration point in a wide variety of cellular processes, including proliferation, apoptosis, metabolism, and immune response (Burotto et al., 2014). In cancer cells, overactivation of ERK signaling promotes mitochondrial fission, tumor invasion, and survival (Cristea and Sage, 2016; Kashatus et al., 2015; Yang and Huang, 2015). However, in normal cells, constitutive activation of Ras/Raf/ERK pathway induces cell cycle arrest and apoptosis through OIS and degradation of pro-survival proteins (Cagnol and Chambard, 2010; Deschenes-Simard et al., 2013). Decreased ERK signaling has shown to sufficiently bypass Ras-induced senescence in primary human fibroblasts (Deschenes-Simard et al., 2013). Similarly, our data also suggests that ERK2 disruption may evade BrafV600E-induced apoptosis. A recent report demonstrated that ERK2 can induce growth arrest independent of ERK1 (Wu et al., 2015), implying that ERK2 may play a more critical role in activating oncogenic response. This may explain the lack of implication of ERK1 in our screening.

Proto-oncogene VAV1 is a member of guanine nucleotide exchange factors for Rho family of GTPases, and its activity is associated with Ras/Raf/ERK pathway activation (Reynolds et al., 2004). VAV1 expression has been reported to increase p53-depedent apoptosis and plays a role as an oncogenic stress activator in cancer (Sebban et al., 2013). In contrast, VAV1 also functions as a tumor suppressor in T cell acute lymphoblastic leukemia; Vav1-deficient mice develop tumors faster and more frequently comparing to the wild-type (Robles-Valero et al., 2017). Consistently, our screening suggests that VAV1 disruption may facilitate cancer development by enabling the escape of OIA.

Among all nine candidates, five were transmembrane proteins including two that have been characterized as G protein-coupled receptors / olfactory receptors (OR6B2 and OR8K1), suggesting that the extracellular signaling plays a significant role in triggering BrafV600E-induced apoptosis. Indeed, previous study has demonstrated that BrafV600E-mediated apoptosis or senescence can be caused by the extracellular signaling of secreted factors, namely IGFBP7 (Wajapeyee et al., 2008). However, our candidates are comprised of multiple types of transmembrane proteins, which indicate that the anti-tumor response can be triggered by a wide range of secreted or extracellular molecules. Since inactivation of any of these genes may promote OIA/OIS bypass, it is like that their pathways may converge at one point. Further investigation may reveal new targets for cancer therapy.

3.5 References

Abraham, A.G., and O'Neill, E. (2014). PI3K/Akt-mediated regulation of p53 in cancer. Biochemical Society transactions *42*, 798-803.

Ananieva, E.A., and Wilkinson, A.C. (2018). Branched-chain amino acid metabolism in cancer. Curr Opin Clin Nutr Metab Care *21*, 64-70.

Aubrey, B.J., Kelly, G.L., Janic, A., Herold, M.J., and Strasser, A. (2018). How does p53 induce apoptosis and how does this relate to p53-mediated tumour suppression? Cell Death Differ *25*, 104-113.

Avruch, J., Zhou, D., and Bardeesy, N. (2012). YAP oncogene overexpression supercharges colon cancer proliferation. Cell cycle *11*, 1090-1096.

Bansal, R., and Nikiforov, M.A. (2010). Pathways of oncogene-induced senescence in human melanocytic cells. Cell cycle *9*, 2782-2788.

Bellelli, R., Vitagliano, D., Federico, G., Marotta, P., Tamburrino, A., Salerno, P., Paciello, O., Papparella, S., Knauf, J.A., Fagin, J.A., *et al.* (2018). Oncogene-induced senescence and its evasion in a mouse model of thyroid neoplasia. Mol Cell Endocrinol *460*, 24-35.

Burotto, M., Chiou, V.L., Lee, J.M., and Kohn, E.C. (2014). The MAPK pathway across different malignancies: a new perspective. Cancer *120*, 3446-3456.

Cagnol, S., and Chambard, J.C. (2010). ERK and cell death: mechanisms of ERK-induced cell death--apoptosis, autophagy and senescence. The FEBS journal *277*, 2-21.

Castellone, R.D., Leffler, N.R., Dong, L., and Yang, L.V. (2011). Inhibition of tumor cell migration and metastasis by the proton-sensing GPR4 receptor. Cancer Lett *312*, 197-208.

Chaussepied, M., and Ginsberg, D. (2004). Transcriptional regulation of AKT activation by E2F. Mol Cell *16*, 831-837.

Cheng, L., Lopez-Beltran, A., Massari, F., MacLennan, G.T., and Montironi, R. (2018). Molecular testing for BRAF mutations to inform melanoma treatment decisions: a move toward precision medicine. Mod Pathol *31*, 24-38.

Childs, B.G., Baker, D.J., Kirkland, J.L., Campisi, J., and van Deursen, J.M. (2014). Senescence and apoptosis: dueling or complementary cell fates? EMBO Rep *15*, 1139-1153.

Cisowski, J., Sayin, V.I., Liu, M., Karlsson, C., and Bergo, M.O. (2016). Oncogene-induced senescence underlies the mutual exclusive nature of oncogenic KRAS and BRAF. Oncogene *35*, 1328-1333.

Cristea, S., and Sage, J. (2016). Is the Canonical RAF/MEK/ERK Signaling Pathway a Therapeutic Target in SCLC? J Thorac Oncol *11*, 1233-1241.

Deschenes-Simard, X., Gaumont-Leclerc, M.F., Bourdeau, V., Lessard, F., Moiseeva, O., Forest, V., Igelmann, S., Mallette, F.A., Saba-El-Leil, M.K., Meloche, S., *et al.* (2013). Tumor suppressor activity of the ERK/MAPK pathway by promoting selective protein degradation. Genes & development *27*, 900-915.

Dong, L., Li, Z., Leffler, N.R., Asch, A.S., Chi, J.T., and Yang, L.V. (2013). Acidosis activation of the proton-sensing GPR4 receptor stimulates vascular endothelial cell inflammatory responses revealed by transcriptome analysis. PloS one *8*, e61991.

Felley-Bosco, E., and Stahel, R. (2014). Hippo/YAP pathway for targeted therapy. Transl Lung Cancer Res *3*, 75-83.

Gitenay, D., Lallet-Daher, H., and Bernard, D. (2014). Caspase-2 regulates oncogene-induced senescence. Oncotarget *5*, 5845-5847.

Gorbunova, V., Seluanov, A., and Pereira-Smith, O.M. (2002). Expression of human telomerase (hTERT) does not prevent stress-induced senescence in normal human fibroblasts but protects the cells from stress-induced apoptosis and necrosis. The Journal of biological chemistry *277*, 38540-38549.

Hattori, A., Tsunoda, M., Konuma, T., Kobayashi, M., Nagy, T., Glushka, J., Tayyari, F., McSkimming, D., Kannan, N., Tojo, A., *et al.* (2017). Cancer progression by reprogrammed

BCAA metabolism in myeloid leukaemia. Nature *545*, 500-504.

Imtiaz, F., Al-Mostafa, A., Allam, R., Ramzan, K., Al-Tassan, N., Tahir, A.I., Al-Numair, N.S., Al-Hamed, M.H., Al-Hassnan, Z., Al-Owain, M., *et al.* (2017). Twenty novel mutations in BCKDHA, BCKDHB and DBT genes in a cohort of 52 Saudi Arabian patients with maple syrup urine disease. Mol Genet Metab Rep *11*, 17-23.

Jing, Z., Xu, H., Chen, X., Zhong, Q., Huang, J., Zhang, Y., Guo, W., Yang, Z., Ding, S., Chen, P., *et al.* (2016). The Proton-Sensing G-Protein Coupled Receptor GPR4 Promotes Angiogenesis in Head and Neck Cancer. PloS one *11*, e0152789.

Joselow, A., Lynn, D., Terzian, T., and Box, N.F. (2017). Senescence-Like Phenotypes in Human Nevi. Methods in molecular biology *1534*, 175-184.

Justus, C.R., and Yang, L.V. (2015). GPR4 decreases B16F10 melanoma cell spreading and regulates focal adhesion dynamics through the G13/Rho signaling pathway. Experimental cell research *334*, 100-113.

Kashatus, J.A., Nascimento, A., Myers, L.J., Sher, A., Byrne, F.L., Hoehn, K.L., Counter, C.M., and Kashatus, D.F. (2015). Erk2 phosphorylation of Drp1 promotes mitochondrial fission and MAPK-driven tumor growth. Mol Cell *57*, 537-551.

Kim, J.J., Lee, S.B., Yi, S.Y., Han, S.A., Kim, S.H., Lee, J.M., Tong, S.Y., Yin, P., Gao, B., Zhang, J., *et al.* (2017). WSB1 overcomes oncogene-induced senescence by targeting ATM for degradation. Cell Res *27*, 274-293.

Komori, H., Enomoto, M., Nakamura, M., Iwanaga, R., and Ohtani, K. (2005). Distinct E2F-mediated transcriptional program regulates p14ARF gene expression. The EMBO journal *24*, 3724-3736.

Kotsantis, P., Petermann, E., and Boulton, S.J. (2018). Mechanisms of Oncogene-Induced Replication Stress: Jigsaw Falling into Place. Cancer Discov *8*, 537-555.

Li, W., Koster, J., Xu, H., Chen, C.H., Xiao, T., Liu, J.S., Brown, M., and Liu, X.S. (2015). Quality control, modeling, and visualization of CRISPR screens with MAGeCK-VISPR. Genome biology *16*, 281.

Liu, X.L., Ding, J., and Meng, L.H. (2018). Oncogene-induced senescence: a double edged sword in cancer. Acta Pharmacol Sin.

Lopez, J., and Tait, S.W. (2015). Mitochondrial apoptosis: killing cancer using the enemy within. Br J Cancer *112*, 957-962.

Manning, B.D., and Toker, A. (2017). AKT/PKB Signaling: Navigating the Network. Cell *169*, 381-405.

Mayers, J.R., Torrence, M.E., Danai, L.V., Papagiannakopoulos, T., Davidson, S.M., Bauer, M.R., Lau, A.N., Ji, B.W., Dixit, P.D., Hosios, A.M., *et al.* (2016). Tissue of origin dictates branched-chain amino acid metabolism in mutant Kras-driven cancers. Science *353*, 1161-1165.

Mayers, J.R., Wu, C., Clish, C.B., Kraft, P., Torrence, M.E., Fiske, B.P., Yuan, C., Bao, Y., Townsend, M.K., Tworoger, S.S., *et al.* (2014). Elevation of circulating branched-chain amino acids is an early event in human pancreatic adenocarcinoma development. Nat Med *20*, 1193-1198.

McHugh, D., and Gil, J. (2018). Senescence and aging: Causes, consequences, and therapeutic avenues. The Journal of cell biology *217*, 65-77.

Munoz-Espin, D., Canamero, M., Maraver, A., Gomez-Lopez, G., Contreras, J., Murillo-Cuesta, S., Rodriguez-Baeza, A., Varela-Nieto, I., Ruberte, J., Collado, M., *et al.* (2013). Programmed cell senescence during mammalian embryonic development. Cell *155*, 1104-1118.

Nie, C., He, T., Zhang, W., Zhang, G., and Ma, X. (2018). Branched Chain Amino Acids: Beyond Nutrition Metabolism. Int J Mol Sci *19*.

Ogawara, Y., Kishishita, S., Obata, T., Isazawa, Y., Suzuki, T., Tanaka, K., Masuyama, N., and Gotoh, Y. (2002). Akt enhances Mdm2-mediated ubiquitination and degradation of p53. The Journal of biological chemistry *277*, 21843-21850.

Ozenne, P., Eymin, B., Brambilla, E., and Gazzeri, S. (2010). The ARF tumor suppressor: structure, functions and status in cancer. Int J Cancer *127*, 2239-2247.

Patel, P.L., Suram, A., Mirani, N., Bischof, O., and Herbig, U. (2016). Derepression of hTERT gene expression promotes escape from oncogene-induced cellular senescence. Proc Natl Acad Sci U S A *113*, E5024-5033.

Pauklin, S., Kristjuhan, A., Maimets, T., and Jaks, V. (2005). ARF and ATM/ATR cooperate in p53-mediated apoptosis upon oncogenic stress. Biochem Biophys Res Commun *334*, 386-394.

Reynolds, L.F., de Bettignies, C., Norton, T., Beeser, A., Chernoff, J., and Tybulewicz, V.L. (2004). Vav1 transduces T cell receptor signals to the activation of the Ras/ERK pathway via LAT, Sos, and RasGRP1. The Journal of biological chemistry *279*, 18239-18246.

Robles-Valero, J., Lorenzo-Martin, L.F., Menacho-Marquez, M., Fernandez-Pisonero, I., Abad, A., Camos, M., Toribio, M.L., Espinosa, L., Bigas, A., and Bustelo, X.R. (2017). A Paradoxical Tumor-Suppressor Role for the Rac1 Exchange Factor Vav1 in T Cell Acute Lymphoblastic Leukemia. Cancer Cell *32*, 608-623 e609.

Sanjana, N.E., Shalem, O., and Zhang, F. (2014). Improved vectors and genome-wide libraries for CRISPR screening. Nature methods *11*, 783-784.

Sebban, S., Farago, M., Gashai, D., Ilan, L., Pikarsky, E., Ben-Porath, I., and Katzav, S. (2013). Vav1 fine tunes p53 control of apoptosis versus proliferation in breast cancer. PloS one *8*, e54321.

Sin, W.C., Zhang, Y., Zhong, W., Adhikarakunnathu, S., Powers, S., Hoey, T., An, S., and Yang, J. (2004). G protein-coupled receptors GPR4 and TDAG8 are oncogenic and overexpressed in human cancers. Oncogene *23*, 6299-6303.

Storer, M., Mas, A., Robert-Moreno, A., Pecoraro, M., Ortells, M.C., Di Giacomo, V., Yosef, R., Pilpel, N., Krizhanovsky, V., Sharpe, J., *et al.* (2013). Senescence is a developmental mechanism that contributes to embryonic growth and patterning. Cell *155*, 1119-1130.

Tao, S.C., Gao, Y.S., Zhu, H.Y., Yin, J.H., Chen, Y.X., Zhang, Y.L., Guo, S.C., and Zhang, C.Q. (2016). Decreased extracellular pH inhibits osteogenesis through proton-sensing GPR4-mediated suppression of yes-associated protein. Scientific reports *6*, 26835.

van Deursen, J.M. (2014). The role of senescent cells in ageing. Nature *509*, 439-446.

Vredeveld, L.C., Possik, P.A., Smit, M.A., Meissl, K., Michaloglou, C., Horlings, H.M., Ajouaou, A., Kortman, P.C., Dankort, D., McMahon, M., *et al.* (2012). Abrogation of BRAFV600E-induced senescence by PI3K pathway activation contributes to melanomagenesis. Genes & development *26*, 1055-1069.

Wajapeyee, N., Serra, R.W., Zhu, X., Mahalingam, M., and Green, M.R. (2008). Oncogenic BRAF induces senescence and apoptosis through pathways mediated by the secreted protein IGFBP7. Cell *132*, 363-374.

Wang, A.X., and Qi, X.Y. (2013). Targeting RAS/RAF/MEK/ERK signaling in metastatic melanoma. IUBMB Life *65*, 748-758.

Wang, X., Su, L., and Ou, Q. (2012). Yes-associated protein promotes tumour development in luminal epithelial derived breast cancer. European journal of cancer *48*, 1227-1234.

Wei, S., Wei, S., and Sedivy, J.M. (1999). Expression of catalytically active telomerase does not prevent premature senescence caused by overexpression of oncogenic Ha-Ras in normal human fibroblasts. Cancer research *59*, 1539-1543.

Wu, P.K., Hong, S.K., Yoon, S.H., and Park, J.I. (2015). Active ERK2 is sufficient to mediate growth arrest and differentiation signaling. The FEBS journal *282*, 1017-1030.

Wyder, L., Suply, T., Ricoux, B., Billy, E., Schnell, C., Baumgarten, B.U., Maira, S.M., Koelbing, C., Ferretti, M., Kinzel, B., *et al.* (2011). Reduced pathological angiogenesis and tumor growth in mice lacking GPR4, a proton sensing receptor. Angiogenesis *14*, 533-544.

Xu, H., Chen, X., Huang, J., Deng, W., Zhong, Q., Yue, C., Wang, P., and Huang, Z. (2013). Identification of GPR65, a novel regulator of matrix metalloproteinases using high through-put

screening. Biochem Biophys Res Commun *436*, 96-103.

Xu, Y., Li, N., Xiang, R., and Sun, P. (2014). Emerging roles of the p38 MAPK and PI3K/AKT/mTOR pathways in oncogene-induced senescence. Trends Biochem Sci *39*, 268-276.

Xue, P., Zeng, F., Duan, Q., Xiao, J., Liu, L., Yuan, P., Fan, L., Sun, H., Malyarenko, O.S., Lu, H., *et al.* (2017). BCKDK of BCAA Catabolism Cross-talking With the MAPK Pathway Promotes Tumorigenesis of Colorectal Cancer. EBioMedicine *20*, 50-60.

Yang, M., and Huang, C.Z. (2015). Mitogen-activated protein kinase signaling pathway and invasion and metastasis of gastric cancer. World J Gastroenterol *21*, 11673-11679.

Zhang, L., Yang, S., Chen, X., Stauffer, S., Yu, F., Lele, S.M., Fu, K., Datta, K., Palermo, N., Chen, Y., *et al.* (2015). The hippo pathway effector YAP regulates motility, invasion, and castration-resistant growth of prostate cancer cells. Molecular and cellular biology *35*, 1350-1362.

Zygulska, A.L., Krzemieniecki, K., and Pierzchalski, P. (2017). Hippo pathway - brief overview of its relevance in cancer. Journal of physiology and pharmacology : an official journal of the Polish Physiological Society *68*, 311-335.

CHAPTER 4
CONCLUDING REMARKS

4.1 Research Summary

By performing genome-wide CRISPR/Cas9 knockout screening, we identified novel genes and biological processes that are implicated in cisplatin sensitivity and resistance in A375 human melanoma as well as novel genes that may contribute to the early-stage tumorigenesis in human immortalized fibroblast and melanocyte.

The major findings are as follows:

1. Protein translation, RNA catabolic processes, and mitochondrial translational elongation and termination were the major processes that contribute to cisplatin sensitivity. In contrast, ubiquitin-dependent protein catabolic process, neddylation, negative regulations of cellular catabolic process, and canonical Wnt signaling were the top biological processes responsible for cisplatin resistance.
2. ZNRF3, a negative regulator of canonical Wnt signaling, is highly responsible for the cisplatin resistance in both melanoma and melanocyte cells. Disruption of tumor suppressor NF2 sensitizes human melanoma to cisplatin but confers resistance in human melanocyte and fibroblast via the regulation of E3 ubiquitin-protein ligase ARIH1.
3. G protein coupled receptors such as pH sensing receptor GPR4 and some olfactory receptors such as OR8K1 and OR6B2 may be important in regulating oncogenic response.
4. DBT, dihydrolipoamide branched chain transacylase E2, is essential in mediating BrafV600E-induced oncogenic stress in human melanocyte. DBT deletion can suppress oncogene-induced apoptosis by regulating p14ARF, AKT, and p53.

4.2 Future Direction

Factors that render the chemoresistance in different tumor types have been elucidated. However, most of these factors are not relevant to melanoma (Kalal et al., 2017). Our loss-of-function genome screening has revealed several novel biological processes that may contribute to the cisplatin resistance. Furthermore, we identified that the depletion of tumor suppressor NF2 can cause cisplatin resistance in normal human cells by upregulating ARIH1 and cisplatin sensitivity in melanoma cells by downregulating ARIH1. The regulation seems to involve the Hippo pathway and the downstream effector YAP, but not through the YAP-mediated transcription. Future study should focus on the molecular details of these biological processes and the mechanism of YAP in relation to ARIH1.

In searching for genes that contribute to tumorigenesis in melanocyte, we found that DBT plays an essential role in mediating oncogene-induced apoptosis through the regulation of p14ARF and AKT. However, how DBT is involved in these regulations is unknown. Future study should focus on finding the mechanism of these regulations.

4.3 Reference

Kalal, B.S., Upadhya, D., and Pai, V.R. (2017). Chemotherapy Resistance Mechanisms in Advanced Skin Cancer. Oncology reviews *11*, 326.

APPENDIX. GENES IMPLICATED IN CISPLATIN SENSITIVITY AND RESISTANCE, AND ONCOGENE-INDUCED APOPTOSIS AND SENESCENCE

Table A1. Top 1000 disrupted genes positively selected by cisplatin

ID	sgRNA number	score	p-value	FDR	rank	goodsgrna
NCMAP	6	3.77E-06	1.76E-05	0.201733	1	2
POLR3G	6	5.42E-06	2.99E-05	0.201733	2	4
CDT1	6	5.86E-06	3.31E-05	0.201733	3	6
RARS	6	6.30E-06	3.73E-05	0.201733	4	5
RPS24	5	1.27E-05	4.96E-05	0.214851	5	4
DHRS4L2	4	2.45E-05	8.80E-05	0.317657	6	4
ZNF207	6	2.51E-05	0.00013507	0.368193	7	5
DUSP23	6	2.53E-05	0.00013598	0.368193	8	3
IRS2	6	4.31E-05	0.00021232	0.464934	9	5
CAMKMT	6	6.55E-05	0.00030374	0.464934	10	4
hsa-mir-6836	4	6.92E-05	0.00025894	0.464934	11	4
TUFM	6	7.05E-05	0.0003275	0.464934	12	4
RGMA	6	7.17E-05	0.00033527	0.464934	13	4
RPUSD4	6	7.59E-05	0.00034762	0.464934	14	3
FBXO39	6	7.85E-05	0.0003595	0.464934	15	2
ZNF234	6	8.10E-05	0.0003723	0.464934	16	4
C2orf49	6	8.63E-05	0.00040292	0.464934	17	5
ZNF561	5	0.00010543	0.00046372	0.464934	18	1
POLDIP3	6	0.00010639	0.00050074	0.464934	19	5
TNIP1	6	0.00011271	0.00052634	0.464934	20	4
NSMCE1	6	0.00011584	0.00053776	0.464934	21	5
NDUFS2	6	0.00012286	0.00056702	0.464934	22	4
EMC6	6	0.00013051	0.00060267	0.464934	23	4
PDZK1	6	0.00013916	0.00064107	0.464934	24	5
hsa-mir-548i-3	2	0.00014457	0.00029002	0.464934	25	2
PSMG4	5	0.00014621	0.00061913	0.464934	26	3
hsa-mir-7515	4	0.00014669	0.0005693	0.464934	27	3
TTYH3	6	0.00014695	0.000679	0.464934	28	5
SREK1IP1	6	0.00015121	0.0006982	0.464934	29	4
NDUFB10	6	0.00015121	0.0006982	0.464934	30	5
SAP30BP	6	0.00015399	0.00071192	0.464934	31	2
PELO	6	0.0001628	0.00075305	0.464934	32	3
PMVK	6	0.00016736	0.00077271	0.464934	33	5
TXLNA	6	0.00016736	0.00077271	0.464934	34	5
ZNF582	6	0.00017711	0.00081842	0.479128	35	1
hsa-mir-4728	4	0.00018223	0.00069317	0.464934	36	4
APBA3	6	0.00019108	0.00087098	0.496483	37	5
MFN2	6	0.00022153	0.00099851	0.537836	38	5

(Table Continued)

ID	sgRNA number	score	p-value	FDR	rank	goodsgrna
SMPDL3A	6	0.00022771	0.0010241	0.537836	39	1
DUSP4	6	0.00023241	0.0010428	0.537836	40	4
FAM60A	6	0.00023245	0.0010428	0.537836	41	5
CDK10	6	0.00024398	0.0010982	0.540617	42	5
STRC	6	0.00027294	0.0012453	0.595243	43	5
SCRN3	6	0.00027831	0.0012641	0.595243	44	2
hsa-mir-6132	4	0.00028675	0.0010831	0.540617	45	2
MTX1	6	0.00030853	0.0013934	0.627917	46	5
SOX10	6	0.00032778	0.0014835	0.627917	47	4
PTPN2	6	0.00032778	0.0014835	0.627917	48	4
GDNF	6	0.00032891	0.0014878	0.627917	49	1
F8	6	0.00033601	0.0015219	0.627917	50	5
TTLL4	6	0.0003592	0.0016233	0.627917	51	2
IL12RB1	6	0.0003592	0.0016233	0.627917	52	3
RAC1	6	0.0003795	0.0017125	0.632591	53	1
ANKRD17	6	0.0003887	0.0017504	0.632591	54	3
TCF7L1	6	0.0003887	0.0017504	0.632591	55	3
C1orf131	6	0.00038897	0.0017522	0.632591	56	4
TRIM74	2	0.00039639	0.00075991	0.464934	57	1
POLR3F	5	0.0004126	0.0016051	0.627917	58	2
hsa-mir-378d-2	4	0.00041487	0.0015603	0.627917	59	4
hsa-mir-877	4	0.00041777	0.0015671	0.627917	60	3
SNRK	6	0.00044522	0.0019904	0.695385	61	4
UFSP1	6	0.00045318	0.0020256	0.696448	62	2
EHD3	6	0.00048068	0.002117	0.716507	63	1
hsa-mir-3163	4	0.00048277	0.0018144	0.644295	64	4
F13A1	6	0.00053126	0.0022994	0.747582	65	1
PPP4R2	6	0.00055957	0.0024002	0.747582	66	3
EIF4A1	6	0.00058185	0.002479	0.747582	67	4
ATP6V0D1	6	0.00061624	0.0025846	0.747582	68	2
MIDN	6	0.00061624	0.0025846	0.747582	69	3
HP1BP3	6	0.00061624	0.0025846	0.747582	70	2
RPL28	6	0.00061624	0.0025846	0.747582	71	2
ZNF442	6	0.00061624	0.0025846	0.747582	72	2
C9orf50	6	0.00063067	0.0026267	0.747582	73	4
PCDH12	6	0.00063243	0.0026335	0.747582	74	1
KRTAP3-2	6	0.00068301	0.0027958	0.747582	75	1
WDR83	6	0.00068747	0.0028113	0.747582	76	4
hsa-mir-1233-1	4	0.00069146	0.0024616	0.747582	77	1
RQCD1	6	0.00069713	0.0028497	0.747582	78	3
VWA1	6	0.00069713	0.0028497	0.747582	79	3
SH2D5	6	0.00070801	0.0028822	0.747582	80	4
BIVM	6	0.00071892	0.0029219	0.747582	81	4
EPB41L1	5	0.00072785	0.0027519	0.747582	82	3
SPINK5	6	0.00072844	0.002953	0.747582	83	2

(Table Continued)

ID	sgRNA number	score	p-value	FDR	rank	goodsgrna
DAW1	6	0.00073359	0.0029681	0.747582	84	1
NKX2-8	6	0.00075992	0.0030426	0.75754	85	2
CWH43	6	0.00078416	0.003134	0.766289	86	2
GPATCH8	6	0.00080199	0.0031898	0.766289	87	3
HRSP12	6	0.00080199	0.0031898	0.766289	88	2
SMAD9	6	0.00083474	0.0033041	0.766289	89	1
hsa-mir-4516	4	0.00085355	0.0028845	0.747582	90	3
RPL13	5	0.00087459	0.0032547	0.766289	91	4
CD63	6	0.00088531	0.0034951	0.766289	92	2
C12orf71	6	0.00089042	0.0035152	0.766289	93	2
TNFAIP1	6	0.00089042	0.0035152	0.766289	94	2
UBR3	6	0.0008928	0.0035194	0.766289	95	4
PDP1	5	0.00092677	0.0034284	0.766289	96	4
MNT	6	0.00093588	0.0036642	0.766289	97	3
ADHFE1	6	0.00094976	0.0037063	0.766289	98	3
HIST1H1E	6	0.00094976	0.0037063	0.766289	99	3
ORC6	6	0.00094976	0.0037063	0.766289	100	3
ARPC3	6	0.00094976	0.0037063	0.766289	101	4
RPS7	6	0.0009781	0.0037963	0.770627	102	4
HLA-DPA1	6	0.00098644	0.0038215	0.770627	103	2
CALHM2	5	0.0010072	0.0037145	0.766289	104	3
NPW	6	0.001081	0.0041405	0.770627	105	4
NOB1	6	0.0010876	0.0041584	0.770627	106	3
CC2D2A	6	0.0010892	0.0041625	0.770627	107	2
MC3R	6	0.0010892	0.0041625	0.770627	108	2
NUDT21	6	0.0010892	0.0041625	0.770627	109	2
USP7	6	0.0010892	0.0041625	0.770627	110	4
CCNJ	6	0.0010892	0.0041625	0.770627	111	2
SPANXF1	5	0.0011034	0.0040605	0.770627	112	3
CCR7	6	0.0011381	0.004327	0.790349	113	3
hsa-mir-6507	4	0.0011565	0.0037008	0.766289	114	3
LYPD3	6	0.0011873	0.0044879	0.790349	115	3
RPLP0	6	0.0011873	0.0044879	0.790349	116	3
LCE1D	6	0.0011873	0.0044879	0.790349	117	4
COQ4	6	0.0011873	0.0044879	0.790349	118	4
RPL38	6	0.0011873	0.0044879	0.790349	119	3
MRPS12	6	0.0012164	0.0045862	0.801142	120	4
FOXD4L5	6	0.0012374	0.0046605	0.802014	121	4
KCNA10	6	0.0012392	0.0046676	0.802014	122	1
hsa-mir-4277	4	0.0012646	0.0039842	0.770627	123	1
CCDC80	6	0.0012846	0.0048189	0.802014	124	3
POP1	6	0.0012898	0.0048381	0.802014	125	1
AMOTL1	6	0.0013404	0.0049948	0.802014	126	1
FAM180B	6	0.0013587	0.0050474	0.802014	127	2
NDUFV1	6	0.0013587	0.0050474	0.802014	128	3

(Table Continued)

ID	sgRNA number	score	p-value	FDR	rank	goodsgrna
ATL2	6	0.0013587	0.0050474	0.802014	129	3
NIPBL	6	0.0013704	0.0050831	0.802014	130	4
VIPR1	6	0.0013832	0.0051265	0.802014	131	3
OTOP3	6	0.0013832	0.0051265	0.802014	132	3
MLPH	6	0.0013909	0.0051539	0.802014	133	1
VPS45	6	0.001414	0.0052339	0.802014	134	4
UBE2E3	6	0.0014324	0.0053015	0.802014	135	4
MAGEC2	6	0.0014324	0.0053015	0.802014	136	4
FASTK	6	0.0014415	0.0053326	0.802014	137	1
FOSL2	6	0.0014567	0.0053687	0.802014	138	3
KLHL14	6	0.0014567	0.0053687	0.802014	139	4
DNAJC2	6	0.0014567	0.0053687	0.802014	140	3
TREX2	6	0.001492	0.0054981	0.815713	141	1
CGA	6	0.0015425	0.0056704	0.824784	142	2
GPT2	6	0.0015705	0.0057641	0.824784	143	3
GLTSCR1	5	0.0015833	0.0057582	0.824784	144	4
PCOLCE	6	0.0015931	0.0058404	0.824784	145	1
hsa-mir-3661	4	0.0016353	0.0049738	0.802014	146	2
PSMA6	6	0.001637	0.0059972	0.824784	147	4
ZMIZ1	6	0.001637	0.0059972	0.824784	148	4
PCGF1	6	0.0016377	0.0060036	0.824784	149	4
RRP1	6	0.0016436	0.006026	0.824784	150	2
PARS2	6	0.0016899	0.0061823	0.824784	151	4
MRPL17	6	0.0016899	0.0061823	0.824784	152	3
TCEB1	6	0.0016942	0.0062038	0.824784	153	2
MRPL32	6	0.0017012	0.006223	0.824784	154	4
hsa-mir-4532	4	0.0017376	0.0052366	0.802014	155	2
HIST1H2BE	6	0.0017447	0.0063597	0.824784	156	1
TCEB3CL2	2	0.0017718	0.0034224	0.766289	157	2
TDRD10	6	0.0018206	0.0066189	0.824784	158	3
ABHD16A	6	0.0018206	0.0066189	0.824784	159	3
KIF3C	6	0.0018206	0.0066189	0.824784	160	3
WAS	6	0.0018458	0.0067048	0.824784	161	3
ADRA2B	6	0.0019427	0.0070398	0.824784	162	3
ANAPC15	6	0.0019468	0.007054	0.824784	163	1
FAM49B	6	0.0020297	0.0073324	0.824784	164	4
SIX5	6	0.002036	0.0073502	0.824784	165	3
TMEM234	6	0.002036	0.0073502	0.824784	166	3
JUP	6	0.0020731	0.0074736	0.824784	167	1
GPR97	6	0.0020731	0.0074736	0.824784	168	1
DMRTC2	6	0.0020731	0.0074736	0.824784	169	2
CAPNS1	6	0.0020731	0.0074736	0.824784	170	2
NFKBIE	6	0.0020753	0.0074796	0.824784	171	4
CCDC64	6	0.0020753	0.0074796	0.824784	172	4
GPN3	6	0.0020999	0.0075586	0.824784	173	3

(Table Continued)

ID	sgRNA number	score	p-value	FDR	rank	goodsgrna
GBA	6	0.0020999	0.0075586	0.824784	174	3
PRPF38A	6	0.0020999	0.0075586	0.824784	175	3
SHOC2	6	0.0020999	0.0075586	0.824784	176	3
ACAD9	6	0.0020999	0.0075586	0.824784	177	2
PTPLAD1	6	0.0020999	0.0075586	0.824784	178	2
LOC10050547 8	6	0.0020999	0.0075586	0.824784	179	2
PNCK	6	0.0020999	0.0075586	0.824784	180	3
CYB5R3	6	0.0020999	0.0075586	0.824784	181	2
CCDC74A	6	0.0020999	0.0075586	0.824784	182	2
ELP3	6	0.0020999	0.0075586	0.824784	183	3
CCDC168	6	0.0020999	0.0075586	0.824784	184	2
OCM2	4	0.002107	0.0062431	0.824784	185	2
ARID4B	6	0.0021218	0.0076226	0.824784	186	4
hsa-mir-181b-2	4	0.0021224	0.0062852	0.824784	187	2
LRRC24	5	0.0021276	0.007672	0.824784	188	4
DSCC1	6	0.0021373	0.0076702	0.824784	189	3
FFAR3	6	0.0021553	0.0077319	0.824784	190	4
SRP68	6	0.0021622	0.0077497	0.824784	191	3
CCR2	6	0.0021773	0.0078036	0.824784	192	4
CER1	6	0.0021901	0.007848	0.824784	193	4
PRPF19	6	0.0021994	0.0078759	0.824784	194	1
OPRD1	6	0.0022154	0.0079257	0.824784	195	4
TNFRSF10B	6	0.0022154	0.0079257	0.824784	196	4
NT5C	6	0.0022499	0.0080409	0.824784	197	2
TXN	6	0.0022588	0.0080628	0.824784	198	3
RNF41	6	0.0022588	0.0080628	0.824784	199	3
RNF4	6	0.0022667	0.0080934	0.824784	200	4
TPM4	6	0.0023012	0.0082045	0.824784	201	4
TGIF1	6	0.0023401	0.0083334	0.824784	202	3
AIF1	6	0.002351	0.0083686	0.824784	203	1
FTH1P18	6	0.002351	0.0083686	0.824784	204	1
YAP1	6	0.002351	0.0083686	0.824784	205	2
CCNA1	6	0.0024089	0.0085533	0.824784	206	3
SHISA5	6	0.0024242	0.0086035	0.824784	207	4
hsa-mir-1249	4	0.0024363	0.0071112	0.824784	208	2
RNF40	6	0.0024554	0.0087155	0.824784	209	4
ANXA3	6	0.0024804	0.0087942	0.824784	210	3
TRAPPC1	6	0.0025025	0.0088636	0.824784	211	2
hsa-mir-302d	4	0.0025028	0.007289	0.824784	212	3
hsa-mir-4441	3	0.0025176	0.0070106	0.824784	213	2
MOGAT3	6	0.002523	0.0089427	0.824784	214	3
hsa-mir-124-1	4	0.0025448	0.0074128	0.824784	215	1
hsa-mir-7848	4	0.0025448	0.0074128	0.824784	216	1
NTN1	6	0.002553	0.0090442	0.824784	217	1

(Table Continued)

ID	sgRNA number	score	p-value	FDR	rank	goodsgrna
DPH7	6	0.0025753	0.0091201	0.824784	218	4
NonTargetingControlGuideForHuman_0979	1	0.0025768	0.0025645	0.747582	219	1
HNRNPM	6	0.002579	0.0091324	0.824784	220	3
RNF165	6	0.0025983	0.0091982	0.824784	221	4
HUS1	6	0.0026035	0.0092138	0.824784	222	3
SRC	6	0.0026131	0.0092407	0.824784	223	4
DHX9	5	0.002633	0.0092549	0.824784	224	3
RSL1D1	6	0.0026496	0.0093641	0.824784	225	3
APTX	6	0.002654	0.0093747	0.824784	226	1
EIF3C	6	0.0027045	0.0095451	0.824784	227	2
SUZ12	6	0.0027256	0.0096142	0.824784	228	4
MARS2	6	0.0027256	0.0096142	0.824784	229	4
DBNDD1	6	0.0027256	0.0096142	0.824784	230	4
KIF20B	6	0.0027256	0.0096142	0.824784	231	4
BANF2	6	0.0027777	0.0097673	0.824784	232	3
TNFSF14	6	0.0028128	0.0098806	0.824784	233	3
hsa-mir-99b	4	0.0028142	0.0081254	0.824784	234	1
GMPPB	6	0.0028376	0.0099657	0.824784	235	3
TTC5	6	0.0028376	0.0099657	0.824784	236	2
HMX2	6	0.0028376	0.0099657	0.824784	237	2
SLX4	6	0.0028376	0.0099657	0.824784	238	3
MUC1	6	0.0028376	0.0099657	0.824784	239	3
C1D	6	0.0028376	0.0099657	0.824784	240	2
CEBPE	6	0.0028559	0.010016	0.824784	241	1
PNPLA1	6	0.0028559	0.010016	0.824784	242	1
SLC22A10	6	0.0028559	0.010016	0.824784	243	2
IGF2BP2	6	0.0028559	0.010016	0.824784	244	2
NTNG1	6	0.0028559	0.010016	0.824784	245	2
RBMX2	5	0.0028629	0.0098066	0.824784	246	2
BCAP29	6	0.0028833	0.010103	0.824784	247	4
HPCA	6	0.0028833	0.010103	0.824784	248	4
AMFR	6	0.0028833	0.010103	0.824784	249	4
NAE1	6	0.0028889	0.01012	0.824784	250	3
ORC4	6	0.0028889	0.01012	0.824784	251	3
GATAD2B	6	0.0028889	0.01012	0.824784	252	3
hsa-mir-6851	3	0.0029069	0.0080742	0.824784	253	3
TRMT112	6	0.00302	0.010546	0.824784	254	3
GNG5	6	0.00302	0.010546	0.824784	255	3
hsa-mir-5692a-1	4	0.0030321	0.0087073	0.824784	256	3
LYRM7	6	0.0030594	0.01067	0.824784	257	2
TMEM200B	6	0.0031386	0.010922	0.824784	258	4
ORMDL1	6	0.0031386	0.010922	0.824784	259	4

(Table Continued)

ID	sgRNA number	score	p-value	FDR	rank	goodsgrna
SNAPIN	6	0.0031398	0.010926	0.824784	260	2
LPO	6	0.0031398	0.010926	0.824784	261	3
PRRT3	6	0.0031588	0.010987	0.824784	262	3
OR2C1	6	0.0031588	0.010987	0.824784	263	1
GML	6	0.0031588	0.010987	0.824784	264	1
hsa-mir-5585	4	0.0032004	0.0091388	0.824784	265	3
LRRD1	6	0.0032242	0.011192	0.824784	266	3
VTCN1	6	0.0032266	0.011198	0.824784	267	2
NFKB2	6	0.0032604	0.011297	0.824784	268	4
ATP2C2	6	0.0032604	0.011297	0.824784	269	4
NIT2	6	0.0032983	0.01141	0.824784	270	2
PLA2G4D	6	0.0033102	0.011449	0.824784	271	1
hsa-mir-5582	2	0.0033205	0.0063647	0.824784	272	1
RAD52	5	0.0033277	0.010932	0.824784	273	2
GTF3C6	6	0.0033543	0.0116	0.824784	274	2
PDLIM3	6	0.0033607	0.011621	0.824784	275	1
NDUFAF3	6	0.0033647	0.011634	0.824784	276	3
ANKRD12	6	0.0033647	0.011634	0.824784	277	3
ANAPC4	6	0.0033647	0.011634	0.824784	278	4
PI16	6	0.0033884	0.011698	0.824784	279	4
VMP1	6	0.0034109	0.011786	0.824784	280	3
GAS8	6	0.0034616	0.011953	0.824784	281	1
CEP97	6	0.0034945	0.012059	0.824784	282	4
SIN3A	6	0.0034945	0.012059	0.824784	283	4
TMEM241	6	0.0034945	0.012059	0.824784	284	4
DDB1	6	0.0035681	0.012309	0.824784	285	3
CNTFR	6	0.0035681	0.012309	0.824784	286	2
SPATA2L	6	0.0035681	0.012309	0.824784	287	2
BHLHB9	6	0.0035681	0.012309	0.824784	288	3
KCNQ2	6	0.0035681	0.012309	0.824784	289	2
TOP1	6	0.0035681	0.012309	0.824784	290	2
FBXO45	6	0.0035833	0.012369	0.824784	291	4
SRSF4	6	0.003592	0.012396	0.824784	292	4
TBC1D3F	2	0.0036467	0.0070179	0.824784	293	2
MANBA	6	0.0036575	0.012594	0.824784	294	4
hsa-mir-5093	4	0.0036751	0.010419	0.824784	295	3
OR1D5	6	0.0036866	0.012692	0.824784	296	4
TUBB6	6	0.0036866	0.012692	0.824784	297	4
hsa-mir-4697	4	0.0036892	0.010462	0.824784	298	1
UFD1L	6	0.0036921	0.012711	0.824784	299	3
XYLT1	6	0.0037592	0.012934	0.824784	300	4
RLIM	5	0.003766	0.011993	0.824784	301	2
LRRIQ3	6	0.0038148	0.013127	0.824784	302	1
RABGEF1	6	0.0038148	0.013127	0.824784	303	1
INSL3	6	0.0038148	0.013127	0.824784	304	1

(Table Continued)

ID	sgRNA number	score	p-value	FDR	rank	goodsgrna
MRP63	6	0.0038148	0.013127	0.824784	305	4
GJB7	6	0.0038148	0.013127	0.824784	306	1
HLA-DRB5	6	0.0038148	0.013127	0.824784	307	4
DUS1L	6	0.0038148	0.013127	0.824784	308	1
OPRK1	6	0.0038148	0.013127	0.824784	309	2
DNAL4	6	0.0038148	0.013127	0.824784	310	2
ABCB1	6	0.0038148	0.013127	0.824784	311	1
HSPBP1	6	0.0038148	0.013127	0.824784	312	2
LCE1E	4	0.0038235	0.010817	0.824784	313	3
LYSMD4	6	0.0038343	0.013189	0.824784	314	3
PFKM	6	0.0038343	0.013189	0.824784	315	3
CEP250	6	0.0038343	0.013189	0.824784	316	3
TADA2B	6	0.0038343	0.013189	0.824784	317	3
FERMT2	6	0.0038343	0.013189	0.824784	318	3
UNC50	6	0.0038343	0.013189	0.824784	319	3
BHLHA9	6	0.0038343	0.013189	0.824784	320	3
PCED1B	6	0.0038343	0.013189	0.824784	321	3
RPLP1	6	0.0038343	0.013189	0.824784	322	3
DESI2	6	0.0038343	0.013189	0.824784	323	3
HMGB3	6	0.0038853	0.013355	0.824784	324	4
LRMP	6	0.0038853	0.013355	0.824784	325	4
HILPDA	6	0.0038853	0.013355	0.824784	326	4
DHX36	6	0.0038853	0.013355	0.824784	327	4
EIF3J	6	0.0038853	0.013355	0.824784	328	4
BIK	6	0.0038853	0.013355	0.824784	329	4
PDCD2	6	0.0038853	0.013355	0.824784	330	4
RAX2	5	0.0039159	0.012367	0.824784	331	2
POLE2	5	0.0039159	0.012367	0.824784	332	1
hsa-mir-548aa-2	4	0.003921	0.01106	0.824784	333	3
hsa-mir-1273a	4	0.003921	0.01106	0.824784	334	3
hsa-mir-3670-1	4	0.0039584	0.011153	0.824784	335	2
SPATA31A6	6	0.0040129	0.01376	0.824784	336	3
HELZ	6	0.0040332	0.013821	0.824784	337	4
SPTSSB	6	0.0040332	0.013821	0.824784	338	4
SPEN	6	0.0040332	0.013821	0.824784	339	4
DUSP10	6	0.0040929	0.014017	0.824784	340	4
SRSF2	6	0.0041153	0.01409	0.824784	341	3
MRPS35	6	0.0041153	0.01409	0.824784	342	3
hsa-mir-30b	4	0.0041214	0.011572	0.824784	343	3
COX16	6	0.0041364	0.014163	0.824784	344	4
SGIP1	6	0.0041679	0.014271	0.824784	345	2
NonTargetingControlGuideForHuman_0089	1	0.0042047	0.0041428	0.770627	346	1

(Table Continued)

ID	sgRNA number	score	p-value	FDR	rank	goodsgrna
APEX2	6	0.0042452	0.014507	0.824784	347	3
MKI67	6	0.0042452	0.014507	0.824784	348	3
OR4K14	6	0.0042452	0.014507	0.824784	349	2
ALDH3B2	6	0.0042452	0.014507	0.824784	350	2
ADAMTSL4	6	0.0042452	0.014507	0.824784	351	3
ADAMTS6	6	0.0042452	0.014507	0.824784	352	2
FBLN1	6	0.0042452	0.014507	0.824784	353	2
TRMT1L	6	0.0042452	0.014507	0.824784	354	3
ERH	6	0.0042452	0.014507	0.824784	355	2
DTNBP1	6	0.0042452	0.014507	0.824784	356	2
CSF2RB	6	0.0042452	0.014507	0.824784	357	2
RILPL2	6	0.0042452	0.014507	0.824784	358	3
TTC23	6	0.0042452	0.014507	0.824784	359	2
SLC35G2	6	0.0042452	0.014507	0.824784	360	3
ASNA1	6	0.0042452	0.014507	0.824784	361	3
TMEM150C	6	0.0042452	0.014507	0.824784	362	3
FOXB2	5	0.0042469	0.01318	0.824784	363	3
IGLON5	5	0.0042469	0.01318	0.824784	364	3
CRYGS	6	0.0042687	0.014589	0.827264	365	1
DACH2	6	0.0043152	0.014737	0.827797	366	3
QRICH2	6	0.0043152	0.014737	0.827797	367	3
BHMT2	6	0.0043192	0.014751	0.827797	368	1
hsa-mir-4252	4	0.0043574	0.012186	0.824784	369	2
CAP1	6	0.0044518	0.015174	0.845179	370	3
MBOAT7	6	0.0044818	0.015256	0.845179	371	4
hsa-mir-4430	4	0.0044911	0.012532	0.824784	372	3
C16orf59	6	0.0045174	0.015378	0.845179	373	4
CCDC112	6	0.00454	0.015457	0.845179	374	4
KRTAP2-3	2	0.0045776	0.0087736	0.824784	375	2
C9orf129	6	0.0045817	0.015587	0.845179	376	4
BDKRB1	6	0.0045817	0.015587	0.845179	377	4
CENPH	2	0.0045832	0.0087827	0.824784	378	1
MRPL40	5	0.0046094	0.014079	0.824784	379	1
USP49	6	0.0046109	0.015681	0.845179	380	3
C10orf118	6	0.0046109	0.015681	0.845179	381	3
RSPH4A	6	0.0046109	0.015681	0.845179	382	3
ENKD1	6	0.0046973	0.015959	0.845179	383	1
EXOSC5	6	0.0046973	0.015959	0.845179	384	2
SEC24B	6	0.0046973	0.015959	0.845179	385	2
TIE1	6	0.0046973	0.015959	0.845179	386	3
CPA1	6	0.0046973	0.015959	0.845179	387	2
TAC4	6	0.0046973	0.015959	0.845179	388	3
PDCD6	6	0.0046973	0.015959	0.845179	389	3
SPC24	6	0.0046973	0.015959	0.845179	390	1
DDIT4	6	0.0046973	0.015959	0.845179	391	2

(Table Continued)

ID	sgRNA number	score	p-value	FDR	rank	goodsgrna
GOLGA4	6	0.0046973	0.015959	0.845179	392	1
hsa-mir-4524a	4	0.0047314	0.013193	0.824784	393	2
TTBK1	6	0.0047926	0.016257	0.851587	394	4
PES1	6	0.0047926	0.016257	0.851587	395	4
RNF32	6	0.0048034	0.016294	0.851587	396	3
VPS52	6	0.0048301	0.016387	0.851587	397	3
MLL	4	0.0048343	0.013454	0.824784	398	3
YY1	6	0.0048866	0.016555	0.851587	399	4
HEY2	6	0.0048922	0.016576	0.851587	400	3
CCDC157	6	0.0049299	0.016694	0.851587	401	3
FARSB	6	0.0049299	0.016694	0.851587	402	3
DHX34	6	0.0049299	0.016694	0.851587	403	2
hsa-mir-6087	2	0.0049531	0.0095223	0.824784	404	2
PCDH1	6	0.0050159	0.01697	0.851587	405	4
CLASRP	6	0.0050159	0.01697	0.851587	406	4
FAM127B	6	0.0050159	0.01697	0.851587	407	4
DAP3	6	0.0050159	0.01697	0.851587	408	4
SLCO6A1	6	0.0050159	0.01697	0.851587	409	4
AFAP1L1	6	0.0050198	0.016982	0.851587	410	2
MRPS11	6	0.0050381	0.017035	0.851587	411	3
PIH1D3	6	0.0050381	0.017035	0.851587	412	3
hsa-mir-4519	4	0.0050512	0.014013	0.824784	413	1
hsa-mir-4707	4	0.0050607	0.014038	0.824784	414	2
OR51B5	6	0.0050727	0.017143	0.851587	415	2
SEC11C	6	0.0050753	0.017152	0.851587	416	2
DYRK3	5	0.0050901	0.015289	0.845179	417	3
hsa-mir-4740	4	0.0051143	0.014184	0.824784	418	3
DNAJC18	6	0.0051257	0.017308	0.854184	419	1
EBNA1BP2	6	0.0051481	0.017385	0.854184	420	3
NPM3	6	0.0051605	0.01743	0.854184	421	4
FOXRED1	6	0.0051605	0.01743	0.854184	422	4
SCAMP4	6	0.0051605	0.01743	0.854184	423	4
hsa-mir-1913	4	0.0055216	0.015238	0.845179	424	3
SOX2	6	0.0055288	0.018609	0.872754	425	1
BLVRA	6	0.0055288	0.018609	0.872754	426	1
SLC25A14	6	0.0055288	0.018609	0.872754	427	2
PDCL2	6	0.0055288	0.018609	0.872754	428	1
FDX1	6	0.0055288	0.018609	0.872754	429	3
SMARCD3	6	0.0055288	0.018609	0.872754	430	2
RNF150	6	0.0055288	0.018609	0.872754	431	2
CBLL1	6	0.0055288	0.018609	0.872754	432	3
BUD13	6	0.0055288	0.018609	0.872754	433	2
RRAGA	6	0.0055288	0.018609	0.872754	434	2
CHCHD6	6	0.0055288	0.018609	0.872754	435	1
hsa-mir-15a	4	0.005559	0.015338	0.845179	436	2

(Table Continued)

ID	sgRNA number	score	p-value	FDR	rank	goodsgrna
HTN1	3	0.0055695	0.013546	0.824784	437	2
RBM33	6	0.0055748	0.018744	0.872754	438	2
RAB3IL1	6	0.0056302	0.018918	0.872754	439	4
EIF3A	6	0.0056302	0.018918	0.872754	440	4
ACTR1B	6	0.0056302	0.018918	0.872754	441	4
RBL2	6	0.0056302	0.018918	0.872754	442	4
SREBF1	6	0.0056302	0.018918	0.872754	443	4
DDX42	6	0.0056302	0.018918	0.872754	444	4
TMEM199	6	0.0056302	0.018918	0.872754	445	4
MRPL34	6	0.0056302	0.018918	0.872754	446	4
DIS3	6	0.0056302	0.018918	0.872754	447	4
ADM2	6	0.0056302	0.018918	0.872754	448	4
NECAB2	6	0.0056302	0.018918	0.872754	449	4
PURB	5	0.0056341	0.01664	0.851587	450	3
hsa-mir-6887	4	0.0056762	0.015628	0.845179	451	2
RGPD6	2	0.005761	0.011028	0.824784	452	1
ZNF8	5	0.0058325	0.01714	0.851587	453	2
POM121C	5	0.0058484	0.01718	0.851587	454	3
C1orf158	6	0.0059267	0.019905	0.872754	455	3
VWCE	6	0.0059267	0.019905	0.872754	456	2
MURC	6	0.0059267	0.019905	0.872754	457	2
GPBP1	6	0.0059267	0.019905	0.872754	458	2
TRIM65	6	0.0059267	0.019905	0.872754	459	2
LEP	6	0.0059267	0.019905	0.872754	460	2
POLRMT	6	0.0059288	0.01991	0.872754	461	3
NAA30	6	0.0059288	0.01991	0.872754	462	3
OTUD1	6	0.0059288	0.01991	0.872754	463	3
GAREML	6	0.0059288	0.01991	0.872754	464	3
GCNT7	6	0.0059288	0.01991	0.872754	465	3
PSMD14	6	0.0059288	0.01991	0.872754	466	3
COA5	6	0.0059288	0.01991	0.872754	467	3
ZMYND15	6	0.0059288	0.01991	0.872754	468	3
CSAG1	6	0.0059288	0.01991	0.872754	469	3
ARMC5	6	0.0059288	0.01991	0.872754	470	3
TOM1L1	6	0.0059288	0.01991	0.872754	471	3
RBM8A	6	0.0059288	0.01991	0.872754	472	3
SSH3	6	0.0059288	0.01991	0.872754	473	3
LETM1	6	0.0059288	0.01991	0.872754	474	3
PSMB3	6	0.0059288	0.01991	0.872754	475	3
hsa-mir-671	4	0.0059523	0.016329	0.851587	476	3
NHLRC4	6	0.005982	0.020078	0.875082	477	2
ASCL4	6	0.0061505	0.020609	0.881703	478	4
PPARA	6	0.0061505	0.020609	0.881703	479	4
DNAJC24	6	0.0061505	0.020609	0.881703	480	4
PUF60	4	0.0061599	0.016855	0.851587	481	1

(Table Continued)

ID	sgRNA number	score	p-value	FDR	rank	goodsgrna
hsa-mir-6500	4	0.0061763	0.016907	0.851587	482	3
hsa-mir-8055	4	0.0061957	0.016956	0.851587	483	3
hsa-mir-516b-1	3	0.006213	0.0147	0.827797	484	2
hsa-mir-6894	4	0.0062374	0.017058	0.851587	485	3
hsa-mir-876	4	0.0062374	0.017058	0.851587	486	3
TDP2	6	0.0062742	0.021008	0.881703	487	4
AMDHD1	6	0.0063107	0.02112	0.881703	488	2
PAK7	6	0.0063781	0.021337	0.881703	489	4
PET112	6	0.0063848	0.021362	0.881703	490	1
PRR15L	6	0.0063848	0.021362	0.881703	491	1
IFNAR1	6	0.0063848	0.021362	0.881703	492	1
LARP7	6	0.0063848	0.021362	0.881703	493	1
PRDM6	6	0.0063848	0.021362	0.881703	494	3
MCF2L2	6	0.0063848	0.021362	0.881703	495	1
SENP8	6	0.0063848	0.021362	0.881703	496	2
TTC13	6	0.0063848	0.021362	0.881703	497	1
HSDL2	6	0.0063848	0.021362	0.881703	498	1
MTO1	6	0.0063848	0.021362	0.881703	499	2
UQCRFS1	6	0.0063848	0.021362	0.881703	500	1
GPR1	6	0.0063848	0.021362	0.881703	501	2
LMO7	6	0.0063848	0.021362	0.881703	502	1
CCL1	6	0.0064339	0.021533	0.881703	503	2
OR1D2	6	0.0064339	0.021533	0.881703	504	2
DDX52	6	0.0064339	0.021533	0.881703	505	2
C11orf87	6	0.0064339	0.021533	0.881703	506	3
NDST3	6	0.0064339	0.021533	0.881703	507	2
DSTN	5	0.0064543	0.018674	0.872754	508	3
GEMIN8	6	0.006472	0.021661	0.88184	509	4
ZNF16	6	0.0065124	0.021801	0.88184	510	4
ADAP2	6	0.0065257	0.021842	0.88184	511	2
P2RX3	6	0.0067176	0.022342	0.88184	512	3
BOK	6	0.0067176	0.022342	0.88184	513	3
MLN	6	0.0067176	0.022342	0.88184	514	3
MRPS6	5	0.0067578	0.019386	0.872754	515	2
CNBD2	6	0.0068023	0.022537	0.88184	516	3
NOP58	6	0.0068023	0.022537	0.88184	517	2
TMEM184C	6	0.0068023	0.022537	0.88184	518	3
CD3E	6	0.0068126	0.022559	0.88184	519	2
NDUFS5	6	0.0068126	0.022559	0.88184	520	2
ADAMTS16	6	0.0068402	0.022617	0.88184	521	3
TEX35	6	0.0068788	0.022698	0.88184	522	3
DLGAP3	6	0.0068788	0.022698	0.88184	523	3
FAM46C	5	0.0069602	0.019875	0.872754	524	1
hsa-mir-320e	4	0.0070559	0.0191	0.872754	525	2
EMC3	6	0.007061	0.023118	0.88184	526	3

(Table Continued)

ID	sgRNA number	score	p-value	FDR	rank	goodsgrna
DSTYK	6	0.007061	0.023118	0.88184	527	2
EHD2	6	0.0071065	0.023216	0.88184	528	3
KATNB1	6	0.0071065	0.023216	0.88184	529	3
TMEM192	6	0.0071065	0.023216	0.88184	530	3
DIAPH2	6	0.0071065	0.023216	0.88184	531	3
ZAP70	6	0.0071065	0.023216	0.88184	532	3
NUP62	6	0.0071065	0.023216	0.88184	533	3
DCUN1D1	5	0.00713	0.020292	0.881703	534	2
ASB16	6	0.0071517	0.023312	0.88184	535	3
GCLM	6	0.0071517	0.023312	0.88184	536	2
RNF169	6	0.0073164	0.023669	0.88184	537	2
SOAT1	6	0.0073164	0.023669	0.88184	538	2
TRIO	6	0.0073164	0.023669	0.88184	539	3
DRAM1	6	0.0073164	0.023669	0.88184	540	2
SHF	6	0.0073164	0.023669	0.88184	541	2
MS4A4A	6	0.0073164	0.023669	0.88184	542	2
NonTargetingControlGuideForHuman_0451	1	0.0073845	0.0073424	0.824784	543	1
hsa-mir-6845	4	0.0073903	0.019948	0.872754	544	3
hsa-mir-5089	4	0.0074018	0.019985	0.872754	545	1
HBG1	6	0.0074127	0.023888	0.88184	546	3
SOWAHA	6	0.0074127	0.023888	0.88184	547	3
BAHD1	6	0.0074127	0.023888	0.88184	548	3
TNNT3	6	0.0074127	0.023888	0.88184	549	3
HIST1H1D	6	0.0074127	0.023888	0.88184	550	3
PUS7	6	0.007443	0.023951	0.88184	551	3
PPAPDC1B	6	0.0075672	0.024251	0.88184	552	1
ADAMTS17	6	0.0075672	0.024251	0.88184	553	2
MYO10	6	0.0075672	0.024251	0.88184	554	2
STAP1	6	0.0075672	0.024251	0.88184	555	1
ZNF649	6	0.0075672	0.024251	0.88184	556	2
CTAGE1	6	0.0075672	0.024251	0.88184	557	2
KANSL1L	6	0.0075672	0.024251	0.88184	558	1
FABP1	6	0.0075672	0.024251	0.88184	559	1
TRAM1L1	6	0.0075672	0.024251	0.88184	560	2
SYT4	6	0.0075672	0.024251	0.88184	561	2
SNX8	6	0.0075672	0.024251	0.88184	562	2
CELA2B	6	0.0075672	0.024251	0.88184	563	2
GOLM1	6	0.0075672	0.024251	0.88184	564	1
C17orf64	6	0.0075672	0.024251	0.88184	565	2
KIAA1239	6	0.0075672	0.024251	0.88184	566	3
PLEKHA6	6	0.0075672	0.024251	0.88184	567	1
KNTC1	6	0.0075672	0.024251	0.88184	568	1
FAM195A	6	0.0075672	0.024251	0.88184	569	1

(Table Continued)

ID	sgRNA number	score	p-value	FDR	rank	goodsgrna
NPR2	6	0.0075672	0.024251	0.88184	570	2
HIST3H2A	5	0.0075953	0.02137	0.881703	571	3
DOCK1	5	0.0075953	0.02137	0.881703	572	3
hsa-mir-4499	4	0.0076093	0.020512	0.881703	573	3
SLC12A7	6	0.0077079	0.024554	0.884664	574	3
hsa-mir-6780a	4	0.0078375	0.021055	0.881703	575	3
hsa-mir-1184-3	3	0.0079169	0.017641	0.86256	576	2
NonTargetingControlGuideForHuman_0873	1	0.0079791	0.0079613	0.824784	577	1
MRPL36	6	0.0079994	0.025197	0.884664	578	3
SARS2	6	0.0079994	0.025197	0.884664	579	3
SYT13	6	0.0079994	0.025197	0.884664	580	3
NDUFB3	6	0.0079994	0.025197	0.884664	581	3
hsa-mir-6823	4	0.008025	0.021503	0.881703	582	3
hsa-mir-3192	4	0.00819	0.021924	0.88184	583	2
ZNF410	6	0.0082197	0.025674	0.884664	584	3
CHTOP	6	0.0082197	0.025674	0.884664	585	3
MAP3K3	6	0.008271	0.025789	0.884664	586	2
hsa-mir-1184-1	4	0.0083089	0.022231	0.88184	587	2
hsa-mir-4262	4	0.0083089	0.022231	0.88184	588	2
TSNARE1	6	0.0083861	0.026042	0.884664	589	3
TDRD5	6	0.0083861	0.026042	0.884664	590	3
CC2D1B	6	0.0083967	0.026067	0.884664	591	1
NCKAP1	6	0.0084412	0.026158	0.884664	592	3
PAGE2B	3	0.0084662	0.018563	0.872754	593	2
GPN1	6	0.008472	0.026235	0.884664	594	1
TFB2M	5	0.0084916	0.023581	0.88184	595	2
LGALS2	6	0.0085748	0.026469	0.884664	596	3
C12orf56	6	0.0086053	0.026547	0.884664	597	2
ARMC7	6	0.0086053	0.026547	0.884664	598	3
NOP10	6	0.0086053	0.026547	0.884664	599	2
C4orf3	6	0.0086053	0.026547	0.884664	600	2
GNB1L	6	0.0086053	0.026547	0.884664	601	2
PDGFA	6	0.0086053	0.026547	0.884664	602	2
MARK1	6	0.0086053	0.026547	0.884664	603	3
SCAPER	6	0.0086053	0.026547	0.884664	604	3
NDUFB11	6	0.0086053	0.026547	0.884664	605	2
PRIM2	6	0.0086053	0.026547	0.884664	606	3
XRCC6	6	0.0086053	0.026547	0.884664	607	3
PPP3CB	6	0.0086053	0.026547	0.884664	608	2
AKT3	6	0.0086053	0.026547	0.884664	609	2
PSMB7	6	0.0086053	0.026547	0.884664	610	2
NEUROD6	6	0.0086053	0.026547	0.884664	611	2
NFS1	6	0.0086053	0.026547	0.884664	612	2

(Table Continued)

ID	sgRNA number	score	p-value	FDR	rank	goodsgrna
SMARCA4	6	0.0086053	0.026547	0.884664	613	2
CHPF2	6	0.0086053	0.026547	0.884664	614	2
NUAK2	6	0.0086053	0.026547	0.884664	615	2
PFN1	6	0.0086053	0.026547	0.884664	616	3
ZC3H18	6	0.0086053	0.026547	0.884664	617	3
GNB2L1	6	0.0086053	0.026547	0.884664	618	3
PIGS	6	0.0086053	0.026547	0.884664	619	3
ZNF569	6	0.0086053	0.026547	0.884664	620	2
SLC25A26	6	0.0086053	0.026547	0.884664	621	2
ABCB11	6	0.0086053	0.026547	0.884664	622	2
NELFB	6	0.0086053	0.026547	0.884664	623	2
NKAIN4	6	0.0086053	0.026547	0.884664	624	2
MRPS30	6	0.0086053	0.026547	0.884664	625	2
hsa-mir-3180-1	4	0.0087054	0.023213	0.88184	626	3
hsa-mir-5003	4	0.0087054	0.023213	0.88184	627	3
ZWINT	6	0.008711	0.026807	0.884664	628	3
TSSC1	6	0.008711	0.026807	0.884664	629	3
SIN3B	6	0.008711	0.026807	0.884664	630	3
COX17	6	0.008711	0.026807	0.884664	631	3
hsa-mir-5705	4	0.0089589	0.023835	0.88184	632	3
ATG4A	6	0.0089783	0.027427	0.884664	633	3
OR5M1	6	0.0090632	0.027622	0.884664	634	3
hsa-mir-6886	4	0.0091453	0.024299	0.88184	635	1
INS-IGF2	4	0.0091453	0.024299	0.88184	636	1
GJC1	6	0.0091606	0.027843	0.884664	637	3
hsa-mir-548q	4	0.0091935	0.024427	0.88184	638	2
hsa-mir-222	4	0.0091935	0.024427	0.88184	639	2
hsa-mir-5787	4	0.0091935	0.024427	0.88184	640	3
hsa-mir-542	4	0.0091935	0.024427	0.88184	641	2
CERS5	6	0.0091936	0.027909	0.884664	642	3
SLC5A10	6	0.0092255	0.027976	0.884664	643	1
ZFYVE27	6	0.0092255	0.027976	0.884664	644	2
RAB25	6	0.0092255	0.027976	0.884664	645	2
ATP1B3	6	0.0092255	0.027976	0.884664	646	2
BASP1	6	0.0092255	0.027976	0.884664	647	3
TWF1	6	0.0092255	0.027976	0.884664	648	2
LOC10028881 4	6	0.0092255	0.027976	0.884664	649	2
AAED1	6	0.0092255	0.027976	0.884664	650	2
MAP2K3	6	0.0092255	0.027976	0.884664	651	1
PPT2	6	0.0092255	0.027976	0.884664	652	1
C11orf42	6	0.0092255	0.027976	0.884664	653	1
CAPN11	6	0.0092255	0.027976	0.884664	654	2
MIB2	6	0.0092255	0.027976	0.884664	655	1
IL1A	6	0.0092255	0.027976	0.884664	656	2

(Table Continued)

ID	sgRNA number	score	p-value	FDR	rank	goodsgrna
TULP1	6	0.0092255	0.027976	0.884664	657	2
RBM46	6	0.0092255	0.027976	0.884664	658	1
TXN2	6	0.0092255	0.027976	0.884664	659	1
CYP17A1	6	0.0092255	0.027976	0.884664	660	1
RNF2	6	0.0092255	0.027976	0.884664	661	2
RNF207	6	0.0092255	0.027976	0.884664	662	2
FBF1	6	0.0092255	0.027976	0.884664	663	2
PARD3B	6	0.0092255	0.027976	0.884664	664	2
ACTR1A	5	0.0092437	0.025322	0.884664	665	2
ART5	5	0.0093962	0.025688	0.884664	666	2
XPO1	6	0.0095495	0.028714	0.901413	667	3
MAFF	6	0.0095495	0.028714	0.901413	668	3
TEX261	6	0.0095495	0.028714	0.901413	669	3
THOC1	5	0.0097088	0.026455	0.884664	670	2
hsa-mir-301b	4	0.0097151	0.025773	0.884664	671	3
PLCL2	6	0.0098485	0.029423	0.904137	672	2
hsa-mir-1273d	4	0.0098812	0.026189	0.884664	673	3
SLC30A2	6	0.0099097	0.029555	0.904137	674	3
RPS15A	6	0.0099097	0.029555	0.904137	675	3
C19orf70	6	0.0099097	0.029555	0.904137	676	3
HMGXB3	6	0.0099097	0.029555	0.904137	677	3
FAM8A1	6	0.0099097	0.029555	0.904137	678	3
PPID	6	0.0099097	0.029555	0.904137	679	3
RIOK1	6	0.0099097	0.029555	0.904137	680	3
CAMK4	6	0.0099284	0.029597	0.904137	681	1
TRIM35	6	0.010004	0.02975	0.904137	682	1
ZFYVE26	6	0.010054	0.029857	0.904137	683	2
hsa-mir-454	4	0.010062	0.026632	0.884664	684	3
hsa-mir-3182	4	0.010062	0.026632	0.884664	685	3
FOXD4L3	4	0.0101	0.026725	0.884664	686	2
TMEM207	6	0.010129	0.030025	0.904137	687	2
PCDHGB2	2	0.010227	0.019389	0.872754	688	2
FAM71E1	6	0.010229	0.030252	0.904137	689	1
hsa-mir-4419b	4	0.010267	0.027154	0.884664	690	2
PEX13	6	0.010275	0.030345	0.904137	691	3
RPUSD3	6	0.010386	0.030601	0.904137	692	3
CASP2	6	0.010386	0.030601	0.904137	693	3
SIGLEC9	6	0.010501	0.030876	0.904137	694	2
TMEM176B	6	0.010501	0.030876	0.904137	695	2
TSPAN2	6	0.010501	0.030876	0.904137	696	3
C11orf93	6	0.010501	0.030876	0.904137	697	3
MKS1	6	0.010501	0.030876	0.904137	698	3
ZFYVE28	6	0.010501	0.030876	0.904137	699	2
SLAMF6	6	0.010501	0.030876	0.904137	700	2
FAM90A1	6	0.010501	0.030876	0.904137	701	2

(Table Continued)

ID	sgRNA number	score	p-value	FDR	rank	goodsgrna
DGKK	6	0.010501	0.030876	0.904137	702	2
HFM1	6	0.010501	0.030876	0.904137	703	2
HSCB	6	0.010501	0.030876	0.904137	704	3
PAFAH1B1	4	0.010542	0.027847	0.884664	705	2
hsa-mir-1229	4	0.010542	0.027847	0.884664	706	2
PDP2	6	0.010545	0.03097	0.904137	707	3
C2orf78	5	0.010564	0.028488	0.898908	708	3
hsa-mir-4758	4	0.010594	0.027973	0.884664	709	3
NonTargetingControlGuideForHuman_0457	1	0.010598	0.010545	0.824784	710	1
hsa-mir-3198-2	4	0.010816	0.02851	0.898908	711	2
DNAJA4	6	0.010937	0.031801	0.904137	712	3
TRIM34	6	0.010937	0.031801	0.904137	713	3
PEA15	6	0.010937	0.031801	0.904137	714	3
NAT1	6	0.010937	0.031801	0.904137	715	3
FUT1	6	0.010937	0.031801	0.904137	716	3
PCDHB15	6	0.010937	0.031801	0.904137	717	3
hsa-mir-7-3	3	0.01108	0.023093	0.88184	718	1
OLFM4	6	0.011082	0.032135	0.904137	719	3
KNDC1	6	0.011082	0.032135	0.904137	720	1
RTN2	6	0.011082	0.032135	0.904137	721	1
EPB41L3	6	0.011082	0.032135	0.904137	722	2
LPIN3	6	0.011082	0.032135	0.904137	723	1
RIMKLA	6	0.011082	0.032135	0.904137	724	1
OSBPL8	6	0.011082	0.032135	0.904137	725	3
PLEKHS1	6	0.011082	0.032135	0.904137	726	1
TMEM222	6	0.011082	0.032135	0.904137	727	2
CLN8	6	0.011082	0.032135	0.904137	728	1
HSPB6	6	0.011082	0.032135	0.904137	729	2
AXDND1	6	0.011082	0.032135	0.904137	730	1
CRISP1	6	0.011082	0.032135	0.904137	731	1
WBP4	6	0.011082	0.032135	0.904137	732	1
GNAS	6	0.011082	0.032135	0.904137	733	2
CBLN4	6	0.011082	0.032135	0.904137	734	2
ZC4H2	6	0.011082	0.032135	0.904137	735	2
CENPN	6	0.011082	0.032135	0.904137	736	1
USPL1	6	0.011082	0.032135	0.904137	737	1
LIMCH1	6	0.011082	0.032135	0.904137	738	1
HMHA1	6	0.011082	0.032135	0.904137	739	1
TTC25	6	0.011082	0.032135	0.904137	740	2
ZSWIM4	6	0.011082	0.032135	0.904137	741	3
KRT15	6	0.011082	0.032135	0.904137	742	2
KIAA0907	6	0.011082	0.032135	0.904137	743	2
DNAJB8	6	0.011082	0.032135	0.904137	744	1

(Table Continued)

ID	sgRNA number	score	p-value	FDR	rank	goodsgrna
PDE10A	6	0.011089	0.032148	0.904137	745	2
ABCA2	6	0.011089	0.032148	0.904137	746	3
INTS3	5	0.011098	0.029758	0.904137	747	3
hsa-mir-3673	2	0.011233	0.021253	0.881703	748	2
MMP24	6	0.01129	0.03261	0.904137	749	3
SPATA31D4	2	0.011304	0.021392	0.881703	750	1
KIR2DL1	6	0.011384	0.03281	0.904137	751	2
ABAT	6	0.011384	0.03281	0.904137	752	3
OR6C4	6	0.011384	0.03281	0.904137	753	2
ZNF581	6	0.011384	0.03281	0.904137	754	2
ATP6V1D	6	0.011384	0.03281	0.904137	755	2
TCP1	6	0.011384	0.03281	0.904137	756	2
LMOD3	6	0.011384	0.03281	0.904137	757	3
FNDC3B	6	0.011384	0.03281	0.904137	758	3
CCNE2	6	0.011384	0.03281	0.904137	759	3
TBCC	5	0.011419	0.030501	0.904137	760	1
HAO1	5	0.011419	0.030501	0.904137	761	2
NLRP11	6	0.011482	0.033007	0.904137	762	3
SEMG1	6	0.011482	0.033007	0.904137	763	3
CFHR1	6	0.011482	0.033007	0.904137	764	3
GOLGA7B	6	0.011482	0.033007	0.904137	765	3
MED9	6	0.011482	0.033007	0.904137	766	3
KPNA6	6	0.011482	0.033007	0.904137	767	3
hsa-mir-4539	4	0.011489	0.030165	0.904137	768	1
FAM5B	4	0.011489	0.030165	0.904137	769	1
FAM86B2	2	0.011514	0.021777	0.88184	770	1
hsa-mir-4769	4	0.011579	0.030394	0.904137	771	3
hsa-mir-6739	4	0.011579	0.030394	0.904137	772	3
hsa-mir-4485	4	0.011579	0.030394	0.904137	773	3
hsa-mir-4638	4	0.011579	0.030394	0.904137	774	3
hsa-mir-3123	4	0.011579	0.030394	0.904137	775	3
hsa-mir-6080	4	0.011579	0.030394	0.904137	776	3
MYBPC2	6	0.01165	0.03338	0.904137	777	2
ZFR2	6	0.011708	0.033496	0.904137	778	3
NDOR1	6	0.011708	0.033496	0.904137	779	3
HOOK2	6	0.011708	0.033496	0.904137	780	3
KRT16	6	0.011708	0.033496	0.904137	781	3
PRL	6	0.011708	0.033496	0.904137	782	3
SAR1A	6	0.011708	0.033496	0.904137	783	3
TCAP	6	0.011708	0.033496	0.904137	784	3
NUS1	6	0.011869	0.033865	0.904137	785	2
CLCA4	6	0.011869	0.033865	0.904137	786	2
NAALADL2	6	0.011869	0.033865	0.904137	787	2
SCAP	6	0.011869	0.033865	0.904137	788	2
MAF	6	0.011909	0.033945	0.904137	789	1

(Table Continued)

ID	sgRNA number	score	p-value	FDR	rank	goodsgrna
CAPN12	6	0.01191	0.033946	0.904137	790	3
DYNLRB1	5	0.01191	0.031639	0.904137	791	3
ARL2	6	0.012031	0.034222	0.904137	792	2
GPR89A	6	0.01206	0.03428	0.904137	793	3
SAMD13	6	0.01206	0.03428	0.904137	794	1
ZDHHC23	6	0.01206	0.03428	0.904137	795	3
POF1B	6	0.01206	0.03428	0.904137	796	2
CCDC115	6	0.012086	0.034339	0.904137	797	3
PRDM8	6	0.01216	0.034499	0.904137	798	2
MDGA1	6	0.01221	0.034606	0.904137	799	2
UBA5	6	0.012287	0.034776	0.904137	800	3
CTNND2	6	0.012287	0.034776	0.904137	801	3
GSN	6	0.012287	0.034776	0.904137	802	3
NPPC	6	0.012287	0.034776	0.904137	803	3
NFYC	6	0.012287	0.034776	0.904137	804	3
LRRC32	6	0.012397	0.035052	0.904137	805	2
RNF19B	6	0.012397	0.035052	0.904137	806	2
TMEM81	6	0.012397	0.035052	0.904137	807	2
SLC25A23	6	0.012397	0.035052	0.904137	808	2
NCAPH2	5	0.012399	0.032773	0.904137	809	2
hsa-mir-1247	4	0.012461	0.032558	0.904137	810	2
GADD45A	6	0.01251	0.035313	0.904137	811	1
DPF1	6	0.01251	0.035313	0.904137	812	1
STXBP2	6	0.01251	0.035313	0.904137	813	1
GALNT1	6	0.01251	0.035313	0.904137	814	1
BRMS1L	6	0.01251	0.035313	0.904137	815	1
DBF4B	6	0.01251	0.035313	0.904137	816	1
SHROOM3	6	0.01251	0.035313	0.904137	817	1
ANKRD33	6	0.01251	0.035313	0.904137	818	1
PPP2R1B	6	0.01251	0.035313	0.904137	819	2
CD4	5	0.012518	0.033037	0.904137	820	2
EPHX4	6	0.012569	0.035448	0.904137	821	2
CMC1	6	0.012569	0.035448	0.904137	822	2
ABTB1	6	0.012569	0.035448	0.904137	823	2
C2CD4D	6	0.012569	0.035448	0.904137	824	2
CMTM1	4	0.012575	0.032829	0.904137	825	2
NUDT14	6	0.01269	0.035699	0.904137	826	2
KRTAP9-7	6	0.01269	0.035699	0.904137	827	2
CLUL1	6	0.012751	0.035843	0.904137	828	3
PFDN2	6	0.012754	0.035848	0.904137	829	3
MCM3AP	6	0.012844	0.036059	0.904137	830	3
SPATA31A5	2	0.012888	0.024312	0.88184	831	1
IARS	6	0.012973	0.036349	0.904137	832	2
MFF	6	0.012973	0.036349	0.904137	833	2
CAMTA2	6	0.012973	0.036349	0.904137	834	3

(Table Continued)

ID	sgRNA number	score	p-value	FDR	rank	goodsgrna
NonTargetingControlGuideForHuman_0581	1	0.013057	0.012982	0.824784	835	1
AK6	6	0.013126	0.036696	0.904137	836	3
MED27	5	0.013298	0.034805	0.904137	837	3
MAT2A	6	0.013331	0.037151	0.904137	838	3
CHRNA2	6	0.013331	0.037151	0.904137	839	2
HSF2	6	0.013331	0.037151	0.904137	840	2
CIAO1	6	0.013331	0.037151	0.904137	841	2
PMP22	6	0.013359	0.03721	0.904137	842	3
KISS1R	6	0.013526	0.037581	0.904137	843	3
ZNF511	6	0.013526	0.037581	0.904137	844	3
EPHA6	6	0.013606	0.037757	0.904137	845	2
MS4A7	6	0.013606	0.037757	0.904137	846	2
SPO11	6	0.013606	0.037757	0.904137	847	2
LRRC56	6	0.013687	0.037954	0.904137	848	1
RAB38	6	0.013687	0.037954	0.904137	849	1
TNIK	6	0.013687	0.037954	0.904137	850	1
DDX6	6	0.013687	0.037954	0.904137	851	2
HS6ST3	6	0.013687	0.037954	0.904137	852	2
CITED4	6	0.013687	0.037954	0.904137	853	1
NRP2	6	0.013687	0.037954	0.904137	854	2
ARID2	6	0.013687	0.037954	0.904137	855	3
AGMO	6	0.013687	0.037954	0.904137	856	1
NEFM	6	0.013687	0.037954	0.904137	857	2
TMEM128	6	0.013687	0.037954	0.904137	858	2
PPP6R2	6	0.013687	0.037954	0.904137	859	2
UGGT2	6	0.013687	0.037954	0.904137	860	2
DROSHA	6	0.013687	0.037954	0.904137	861	2
PRR14L	6	0.013687	0.037954	0.904137	862	2
LIPE	6	0.013687	0.037954	0.904137	863	2
GFRA3	6	0.013687	0.037954	0.904137	864	1
ZNF160	6	0.013687	0.037954	0.904137	865	1
CCNYL1	6	0.013687	0.037954	0.904137	866	1
DFNA5	6	0.013687	0.037954	0.904137	867	1
XPNPEP3	6	0.013687	0.037954	0.904137	868	2
ARHGAP21	6	0.013687	0.037954	0.904137	869	2
REM2	6	0.013687	0.037954	0.904137	870	1
APBB3	6	0.013687	0.037954	0.904137	871	1
RBM39	6	0.013687	0.037954	0.904137	872	2
NCCRP1	6	0.013687	0.037954	0.904137	873	1
PADI2	6	0.013715	0.038013	0.904137	874	2
CENPC1	4	0.013733	0.035123	0.904137	875	2
TACR1	6	0.013799	0.038204	0.904137	876	2
ALX1	6	0.013799	0.038204	0.904137	877	3

(Table Continued)

ID	sgRNA number	score	p-value	FDR	rank	goodsgrna
RNF223	6	0.013816	0.038234	0.904137	878	3
TNKS1BP1	6	0.013816	0.038234	0.904137	879	3
CLMP	6	0.013816	0.038234	0.904137	880	3
IER5L	6	0.01411	0.0389	0.904137	881	3
C9orf96	6	0.014178	0.039056	0.904137	882	3
IMP3	6	0.014253	0.039213	0.904137	883	2
DPP3	6	0.014253	0.039213	0.904137	884	2
HERC1	6	0.014253	0.039213	0.904137	885	2
RAB21	6	0.014253	0.039213	0.904137	886	2
YARS	6	0.014253	0.039213	0.904137	887	2
EML3	6	0.014253	0.039213	0.904137	888	2
RNF122	6	0.014253	0.039213	0.904137	889	2
AP2A1	6	0.014253	0.039213	0.904137	890	2
CASP8	6	0.014253	0.039213	0.904137	891	2
GAB2	6	0.014253	0.039213	0.904137	892	2
ACD	6	0.014253	0.039213	0.904137	893	2
LOC10050746 2	5	0.01434	0.037243	0.904137	894	1
KRTDAP	5	0.01434	0.037243	0.904137	895	1
DDX59	5	0.01434	0.037243	0.904137	896	3
CXXC1	6	0.014508	0.039789	0.904137	897	3
DUSP14	6	0.014508	0.039789	0.904137	898	3
ATXN7L1	6	0.014508	0.039789	0.904137	899	3
GABRR2	6	0.014508	0.039789	0.904137	900	3
PIAS4	6	0.014508	0.039789	0.904137	901	3
ZW10	6	0.014508	0.039789	0.904137	902	3
HSH2D	6	0.014508	0.039789	0.904137	903	3
ZDHHC8	6	0.014508	0.039789	0.904137	904	3
ATP6AP2	6	0.014508	0.039789	0.904137	905	3
SLC30A5	4	0.014746	0.036786	0.904137	906	1
hsa-mir-4773-1	4	0.014746	0.036786	0.904137	907	1
hsa-mir-7151	4	0.014746	0.036786	0.904137	908	1
hsa-mir-5195	4	0.014746	0.036786	0.904137	909	1
hsa-mir-200b	4	0.014746	0.036786	0.904137	910	2
TRRAP	4	0.014763	0.036817	0.904137	911	2
hsa-mir-4632	4	0.014763	0.036817	0.904137	912	2
hsa-mir-548f-2	4	0.014763	0.036817	0.904137	913	2
INPP5J	6	0.014812	0.040403	0.904137	914	2
SLAMF8	6	0.014812	0.040403	0.904137	915	1
ATOH1	6	0.014812	0.040403	0.904137	916	2
SLC28A2	6	0.014812	0.040403	0.904137	917	3
FAM126A	5	0.014914	0.038603	0.904137	918	3
CAPSL	5	0.014914	0.038603	0.904137	919	2
CHRNA10	6	0.014942	0.040688	0.904137	920	3
TSGA10IP	6	0.014942	0.040688	0.904137	921	3

(Table Continued)

ID	sgRNA number	score	p-value	FDR	rank	goodsgrna
ADSL	6	0.015012	0.040839	0.904137	922	1
SSC5D	6	0.015053	0.040924	0.904137	923	3
CXorf27	6	0.015112	0.041054	0.904137	924	1
CDC16	6	0.015361	0.041601	0.904137	925	3
UBE2QL1	6	0.015361	0.041601	0.904137	926	1
SLC9A3R2	6	0.015361	0.041601	0.904137	927	2
HNF1A	6	0.015361	0.041601	0.904137	928	1
LRRC57	6	0.015364	0.041604	0.904137	929	3
ALDH16A1	6	0.015391	0.041679	0.904137	930	3
RAP2A	6	0.015391	0.041679	0.904137	931	2
AMMECR1L	6	0.015391	0.041679	0.904137	932	2
GUK1	6	0.015391	0.041679	0.904137	933	2
SLC39A10	6	0.015391	0.041679	0.904137	934	2
GNA15	6	0.015391	0.041679	0.904137	935	2
NEDD8	6	0.015391	0.041679	0.904137	936	2
ZNF430	6	0.015391	0.041679	0.904137	937	2
RAB1A	6	0.015391	0.041679	0.904137	938	3
TMBIM1	6	0.015391	0.041679	0.904137	939	2
KATNAL2	6	0.015391	0.041679	0.904137	940	2
RASA4B	2	0.01551	0.02908	0.904137	941	1
hsa-mir-1255b-1	2	0.01551	0.02908	0.904137	942	1
FURIN	6	0.01553	0.041985	0.904137	943	3
STRN4	6	0.015749	0.042477	0.904137	944	3
PKLR	6	0.015749	0.042477	0.904137	945	3
PFAS	6	0.015749	0.042477	0.904137	946	3
OPN4	6	0.015749	0.042477	0.904137	947	3
SP2	6	0.015749	0.042477	0.904137	948	3
hsa-mir-548h-1	4	0.01585	0.038521	0.904137	949	2
BIVM-ERCC5	2	0.01592	0.029821	0.904137	950	1
DNHD1	6	0.015971	0.042978	0.904137	951	3
CYSLTR2	6	0.015971	0.042978	0.904137	952	3
IGFL1	6	0.015971	0.042978	0.904137	953	3
SLC25A47	6	0.015971	0.042978	0.904137	954	3
SENP5	6	0.015971	0.042978	0.904137	955	3
TNNI3	5	0.015986	0.041122	0.904137	956	1
DDX28	6	0.016052	0.043144	0.904137	957	2
RHOC	6	0.016052	0.043144	0.904137	958	2
MPV17L2	6	0.01614	0.043321	0.904137	959	3
SLAMF1	6	0.01614	0.043321	0.904137	960	3
ST3GAL1	6	0.01614	0.043321	0.904137	961	3
MSL2	6	0.01614	0.043321	0.904137	962	3
HGC6.3	6	0.01614	0.043321	0.904137	963	3
CEP192	5	0.016238	0.041726	0.904137	964	3
OSBPL9	4	0.016241	0.039162	0.904137	965	2

(Table Continued)

ID	sgRNA number	score	p-value	FDR	rank	goodsgrna
B4GALT5	6	0.016289	0.043633	0.904137	966	3
DAND5	6	0.01634	0.043747	0.904137	967	3
C6orf203	6	0.01634	0.043747	0.904137	968	2
PAFAH1B3	6	0.016349	0.043767	0.904137	969	3
AURKA	6	0.0164	0.043878	0.904137	970	3
NEDD8-MDP1	3	0.016519	0.032378	0.904137	971	2
PRKRIP1	6	0.016538	0.044189	0.904137	972	2
HLA-DQB1	6	0.016538	0.044189	0.904137	973	3
ACOT9	6	0.016538	0.044189	0.904137	974	2
TRABD	6	0.016653	0.044451	0.904137	975	2
NME7	5	0.01673	0.042883	0.904137	976	3
PTPMT1	6	0.016743	0.044648	0.904137	977	3
UCKL1	6	0.016743	0.044648	0.904137	978	3
GPAT2	6	0.016743	0.044648	0.904137	979	3
RHOA	6	0.016743	0.044648	0.904137	980	3
PDE6B	6	0.016743	0.044648	0.904137	981	3
PSMA3	6	0.016743	0.044648	0.904137	982	3
SH3BGRL	6	0.016743	0.044648	0.904137	983	3
PIFO	6	0.016743	0.044648	0.904137	984	3
AKAP13	6	0.016743	0.044648	0.904137	985	3
EIF3I	5	0.016757	0.042947	0.904137	986	2
C19orf57	6	0.01683	0.044829	0.904137	987	2
OCLN	6	0.01683	0.044829	0.904137	988	2
PGLYRP2	6	0.01683	0.044829	0.904137	989	3
OSBPL3	6	0.01683	0.044829	0.904137	990	2
OR52K1	6	0.01683	0.044829	0.904137	991	2
NEU3	6	0.01683	0.044829	0.904137	992	2
GRIK3	6	0.01683	0.044829	0.904137	993	2
SLC52A3	5	0.017068	0.043659	0.904137	994	2
PSMG2	5	0.017068	0.043659	0.904137	995	2
OR13G1	6	0.017077	0.045356	0.904137	996	3
WNT2B	6	0.017125	0.045454	0.904137	997	3
MTERFD1	6	0.017164	0.045537	0.904137	998	3
RAMP3	6	0.017164	0.045537	0.904137	999	3
hsa-mir-548aw	4	0.017177	0.040651	0.904137	1000	2

Table A2. Top 1000 disrupted genes negatively selected by cisplatin

ID	sgRNA num	score	p-value	FDR	rank	goodsgrna
ZNRF3	6	3.08E-11	2.29E-07	0.00165	1	6
RNF7	6	3.26E-11	2.29E-07	0.00165	2	6
UBE2F	6	3.04E-08	2.29E-07	0.00165	3	5
HES1	6	2.53E-07	1.14E-06	0.006188	4	6
CUL3	6	5.76E-07	2.97E-06	0.012871	5	4
UBE2J1	6	3.75E-06	1.76E-05	0.063531	6	6
JUNB	6	5.93E-06	3.36E-05	0.10396	7	6
CUL5	6	1.56E-05	9.26E-05	0.222772	8	4
AMBRA1	6	1.94E-05	0.00011359	0.238974	9	5
GPRC5B	6	2.07E-05	0.00012136	0.238974	10	5
CD4	5	2.11E-05	8.71E-05	0.222772	11	1
ADAMTS18	5	3.34E-05	0.00014604	0.263614	12	4
BRPF1	6	4.19E-05	0.00023746	0.367397	13	3
COPS8	6	4.82E-05	0.00026671	0.381498	14	6
TMEM55A	6	5.21E-05	0.00028179	0.381498	15	6
hsa-mir-215	4	6.28E-05	0.00023289	0.367397	16	3
MMAA	6	7.59E-05	0.00040475	0.487074	17	3
HOXC5	6	8.31E-05	0.00044543	0.507544	18	5
hsa-mir-361	4	8.43E-05	0.00032293	0.411474	19	1
HRASLS	6	8.96E-05	0.0004852	0.507544	20	4
NDUFAF2	6	9.11E-05	0.00049206	0.507544	21	6
MCCC1	6	9.82E-05	0.00053914	0.507749	22	5
LRRIQ4	6	0.00011396	0.0006237	0.562913	23	5
ATXN2	6	0.00011985	0.00065158	0.564554	24	6
SLC26A4	6	0.00012932	0.00070643	0.588538	25	4
hsa-mir-6750	4	0.00013349	0.00052085	0.507749	26	2
PLEKHA7	6	0.00014498	0.00079236	0.598447	27	5
KLC3	6	0.00014684	0.00080242	0.598447	28	3
WAPAL	6	0.00014707	0.00080333	0.598447	29	5
ADAMTS6	6	0.00017711	0.00096926	0.598447	30	1
SLC38A11	6	0.00017804	0.000972	0.598447	31	4
SYNGR4	6	0.00018004	0.00098068	0.598447	32	3
CCDC11	6	0.00019223	0.0010337	0.598447	33	6
OR5D14	6	0.00019584	0.001052	0.598447	34	6
HOXA6	6	0.00020117	0.001079	0.598447	35	5
NF2	6	0.00020595	0.0011041	0.598447	36	4
ZNF607	6	0.00020861	0.0011164	0.598447	37	6
CEBPE	6	0.00021297	0.0011356	0.598447	38	3
PLRG1	6	0.00021527	0.001148	0.598447	39	3
SCAF4	6	0.00021647	0.0011525	0.598447	40	4
WNT4	6	0.00021915	0.0011704	0.598447	41	3
NLRP6	6	0.00022771	0.0012115	0.598447	42	2
PHF21A	6	0.00022905	0.0012156	0.598447	43	5

(Table Continued)

ID	sgRNA num	score	p-value	FDR	rank	goodsgrna
SUDS3	6	0.00027444	0.0014757	0.678321	44	5
LATS2	6	0.00027831	0.0014917	0.678321	45	3
OAT	6	0.00029896	0.0015978	0.692439	46	4
hsa-mir-4694	4	0.00030022	0.0011352	0.598447	47	3
SLC1A7	6	0.00031183	0.0016595	0.692439	48	4
WDHD1	5	0.00031804	0.0014922	0.678321	49	3
OR4S2	6	0.0003205	0.0017093	0.692439	50	5
DNAJA2	6	0.00032461	0.0017335	0.692439	51	6
RBX1	6	0.00032885	0.0017545	0.692439	52	5
SLC6A4	6	0.00032988	0.0017582	0.692439	53	4
PIK3R4	6	0.00037709	0.0020059	0.705925	54	6
WRN	6	0.0003795	0.002016	0.705925	55	2
C6orf222	6	0.00038034	0.0020206	0.705925	56	5
KIF21A	6	0.00038034	0.0020206	0.705925	57	3
C2orf54	5	0.00039566	0.0018272	0.705925	58	4
ORC3	6	0.000404	0.0021339	0.730759	59	5
RFWD2	6	0.00041473	0.0021901	0.730759	60	6
REXO1L1	6	0.00042091	0.0022249	0.730759	61	4
GFRA3	6	0.00042575	0.0022454	0.730759	62	3
STAC3	6	0.00043009	0.002266	0.730759	63	3
GOLGA8B	4	0.00043263	0.0016215	0.692439	64	2
PHF23	6	0.00045286	0.0023794	0.730759	65	6
TNFRSF8	6	0.00045455	0.0023858	0.730759	66	4
KLHDC2	6	0.000468	0.002447	0.730759	67	5
NXPE2	6	0.00047117	0.0024616	0.730759	68	3
PTPN14	6	0.00047277	0.002468	0.730759	69	5
KIAA1524	6	0.00048029	0.0025037	0.730759	70	5
HIGD1A	6	0.00048068	0.002506	0.730759	71	5
NUDT11	6	0.00048613	0.0025302	0.730759	72	5
GPR75-ASB3	3	0.00051864	0.0015031	0.678321	73	3
RGP1	6	0.00052965	0.0027766	0.741982	74	5
hsa-mir-6069	4	0.00053025	0.0019831	0.705925	75	4
ADAM17	6	0.00055267	0.0028945	0.741982	76	6
C12orf60	6	0.00055536	0.0029069	0.741982	77	6
OR10H2	6	0.00055713	0.0029142	0.741982	78	2
RAI2	6	0.00056409	0.0029548	0.741982	79	6
DMXL1	6	0.00058119	0.0030454	0.741982	80	4
UTP15	6	0.00059099	0.0030897	0.741982	81	2
MAPK14	6	0.00059129	0.003092	0.741982	82	6
KRTAP19-7	6	0.00059341	0.0031039	0.741982	83	6
TAOK1	6	0.00059481	0.0031137	0.741982	84	6
AACS	6	0.00060253	0.0031496	0.741982	85	6
ACVR2A	6	0.00060297	0.0031514	0.741982	86	5
GPR75	5	0.00062128	0.0028406	0.741982	87	5
PPP1CB	6	0.00063165	0.0032885	0.744046	88	4

(Table Continued)

ID	sgRNA num	score	p-value	FDR	rank	goodsgrna
GPRC6A	6	0.00063794	0.0033159	0.744046	89	2
FUBP1	5	0.00063902	0.0029233	0.741982	90	4
GDPD4	6	0.00064526	0.003353	0.744046	91	4
TMPRSS7	6	0.00064636	0.0033562	0.744046	92	5
CSK	6	0.00065653	0.003401	0.744046	93	5
LAMTOR5	5	0.00066374	0.0030435	0.741982	94	4
HMGA2	6	0.00067206	0.0034796	0.744046	95	5
PARP14	6	0.00067294	0.0034846	0.744046	96	6
TEX38	6	0.00068833	0.0035545	0.744046	97	2
CDIP1	6	0.00069893	0.0036176	0.744046	98	3
HSP90AB1	6	0.00070977	0.003667	0.744046	99	5
DAGLB	6	0.00071007	0.0036693	0.744046	100	5
NDEL1	6	0.00071298	0.0036862	0.744046	101	4
PIGC	6	0.00071298	0.0036862	0.744046	102	4
GPX7	6	0.00071876	0.0037154	0.744046	103	5
LCN2	6	0.00072562	0.0037488	0.744046	104	5
CD1C	6	0.00073179	0.0037803	0.744046	105	3
OSGEP	6	0.00073359	0.0037863	0.744046	106	4
EIF2AK3	6	0.00074887	0.0038571	0.745978	107	6
THNSL2	6	0.00076497	0.003928	0.752957	108	6
FAHD2A	6	0.00078416	0.0040281	0.758717	109	4
KANSL1	6	0.0007995	0.0041044	0.759952	110	4
hsa-mir-583	4	0.00083163	0.0030746	0.741982	111	3
PTPRH	6	0.00083474	0.0042772	0.759952	112	3
NPFF	6	0.00085263	0.0043787	0.759952	113	3
AMPH	6	0.00085263	0.0043787	0.759952	114	3
C1orf168	6	0.0008605	0.0044166	0.759952	115	6
TMEM14B	6	0.0008605	0.0044166	0.759952	116	6
FNDC4	6	0.00086817	0.0044518	0.759952	117	4
KIF12	6	0.00086894	0.004455	0.759952	118	6
ENTPD3	6	0.00088531	0.0045473	0.759952	119	2
FRYL	6	0.00090619	0.0046424	0.759952	120	4
RANBP1	6	0.00090865	0.0046552	0.759952	121	4
MAGEA11	6	0.00090868	0.0046552	0.759952	122	4
ZBTB37	6	0.00090868	0.0046552	0.759952	123	4
SNRPC	4	0.00091221	0.0033708	0.744046	124	4
LRRFIP2	6	0.00091828	0.0047009	0.759952	125	5
UBL7	6	0.00092213	0.0047169	0.759952	126	6
PBK	6	0.00092984	0.0047576	0.759952	127	5
STARD3	6	0.00093424	0.0047805	0.759952	128	6
IL12A	6	0.00093572	0.0047891	0.759952	129	4
KLHL8	6	0.00093588	0.0047891	0.759952	130	4
RASL10A	6	0.0009471	0.0048376	0.759952	131	4
EPPIN	6	0.00095996	0.0049002	0.759952	132	5
KLK12	6	0.0009781	0.0049784	0.759952	133	5

(Table Continued)

ID	sgRNA num	score	p-value	FDR	rank	goodsgrna
ARRDC3	6	0.00097996	0.0049866	0.759952	134	5
SAT1	6	0.00098644	0.005014	0.759952	135	4
CCND1	6	0.0009895	0.0050314	0.759952	136	4
KY	6	0.00099745	0.0050753	0.759952	137	3
FAM65C	6	0.0009999	0.0050872	0.759952	138	6
CCDC17	6	0.0010151	0.0051571	0.765123	139	6
hsa-mir-3689c	2	0.0010372	0.0019634	0.705925	140	1
hsa-mir-643	4	0.0010382	0.0038128	0.744046	141	2
CHPT1	6	0.0010853	0.0054958	0.777139	142	3
HNRNPA1	6	0.0010853	0.0054958	0.777139	143	3
MS4A6A	6	0.0010876	0.0055077	0.777139	144	3
TCEB3	5	0.0011241	0.0050113	0.759952	145	4
AGMO	6	0.0011381	0.0057198	0.777139	146	3
GPR132	6	0.0011499	0.0057659	0.777139	147	5
TMEM67	6	0.0011566	0.0057934	0.777139	148	2
NFE2	6	0.0011566	0.0057934	0.777139	149	2
TDRKH	6	0.0011566	0.0057934	0.777139	150	2
CD5L	6	0.0011566	0.0057934	0.777139	151	3
SCARA3	6	0.0011566	0.0057934	0.777139	152	3
DTHD1	6	0.0011682	0.0058427	0.777139	153	5
C1orf53	5	0.001173	0.0052119	0.768	154	4
hsa-let-7f-1	4	0.0011751	0.0043179	0.759952	155	3
ARR3	6	0.0011887	0.00592	0.777139	156	3
RNGTT	6	0.0011972	0.0059597	0.777139	157	4
TCP1	6	0.0012142	0.0060274	0.777139	158	3
RAB5B	6	0.0012142	0.0060274	0.777139	159	5
ARSF	6	0.0012142	0.0060274	0.777139	160	3
PRPF18	6	0.0012142	0.0060274	0.777139	161	3
GOLPH3	6	0.0012333	0.006101	0.781973	162	5
DOCK5	6	0.0012482	0.0061641	0.784682	163	5
C12orf43	6	0.0012645	0.0062308	0.784682	164	2
HPRT1	6	0.0012645	0.0062308	0.784682	165	3
ARNT	6	0.0012755	0.0062733	0.785469	166	3
PDE4C	6	0.0012967	0.0063579	0.791372	167	4
KIAA1598	6	0.0013064	0.0063935	0.791372	168	3
hsa-mir-3137	4	0.00133	0.0048728	0.759952	169	2
LYSMD2	6	0.0013404	0.0065105	0.801277	170	3
CDH2	6	0.0013909	0.0067066	0.820747	171	5
ENTPD5	6	0.0014069	0.0067747	0.824424	172	3
RD3	6	0.0014415	0.006921	0.837141	173	1
ICK	6	0.0014704	0.0070165	0.837141	174	4
C14orf182	6	0.0014895	0.0071002	0.837141	175	3
ZNF696	6	0.001492	0.0071112	0.837141	176	2
ERCC8	6	0.0015541	0.0073571	0.837141	177	4
hsa-mir-16-1	4	0.0015657	0.0057271	0.777139	178	4

(Table Continued)

ID	sgRNA num	score	p-value	FDR	rank	goodsgrna
LRRC4B	6	0.0015678	0.0074137	0.837141	179	3
ANKRD35	6	0.0015754	0.0074526	0.837141	180	5
GALK2	6	0.0015782	0.0074617	0.837141	181	5
ROS1	6	0.0015817	0.00748	0.837141	182	4
FAM133B	6	0.0015817	0.00748	0.837141	183	4
LTA4H	6	0.0015999	0.0075362	0.837141	184	5
SF1	6	0.0015999	0.0075362	0.837141	185	4
PLEKHM1	6	0.0015999	0.0075362	0.837141	186	4
GRAMD2	6	0.0015999	0.0075362	0.837141	187	4
MIF	6	0.0015999	0.0075362	0.837141	188	4
hsa-mir-3923	4	0.0016223	0.0059214	0.777139	189	3
hsa-mir-1237	4	0.0016348	0.0059634	0.777139	190	3
ASB5	6	0.0016363	0.0076926	0.844274	191	5
TPM4	6	0.0016436	0.0077232	0.844274	192	1
EIF4EBP1	6	0.0016673	0.0078146	0.844274	193	4
CLP1	6	0.0016856	0.0078864	0.844274	194	3
YARS	6	0.0016856	0.0078864	0.844274	195	3
AP1S2	6	0.0016856	0.0078864	0.844274	196	3
KDM4A	6	0.0016942	0.0079271	0.844274	197	2
ZNF708	6	0.0017053	0.0079645	0.844274	198	5
MYL6	6	0.0017486	0.0081309	0.844274	199	4
VSX2	6	0.0017509	0.0081423	0.844274	200	4
OR5AR1	6	0.0017509	0.0081423	0.844274	201	5
RRP8	6	0.0018177	0.0084166	0.844274	202	3
POLR1D	6	0.0018289	0.0084646	0.844274	203	4
ZBTB40	6	0.0018333	0.0084788	0.844274	204	2
TMEM99	6	0.001838	0.0085007	0.844274	205	4
KCNMB4	6	0.0018458	0.0085359	0.844274	206	2
LYPD1	6	0.0018458	0.0085359	0.844274	207	2
DGKB	6	0.0018458	0.0085359	0.844274	208	2
NISCH	6	0.0018667	0.0086205	0.844774	209	5
SLC25A15	6	0.0018837	0.0086945	0.844774	210	4
OR5K4	6	0.0018897	0.0087206	0.844774	211	4
EGFL7	6	0.0018971	0.0087535	0.844774	212	4
NR2C1	6	0.0019468	0.0089555	0.846615	213	2
BRIP1	6	0.0019532	0.0089838	0.846615	214	5
CLRN1	6	0.0019631	0.0090282	0.846615	215	4
DDX5	6	0.0019883	0.0091233	0.846615	216	4
PDHA2	6	0.0019954	0.0091489	0.846615	217	2
KIAA1671	6	0.0019973	0.0091562	0.846615	218	1
LACTB2	6	0.0020479	0.0093504	0.846615	219	1
CATSPER2	6	0.002048	0.0093518	0.846615	220	5
SPG11	6	0.0020529	0.0093715	0.846615	221	5
UVRAG	6	0.0020529	0.0093715	0.846615	222	5
TGFBR2	6	0.0020569	0.0093865	0.846615	223	5

(Table Continued)

ID	sgRNA num	score	p-value	FDR	rank	goodsgrna
PUS7L	6	0.0020922	0.0095122	0.846615	224	5
MLLT1	6	0.0020964	0.0095282	0.846615	225	5
SMR3A	6	0.0021088	0.0095685	0.846615	226	5
ATAD1	6	0.0021236	0.0096197	0.846615	227	2
CCT5	6	0.0021236	0.0096197	0.846615	228	3
PTEN	5	0.0021259	0.0092951	0.846615	229	3
PALMD	5	0.0021279	0.0093029	0.846615	230	2
GPRIN2	6	0.0021336	0.0096539	0.846615	231	4
STAT3	6	0.0021523	0.0097312	0.849948	232	4
hsa-mir-3169	4	0.0021912	0.0079399	0.844274	233	1
HECW1	6	0.0021994	0.0099158	0.858382	234	3
HIST1H2AI	6	0.0022219	0.010002	0.858382	235	2
TEX26	6	0.0022499	0.010113	0.858382	236	4
AQP7	6	0.0022646	0.010168	0.858382	237	4
ZNF518B	6	0.0022793	0.010223	0.858382	238	5
HNRNPU	6	0.0022793	0.010223	0.858382	239	5
FTL	6	0.0022793	0.010223	0.858382	240	5
ZNF721	6	0.0022793	0.010223	0.858382	241	5
STYK1	6	0.0023004	0.010297	0.858382	242	2
ZNF280A	6	0.0023039	0.010314	0.858382	243	3
hsa-mir-3162	4	0.002308	0.008343	0.844274	244	2
CDRT1	6	0.0023166	0.010361	0.858382	245	2
JPH4	6	0.0023166	0.010361	0.858382	246	3
MOCS3	6	0.0023166	0.010361	0.858382	247	4
RNF31	6	0.002351	0.01049	0.858729	248	3
RIMBP3B	6	0.0023977	0.010665	0.858729	249	5
CEP290	6	0.0024015	0.01068	0.858729	250	1
CCDC27	6	0.0024124	0.010718	0.858729	251	3
hsa-mir-6729	4	0.0024309	0.008775	0.844774	252	4
GABRD	6	0.0025117	0.011116	0.858729	253	4
ACP1	6	0.0025151	0.011128	0.858729	254	5
DNAJC3	6	0.0025151	0.011128	0.858729	255	5
CRCT1	6	0.0025464	0.011247	0.858729	256	4
ARHGAP26	6	0.0025464	0.011247	0.858729	257	4
HARS2	6	0.00255	0.011266	0.858729	258	2
RPL11	6	0.00255	0.011266	0.858729	259	2
OR4D11	6	0.00255	0.011266	0.858729	260	3
PSMC1	6	0.00255	0.011266	0.858729	261	3
APPL1	6	0.00255	0.011266	0.858729	262	2
C9orf142	6	0.00255	0.011266	0.858729	263	2
NPEPL1	6	0.00255	0.011266	0.858729	264	4
EEF2	6	0.00255	0.011266	0.858729	265	2
SOX14	6	0.002553	0.011278	0.858729	266	2
WDR61	6	0.002553	0.011278	0.858729	267	1
A4GALT	6	0.0025578	0.011299	0.858729	268	5

(Table Continued)

ID	sgRNA num	score	p-value	FDR	rank	goodsgrna
OR13H1	6	0.0025947	0.011437	0.864452	269	5
AXIN1	6	0.0026215	0.011546	0.864452	270	3
AZI2	6	0.0026215	0.011546	0.864452	271	5
CCAR1	6	0.0026426	0.011624	0.864452	272	4
DDX18	6	0.0026426	0.011624	0.864452	273	4
RPL19	5	0.0026602	0.011474	0.864452	274	5
hsa-mir-578	4	0.0026685	0.0095749	0.846615	275	3
RMND5B	6	0.0026859	0.011795	0.864452	276	5
EMILIN2	6	0.0026934	0.011829	0.864452	277	5
COQ10B	6	0.0026973	0.011846	0.864452	278	4
HEMK1	6	0.0026973	0.011846	0.864452	279	5
TMEM107	6	0.0027045	0.011873	0.864452	280	3
C4orf47	6	0.0027239	0.011945	0.864452	281	5
ZNF350	6	0.0027247	0.011949	0.864452	282	3
ACAP1	6	0.0027461	0.01202	0.864452	283	2
TGDS	6	0.0027461	0.01202	0.864452	284	3
PAPOLB	6	0.002755	0.012052	0.864452	285	2
HTT	6	0.0027661	0.012093	0.864474	286	5
JKAMP	6	0.0027983	0.012214	0.869615	287	5
CCDC121	6	0.0028054	0.012245	0.869615	288	1
SDAD1	6	0.0028285	0.012336	0.8704	289	4
HIST1H2BD	6	0.0028559	0.012427	0.873939	290	2
SLC4A1AP	5	0.0028658	0.012308	0.8704	291	4
SMG6	6	0.0028895	0.012554	0.879601	292	4
OR5M10	6	0.0029242	0.012684	0.879601	293	4
OR6B2	6	0.0029253	0.012688	0.879601	294	4
NSL1	6	0.0029317	0.012715	0.879601	295	3
VPS29	6	0.0029509	0.012791	0.879601	296	5
ZDHHC21	6	0.0029509	0.012791	0.879601	297	4
RNASE10	6	0.0029509	0.012791	0.879601	298	3
TRIP12	6	0.0029761	0.012891	0.882163	299	4
SLC41A1	6	0.0029813	0.01291	0.882163	300	5
SDF2	6	0.002997	0.012972	0.882163	301	3
BAP1	6	0.0030074	0.013009	0.882163	302	1
BANK1	6	0.0030127	0.013032	0.882163	303	3
HIST1H4K	1	0.0030196	0.0029942	0.741982	304	1
ZNF609	6	0.0030447	0.013152	0.882609	305	4
MTA2	6	0.0030536	0.013189	0.882609	306	4
GOLGA8O	6	0.0030579	0.013202	0.882609	307	2
FBN2	6	0.0030809	0.013289	0.885712	308	3
MZT2B	4	0.0030835	0.011032	0.858729	309	1
PTBP1	6	0.0031099	0.013398	0.889711	310	4
GARS	6	0.003119	0.013431	0.889711	311	4
hsa-mir-556	3	0.003125	0.0086662	0.844774	312	3
hsa-mir-548f-1	4	0.0031415	0.011234	0.858729	313	2

(Table Continued)

ID	sgRNA num	score	p-value	FDR	rank	goodsgrna
DPY19L4	6	0.0031588	0.013576	0.896568	314	3
SPIRE1	6	0.003175	0.013633	0.897574	315	4
LRRC26	6	0.0032044	0.013741	0.898383	316	3
BTNL8	6	0.0032221	0.013802	0.898383	317	5
GPATCH4	6	0.003232	0.013837	0.898383	318	4
ADAM19	6	0.00324	0.013865	0.898383	319	5
DHRS7C	6	0.0032624	0.01394	0.898383	320	5
CEP135	6	0.0032803	0.014001	0.898383	321	4
ZNF226	6	0.0032803	0.014001	0.898383	322	4
EFNA5	6	0.003285	0.014018	0.898383	323	5
ZNF32	6	0.0033181	0.014139	0.903458	324	3
hsa-mir-4459	3	0.0033331	0.0092252	0.846615	325	3
hsa-mir-1302-5	4	0.0033528	0.011976	0.864452	326	1
PSD	6	0.0033607	0.014312	0.90679	327	2
TMEM138	6	0.0033699	0.014345	0.90679	328	5
RAB26	6	0.0033835	0.014392	0.90679	329	4
DENND4A	6	0.0034112	0.01451	0.910992	330	2
LGR6	6	0.0034442	0.01464	0.912579	331	4
PIK3CA	6	0.0034476	0.014651	0.912579	332	4
LOC391322	6	0.0034616	0.014703	0.912579	333	2
KCNK18	6	0.0034863	0.014795	0.913114	334	3
CKS2	6	0.0035495	0.015053	0.913114	335	4
RPS6KC1	6	0.0035512	0.01506	0.913114	336	5
ACTB	6	0.0035625	0.015102	0.913114	337	4
AIP	6	0.0035802	0.015177	0.913114	338	5
ATP5G2	6	0.0035802	0.015177	0.913114	339	5
BPI	6	0.0035881	0.01521	0.913114	340	4
TENM1	6	0.003613	0.015302	0.913114	341	2
TMEM130	6	0.003613	0.015302	0.913114	342	1
EIF4E1B	6	0.003613	0.015302	0.913114	343	3
TEAD1	6	0.003613	0.015302	0.913114	344	3
DARS2	6	0.0036134	0.015302	0.913114	345	3
HIATL1	6	0.0036134	0.015302	0.913114	346	3
H2AFX	6	0.0036584	0.015467	0.920425	347	4
FOXN3	6	0.0036864	0.015583	0.922689	348	5
SPACA1	6	0.0036988	0.015638	0.922689	349	3
SERPINB5	6	0.0037644	0.015882	0.927518	350	4
LGALS7B	2	0.0037667	0.0072565	0.837141	351	1
MYO18B	6	0.0037785	0.015949	0.927518	352	4
ITGB1	6	0.0037931	0.015997	0.927518	353	4
DCK	6	0.0038096	0.01607	0.927518	354	4
COL17A1	6	0.0038148	0.016092	0.927518	355	3
BHLHE41	6	0.0038278	0.016141	0.927518	356	5
EFHB	6	0.0038399	0.01619	0.927518	357	5
hsa-mir-587	4	0.0038552	0.013735	0.898383	358	4

(Table Continued)

ID	sgRNA num	score	p-value	FDR	rank	goodsgrna
ANKRD40	6	0.0038653	0.016275	0.927518	359	3
FUT7	6	0.003882	0.016343	0.927518	360	5
MEIS2	6	0.003882	0.016343	0.927518	361	5
FLJ44635	6	0.0038858	0.016354	0.927518	362	4
KIAA1429	6	0.0039883	0.016726	0.927518	363	5
WDR83OS	6	0.0039968	0.016753	0.927518	364	3
BORA	6	0.0039968	0.016753	0.927518	365	4
TRAF5	6	0.0039968	0.016753	0.927518	366	3
KLHL5	6	0.0039968	0.016753	0.927518	367	2
C8orf86	6	0.0040088	0.016795	0.927518	368	5
SLC35B2	6	0.0040166	0.016823	0.927518	369	1
TYRP1	6	0.0040166	0.016823	0.927518	370	5
TOX2	6	0.0040166	0.016823	0.927518	371	3
SPRR2B	1	0.0040866	0.0040235	0.758717	372	1
hsa-mir-30c-2	4	0.0041376	0.014681	0.912579	373	3
TIMM10B	6	0.0041403	0.01729	0.927518	374	4
STK36	6	0.0041419	0.017295	0.927518	375	5
RDH5	6	0.0041419	0.017295	0.927518	376	5
TMEM163	6	0.0041419	0.017295	0.927518	377	5
RNF19A	6	0.0041482	0.017324	0.927518	378	5
MEF2C	6	0.0041482	0.017324	0.927518	379	4
ATP6V0C	6	0.0041482	0.017324	0.927518	380	4
GATSL3	6	0.0041482	0.017324	0.927518	381	4
CAGE1	6	0.0041482	0.017324	0.927518	382	4
MECR	6	0.0041482	0.017324	0.927518	383	4
FSBP	6	0.0041482	0.017324	0.927518	384	4
GGT6	6	0.0041614	0.017378	0.927518	385	4
RTP4	6	0.0041679	0.017405	0.927518	386	2
NEK8	5	0.0041892	0.016908	0.927518	387	2
GGT1	5	0.0041892	0.016908	0.927518	388	2
HIST1H2AL	6	0.0042687	0.017781	0.94172	389	1
EFNB3	6	0.0042687	0.017781	0.94172	390	1
FAH	6	0.0042985	0.017892	0.945291	391	4
VWA3B	6	0.0043099	0.017938	0.945376	392	5
SPRYD7	6	0.0043696	0.018159	0.951232	393	3
VSIG4	6	0.0043889	0.018232	0.951232	394	5
hsa-mir-3655	4	0.0044139	0.015613	0.922689	395	4
SLC6A20	6	0.00442	0.01834	0.951232	396	3
NEO1	6	0.0044279	0.018365	0.951232	397	3
hsa-mir-1249	4	0.0044292	0.015676	0.922689	398	2
TSPAN32	6	0.0044518	0.018462	0.951232	399	3
PDE4D	6	0.0044632	0.018506	0.951232	400	5
DGKD	6	0.0044693	0.018523	0.951232	401	5
ZMYND10	6	0.0044704	0.018526	0.951232	402	2
CPED1	6	0.0044861	0.018576	0.951232	403	4

(Table Continued)

ID	sgRNA num	score	p-value	FDR	rank	goodsgrna
PDLIM3	6	0.0045229	0.018722	0.955092	404	5
NAALAD2	6	0.004542	0.018803	0.955092	405	4
GPR183	6	0.0045594	0.018867	0.955092	406	4
MLLT3	6	0.0045901	0.01899	0.955092	407	5
KAT8	6	0.0045901	0.01899	0.955092	408	5
IDE	6	0.0046032	0.019036	0.955092	409	4
RBMXL3	6	0.0046217	0.019105	0.955092	410	3
PCSK2	6	0.0046217	0.019105	0.955092	411	4
OR10W1	6	0.004629	0.019136	0.955092	412	3
TRIM36	6	0.0046638	0.019259	0.958234	413	4
SRGAP2B	4	0.0046814	0.016542	0.927518	414	3
IHH	6	0.0047057	0.019414	0.958234	415	4
CHODL	5	0.0047132	0.018543	0.951232	416	3
OR8H1	6	0.0047206	0.019477	0.958234	417	5
ZNF20	6	0.0047225	0.019484	0.958234	418	2
RHOXF1	6	0.0047569	0.019609	0.958234	419	2
DBT	6	0.0047729	0.019665	0.958234	420	4
DNAJC17	6	0.0047762	0.019675	0.958234	421	3
HIST1H4D	6	0.0047762	0.019675	0.958234	422	3
PRSS53	6	0.004808	0.019798	0.958234	423	5
KLRC4	6	0.0048198	0.019842	0.958234	424	5
SRGAP2D	6	0.0048278	0.019879	0.958234	425	5
TYMS	6	0.0048326	0.019897	0.958234	426	3
CASP8AP2	6	0.0048474	0.019951	0.958234	427	2
KIAA0368	6	0.0048474	0.019951	0.958234	428	4
MYO7A	6	0.0048474	0.019951	0.958234	429	2
FAM78B	6	0.0048474	0.019951	0.958234	430	2
ARRDC1	5	0.0048479	0.018963	0.955092	431	3
ARHGAP25	6	0.0048662	0.020012	0.958287	432	5
hsa-mir-6500	4	0.0048663	0.017194	0.927518	433	1
BRI3BP	6	0.0048737	0.020041	0.958287	434	1
PNN	6	0.0049267	0.020234	0.964077	435	4
hsa-mir-4460	4	0.0049335	0.017428	0.927518	436	1
PATL2	6	0.004937	0.020272	0.964077	437	4
ZNF782	6	0.004965	0.020377	0.964077	438	5
NUP153	6	0.004965	0.020377	0.964077	439	5
AP2A2	6	0.0050063	0.020537	0.964077	440	3
NPFFR2	6	0.0050249	0.020597	0.964077	441	3
WWC2	6	0.0050249	0.020597	0.964077	442	3
ZNF658	6	0.0050308	0.020614	0.964077	443	3
NBEAL2	6	0.0050662	0.020735	0.964077	444	5
SLAMF9	6	0.00507	0.020755	0.964077	445	3
KLF3	6	0.0050834	0.020802	0.964077	446	4
POLG2	6	0.0050838	0.020804	0.964077	447	2
RPS18	6	0.0051256	0.020951	0.965389	448	5

(Table Continued)

ID	sgRNA num	score	p-value	FDR	rank	goodsgrna
ZNF425	6	0.0051256	0.020951	0.965389	449	5
FNTA	5	0.0051356	0.019877	0.958234	450	4
NSF	6	0.0051761	0.021148	0.967655	451	1
TECTB	6	0.0051803	0.021171	0.967655	452	5
TBC1D10B	6	0.0051816	0.021175	0.967655	453	3
RPRD1A	6	0.0052265	0.021344	0.967727	454	3
hsa-mir-4519	4	0.0052286	0.018395	0.951232	455	2
SCFD1	6	0.0052346	0.021376	0.967727	456	5
TCTN1	6	0.0052424	0.021406	0.967727	457	5
DHDDS	6	0.0052574	0.021472	0.967727	458	4
SATB1	6	0.0052596	0.021478	0.967727	459	4
HBE1	6	0.0052873	0.021582	0.967727	460	5
KLK15	6	0.0052916	0.021599	0.967727	461	2
SYPL1	6	0.0053021	0.021635	0.967727	462	4
KIAA0408	6	0.0053021	0.021635	0.967727	463	3
OR5P3	6	0.0053268	0.02172	0.967727	464	4
TEX2	6	0.0053572	0.021826	0.967727	465	5
NOD2	6	0.0053599	0.021835	0.967727	466	5
KLHDC7A	6	0.0053599	0.021835	0.967727	467	5
FOXI3	6	0.0053599	0.021835	0.967727	468	5
ANKZF1	6	0.0053844	0.021919	0.967727	469	5
GLYCTK	6	0.005428	0.022083	0.967727	470	4
CLDN4	6	0.005428	0.022083	0.967727	471	2
SHISA4	6	0.005428	0.022083	0.967727	472	3
PLCB4	6	0.0054362	0.022115	0.967727	473	5
hsa-mir-1910	4	0.0054376	0.019093	0.955092	474	3
RPAIN	5	0.0054517	0.02083	0.964077	475	4
LOC100130357	6	0.005481	0.022283	0.973142	476	4
SLC45A4	6	0.0055247	0.022441	0.976788	477	5
EMILIN3	6	0.0055288	0.022457	0.976788	478	2
UPRT	6	0.0055794	0.022622	0.981994	479	4
ADAM11	6	0.0056295	0.022797	0.986243	480	2
hsa-mir-548ae-2	1	0.0056849	0.0056466	0.777139	481	1
FER	6	0.0056886	0.023043	0.986243	482	2
BBX	6	0.0057168	0.02315	0.986243	483	4
DPEP2	6	0.0057806	0.02339	0.986243	484	5
DYDC2	6	0.0057806	0.02339	0.986243	485	3
PKIA	6	0.0057806	0.02339	0.986243	486	2
STK33	6	0.0057945	0.023436	0.986243	487	4
AHSA2	6	0.0057945	0.023436	0.986243	488	4
PPP4C	6	0.0057945	0.023436	0.986243	489	4
TMEM92	6	0.0058063	0.023482	0.986243	490	5
LANCL1	6	0.0058063	0.023482	0.986243	491	5
FABP6	6	0.0058318	0.023565	0.986243	492	2
DVL2	6	0.0058318	0.023565	0.986243	493	3

(Table Continued)

ID	sgRNA num	score	p-value	FDR	rank	goodsgrna
STON1	6	0.0058395	0.023592	0.986243	494	5
hsa-mir-4649	4	0.0058408	0.020408	0.964077	495	2
H1F0	6	0.0058581	0.023678	0.986243	496	5
YWHAZ	6	0.0058813	0.023771	0.986243	497	4
HGF	6	0.0059298	0.023953	0.986243	498	3
GNG3	6	0.0059298	0.023953	0.986243	499	4
hsa-mir-6078	4	0.005936	0.020715	0.964077	500	3
AKAP7	6	0.0059454	0.024006	0.986243	501	4
WNT1	6	0.0059454	0.024006	0.986243	502	4
PRSS27	6	0.0059569	0.024045	0.986243	503	2
SLC38A3	6	0.0059569	0.024045	0.986243	504	3
USP15	6	0.0059591	0.024054	0.986243	505	5
hsa-mir-7844	4	0.0060194	0.020992	0.965389	506	4
SRR	6	0.006031	0.024334	0.986243	507	4
MC1R	6	0.0060324	0.024341	0.986243	508	1
ANKRD13B	6	0.0061331	0.024713	0.986243	509	3
CWF19L2	6	0.0061835	0.024908	0.986243	510	3
UBE2G2	6	0.006199	0.024966	0.986243	511	4
DNASE1L1	6	0.006204	0.024982	0.986243	512	5
S100A1	6	0.0062338	0.02509	0.986243	513	5
PDE4A	6	0.0062338	0.02509	0.986243	514	5
MUTYH	6	0.0062338	0.02509	0.986243	515	4
AAK1	5	0.006247	0.02328	0.986243	516	2
TACR1	6	0.0062841	0.025263	0.986243	517	1
hsa-mir-3198-1	4	0.0062962	0.021899	0.967727	518	3
OR52A5	6	0.0063068	0.025348	0.986243	519	5
PTK2	6	0.0063328	0.025444	0.986243	520	3
KCNRG	6	0.0063328	0.025444	0.986243	521	5
SNX10	6	0.0063328	0.025444	0.986243	522	2
PIGW	6	0.0063328	0.025444	0.986243	523	5
WASH1	6	0.0063328	0.025444	0.986243	524	2
REXO4	6	0.0063328	0.025444	0.986243	525	4
HAUS4	6	0.0063328	0.025444	0.986243	526	2
RPL31	6	0.0063383	0.025463	0.986243	527	5
ZSCAN5B	6	0.0063383	0.025463	0.986243	528	5
NFKBIA	6	0.0063833	0.025631	0.986243	529	3
CD40	6	0.0063923	0.025665	0.986243	530	5
GMPR	6	0.0064286	0.025807	0.986243	531	4
LRP10	6	0.0064319	0.02582	0.986243	532	4
TH	6	0.0064352	0.025833	0.986243	533	3
GDNF	6	0.0064352	0.025833	0.986243	534	4
C16orf97	6	0.0064352	0.025833	0.986243	535	5
PDZD11	6	0.0064352	0.025833	0.986243	536	2
SLC6A5	6	0.0064605	0.025935	0.986243	537	5
TIMM21	6	0.0064793	0.026007	0.986243	538	4

(Table Continued)

ID	sgRNA num	score	p-value	FDR	rank	goodsgrna
DNAJC28	6	0.0064916	0.026052	0.986243	539	5
TECR	5	0.006521	0.024137	0.986243	540	4
SCGB1D2	6	0.0065862	0.026396	0.986243	541	2
PIWIL3	6	0.0066522	0.026639	0.986243	542	5
PLEKHH3	6	0.0066554	0.02665	0.986243	543	4
ELAVL2	6	0.0066868	0.02676	0.986243	544	4
SLTM	3	0.0066905	0.018211	0.951232	545	1
TLR9	6	0.0067195	0.026871	0.986243	546	4
GKAP1	6	0.0067195	0.026871	0.986243	547	4
TMED10	6	0.0067196	0.026871	0.986243	548	5
SAV1	6	0.0067238	0.026886	0.986243	549	3
ELOVL3	6	0.0067371	0.026934	0.986243	550	3
LRIG2	5	0.0067661	0.024844	0.986243	551	3
SLC23A1	6	0.0067875	0.027121	0.986243	552	2
C9orf129	6	0.0067947	0.027146	0.986243	553	2
CSTF2	6	0.0068116	0.027203	0.986243	554	3
SLC5A9	6	0.0068468	0.027326	0.986243	555	3
LRCH1	6	0.0068533	0.027348	0.986243	556	4
ABO	6	0.0068543	0.027351	0.986243	557	5
SUV420H1	6	0.006886	0.027458	0.986243	558	5
KBTBD2	6	0.0069126	0.027557	0.986243	559	4
PRSS23	6	0.0069349	0.027621	0.986243	560	5
SERBP1	6	0.006975	0.027773	0.986243	561	4
DHCR7	6	0.0070008	0.027864	0.986243	562	5
RGPD3	6	0.00701	0.027904	0.986243	563	3
GUCA1B	6	0.0070139	0.027921	0.986243	564	2
ARHGEF11	6	0.0070139	0.027921	0.986243	565	5
GPR56	6	0.0070139	0.027921	0.986243	566	2
PPM1N	6	0.0070139	0.027921	0.986243	567	3
TPT1	6	0.0070139	0.027921	0.986243	568	1
CMAS	6	0.0070139	0.027921	0.986243	569	3
hsa-mir-4273	4	0.0070347	0.024264	0.986243	570	3
KLHL1	6	0.0070636	0.02811	0.986243	571	4
URM1	6	0.0070659	0.028118	0.986243	572	4
ACTA2	6	0.0070659	0.028118	0.986243	573	4
CXorf58	6	0.0070659	0.028118	0.986243	574	4
PNPT1	6	0.0070659	0.028118	0.986243	575	5
DALRD3	6	0.0070659	0.028118	0.986243	576	4
DTWD2	6	0.0070862	0.028194	0.986243	577	3
LMNB1	6	0.0071283	0.02835	0.986243	578	5
hsa-mir-527	1	0.0071821	0.0071422	0.837141	579	1
TUBA1A	6	0.0071902	0.028556	0.986243	580	3
ATF2	6	0.0072403	0.028722	0.986243	581	3
DEFB126	6	0.0072508	0.028762	0.986243	582	3
hsa-mir-3912	4	0.007318	0.025195	0.986243	583	1

(Table Continued)

ID	sgRNA num	score	p-value	FDR	rank	goodsgrna
FOXO1	6	0.0073409	0.029081	0.986243	584	1
ZNF536	6	0.0073479	0.029103	0.986243	585	2
SPATA18	6	0.0073479	0.029103	0.986243	586	3
DEPDC7	6	0.0073795	0.029221	0.986243	587	3
NRM	6	0.0074092	0.029322	0.986243	588	3
DEFB110	6	0.0074092	0.029322	0.986243	589	3
hsa-mir-217	4	0.0074338	0.025578	0.986243	590	3
OVGP1	6	0.0074469	0.029455	0.986243	591	5
S100A12	6	0.0074918	0.029627	0.986243	592	3
POLR2F	6	0.0074918	0.029627	0.986243	593	1
hsa-mir-197	4	0.0075193	0.025872	0.986243	594	1
hsa-mir-2113	4	0.0075193	0.025872	0.986243	595	1
TDG	6	0.0075408	0.029821	0.986243	596	5
MORN1	6	0.007563	0.029907	0.986243	597	5
SETD3	6	0.007563	0.029907	0.986243	598	5
hsa-mir-548ar	2	0.0075673	0.014401	0.90679	599	2
CRIPT	5	0.0075729	0.027214	0.986243	600	2
IGSF22	6	0.007577	0.029963	0.986243	601	4
HINT2	6	0.0075801	0.029974	0.986243	602	4
FBLN7	6	0.0075923	0.030007	0.986243	603	4
ZNF470	6	0.0076929	0.030371	0.986243	604	3
AQP4	6	0.0076929	0.030371	0.986243	605	2
COA1	6	0.0076929	0.030371	0.986243	606	1
FKBP14	6	0.0077071	0.030414	0.986243	607	4
NUP43	6	0.0077248	0.030483	0.986243	608	5
INHBA	6	0.0077248	0.030483	0.986243	609	5
OTUB2	6	0.0077248	0.030483	0.986243	610	5
KHNYN	6	0.0077248	0.030483	0.986243	611	5
SENP8	6	0.0077411	0.030543	0.986243	612	3
CDHR5	6	0.0077411	0.030543	0.986243	613	3
MTMR9	6	0.0077685	0.030644	0.986243	614	4
UBE2Q2	6	0.0077685	0.030644	0.986243	615	4
hsa-mir-6499	4	0.0077746	0.026675	0.986243	616	4
ZNF148	6	0.0077935	0.030732	0.986243	617	3
STATH	6	0.0078437	0.030919	0.986243	618	4
GLUL	6	0.0078474	0.030928	0.986243	619	3
STK11	6	0.007887	0.031074	0.986243	620	4
HHATL	6	0.007887	0.031074	0.986243	621	3
CDKN2D	6	0.007894	0.031099	0.986243	622	3
RPUSD1	6	0.0079241	0.031203	0.986243	623	2
SLC5A7	6	0.0079241	0.031203	0.986243	624	2
HOXB4	6	0.0079263	0.031211	0.986243	625	5
SAPCD2	6	0.0079281	0.031216	0.986243	626	4
LCORL	6	0.0079443	0.031269	0.986243	627	3
ITGBL1	6	0.0079461	0.031274	0.986243	628	3

(Table Continued)

ID	sgRNA num	score	p-value	FDR	rank	goodsgrna
hsa-mir-488	4	0.0079553	0.027234	0.986243	629	1
CAMKK2	6	0.0079703	0.031354	0.986243	630	3
UNC13A	6	0.0079735	0.031366	0.986243	631	5
TTLL9	6	0.00798	0.031388	0.986243	632	3
ENO1	5	0.0079879	0.028454	0.986243	633	3
SPEM1	6	0.0079946	0.031431	0.986243	634	2
SEC31A	6	0.0080448	0.031616	0.986243	635	3
PLN	1	0.0081183	0.0081062	0.844274	636	1
ASRGL1	6	0.0081454	0.031952	0.986243	637	3
ITPKA	6	0.0081454	0.031952	0.986243	638	2
PROKR2	6	0.0081519	0.031977	0.986243	639	3
HINT1	6	0.0081626	0.032017	0.986243	640	5
NonTargetingControlGuideForHuman_0437	1	0.0081689	0.0081529	0.844274	641	1
MKRN3	6	0.0081768	0.032071	0.986243	642	4
IFIT1B	6	0.0081852	0.032096	0.986243	643	3
ATRIP	6	0.0081852	0.032096	0.986243	644	4
DSE	6	0.0081852	0.032096	0.986243	645	3
hsa-mir-431	4	0.0081968	0.028004	0.986243	646	4
NonTargetingControlGuideForHuman_0912	1	0.0082111	0.0081899	0.844274	647	1
ZDHHC5	6	0.0082211	0.032224	0.986243	648	4
RPS6KL1	6	0.008244	0.032298	0.986243	649	5
TBC1D15	6	0.0082459	0.032307	0.986243	650	3
KIAA1549	6	0.0082961	0.032494	0.986243	651	1
MIR205HG	6	0.0083073	0.032533	0.986243	652	3
GPR89B	4	0.0083124	0.028374	0.986243	653	3
NonTargetingControlGuideForHuman_0828	1	0.0083418	0.0083165	0.844274	654	1
FOSB	6	0.0083464	0.032661	0.986243	655	3
NBAS	6	0.0083936	0.032836	0.986243	656	3
SLC27A5	6	0.0083967	0.032846	0.986243	657	2
hsa-mir-548a-1	4	0.0084065	0.028677	0.986243	658	4
SEMA3C	6	0.0084136	0.0329	0.986243	659	2
PCDH20	6	0.0084304	0.032953	0.986243	660	3
EDEM2	6	0.0084319	0.032956	0.986243	661	4
TWIST1	6	0.0084343	0.032966	0.986243	662	5
ATP2C1	6	0.0084343	0.032966	0.986243	663	5
PINK1	6	0.0084469	0.033012	0.986243	664	1
FKBP2	6	0.00847	0.033101	0.986243	665	4
ZNF664	6	0.0084972	0.033205	0.986243	666	3
FLCN	6	0.0085199	0.033287	0.986243	667	5

(Table Continued)

ID	sgRNA num	score	p-value	FDR	rank	goodsgrna
ZFPM2	6	0.0085317	0.033332	0.986243	668	4
KCNQ3	6	0.0085317	0.033332	0.986243	669	2
JAK1	6	0.00858	0.03351	0.986243	670	4
KLLN	6	0.0085936	0.033561	0.986243	671	5
SLC9A8	6	0.0085936	0.033561	0.986243	672	5
GPR107	6	0.0086228	0.033686	0.986243	673	4
MEGF10	6	0.0086383	0.033744	0.986243	674	3
TTLL1	6	0.0087019	0.033987	0.986243	675	2
NOSTRIN	5	0.0087203	0.030623	0.986243	676	2
APOD	6	0.0087484	0.034153	0.986243	677	3
RNASEL	6	0.0087484	0.034153	0.986243	678	2
RASD2	6	0.0087484	0.034153	0.986243	679	3
SEL1L3	6	0.0087484	0.034153	0.986243	680	2
OTUD4	6	0.0087484	0.034153	0.986243	681	2
TRNT1	6	0.0087484	0.034153	0.986243	682	3
LRRK1	6	0.0087484	0.034153	0.986243	683	3
GRIN2B	6	0.0087546	0.034174	0.986243	684	5
R3HDM1	6	0.0087782	0.034265	0.986243	685	5
CXCR5	6	0.0087818	0.034275	0.986243	686	3
C1orf174	6	0.0087946	0.03432	0.986243	687	5
IL6ST	6	0.0088498	0.034519	0.986243	688	4
GALC	6	0.0088498	0.034519	0.986243	689	3
hsa-mir-6758	4	0.0088607	0.030108	0.986243	690	2
KRTAP2-2	1	0.0088859	0.0088531	0.846615	691	1
LOC100287399	6	0.0088933	0.034686	0.986243	692	5
SRD5A2	6	0.0089029	0.034721	0.986243	693	4
hsa-mir-363	4	0.0089108	0.030271	0.986243	694	2
GRAMD1C	6	0.0089295	0.034805	0.986243	695	5
NR0B1	6	0.0089295	0.034805	0.986243	696	5
ZNF705D	2	0.0089361	0.016994	0.927518	697	2
SMNDC1	6	0.0089513	0.034882	0.986243	698	3
CDKL2	6	0.008967	0.03495	0.986243	699	4
PPAPDC3	6	0.0089811	0.034996	0.986243	700	5
BEX5	6	0.0089946	0.035037	0.986243	701	3
NREP	6	0.0089995	0.035053	0.986243	702	3
TOPAZ1	6	0.0090174	0.035118	0.986243	703	3
ETAA1	6	0.0090177	0.035121	0.986243	704	5
hsa-let-7a-2	4	0.0090234	0.030619	0.986243	705	3
ACADL	6	0.0090468	0.035219	0.986243	706	4
MXD3	6	0.0090498	0.035228	0.986243	707	3
CSN3	6	0.009061	0.035275	0.986243	708	5
DNAI1	6	0.009061	0.035275	0.986243	709	5
CUX2	6	0.0090853	0.035368	0.986243	710	5
ESYT2	6	0.0090874	0.035374	0.986243	711	4
AGPAT2	6	0.0090932	0.035396	0.986243	712	3

(Table Continued)

ID	sgRNA num	score	p-value	FDR	rank	goodsgrna
SEC61A1	6	0.0091052	0.03544	0.986243	713	3
SMPD3	6	0.0091398	0.03557	0.986243	714	2
ZNF229	6	0.0091502	0.035602	0.986243	715	3
HIST1H2BG	6	0.0091661	0.035648	0.986243	716	3
CIDEB	6	0.0091857	0.035709	0.986243	717	5
PGBD3	6	0.0092004	0.035756	0.986243	718	3
RAB5A	6	0.009235	0.035881	0.986243	719	5
PLCD4	6	0.0092507	0.035935	0.986243	720	2
ETNK2	6	0.0093009	0.036108	0.986243	721	3
IFNA1	6	0.0093071	0.036128	0.986243	722	4
SMARCD2	6	0.0093071	0.036128	0.986243	723	4
STOM	6	0.0093511	0.036293	0.986243	724	3
RCVRN	6	0.0094004	0.036478	0.986243	725	4
SIGLEC14	6	0.0094004	0.036478	0.986243	726	5
hsa-mir-6850	4	0.0094083	0.031851	0.986243	727	3
hsa-mir-6508	4	0.0094134	0.031874	0.986243	728	1
SCTR	6	0.0094268	0.036558	0.986243	729	5
SESN2	5	0.0094353	0.032714	0.986243	730	4
TAC3	6	0.0094515	0.03665	0.986243	731	3
PMPCA	6	0.0094712	0.036725	0.986243	732	4
ARMCX5-GPRASP2	6	0.0094719	0.036728	0.986243	733	4
MAGEA12	6	0.0094837	0.036771	0.986243	734	3
AP1S3	6	0.0094837	0.036771	0.986243	735	3
CCL2	6	0.0095013	0.036844	0.986243	736	4
APOBEC3F	6	0.0095149	0.036892	0.986243	737	5
hsa-mir-21	4	0.0095306	0.032211	0.986243	738	2
PTPN7	6	0.0095672	0.037075	0.986243	739	5
KCNAB1	6	0.0095672	0.037075	0.986243	740	5
CD81	6	0.0096021	0.037202	0.986243	741	3
KHK	6	0.0096021	0.037202	0.986243	742	2
TYRO3	6	0.0096021	0.037202	0.986243	743	3
DNER	6	0.0096021	0.037202	0.986243	744	3
NKG7	6	0.0096169	0.037257	0.986243	745	4
GBA2	6	0.0096204	0.037271	0.986243	746	4
SFTPB	6	0.0096282	0.037293	0.986243	747	5
HNRNPDL	6	0.0096282	0.037293	0.986243	748	5
KCTD21	6	0.0096432	0.037343	0.986243	749	3
FANCC	6	0.0096564	0.03739	0.986243	750	4
ZNF624	6	0.0096798	0.037463	0.986243	751	4
CENPI	6	0.0097252	0.037641	0.986243	752	3
TRIM35	6	0.0097252	0.037641	0.986243	753	4
MORC3	6	0.0097334	0.037667	0.986243	754	5
ALDH8A1	6	0.0097622	0.037774	0.986243	755	3
ZNF599	6	0.0097622	0.037774	0.986243	756	3

(Table Continued)

ID	sgRNA num	score	p-value	FDR	rank	goodsgrna
REV1	6	0.00979	0.037875	0.986243	757	5
C1orf127	6	0.00979	0.037875	0.986243	758	5
SLC24A3	6	0.0098029	0.037924	0.986243	759	3
BNC2	6	0.0098033	0.037927	0.986243	760	4
hsa-mir-3185	4	0.0098317	0.033194	0.986243	761	2
KRAS	6	0.0098434	0.038072	0.986243	762	4
KNG1	6	0.0098531	0.038105	0.986243	763	3
LRSAM1	6	0.0098866	0.038229	0.986243	764	5
STX16	6	0.0098866	0.038229	0.986243	765	5
AVPR1B	6	0.0098866	0.038229	0.986243	766	5
DCAF8L1	6	0.0098866	0.038229	0.986243	767	5
FADS2	6	0.0099033	0.038286	0.986243	768	3
ZNF423	6	0.0099249	0.038356	0.986243	769	5
SRSF7	6	0.0099388	0.038389	0.986243	770	4
SRGAP2	6	0.0099588	0.038453	0.986243	771	4
SLC25A26	6	0.0099695	0.038482	0.986243	772	3
ISL1	6	0.0099695	0.038482	0.986243	773	2
CHRNA9	6	0.010004	0.038606	0.986243	774	2
LEKR1	6	0.010004	0.038606	0.986243	775	3
TMEM161B	6	0.010021	0.038668	0.986243	776	5
UBXN4	6	0.010033	0.038709	0.986243	777	3
OSTN	6	0.010053	0.038775	0.986243	778	4
C14orf2	6	0.010059	0.038793	0.986243	779	3
hsa-mir-1343	4	0.010073	0.033954	0.986243	780	2
CD302	6	0.010085	0.038893	0.986243	781	4
SYT1	6	0.010095	0.038929	0.986243	782	4
BAIAP2L2	6	0.010095	0.038929	0.986243	783	4
TTC9C	6	0.010104	0.038961	0.986243	784	4
HPDL	6	0.010113	0.038984	0.986243	785	3
OLR1	6	0.01012	0.03901	0.986243	786	5
hsa-mir-5704	4	0.010151	0.0342	0.986243	787	3
CACNA1H	6	0.010152	0.039129	0.986243	788	2
PHLDA3	6	0.010173	0.039203	0.986243	789	5
SPTY2D1	6	0.010173	0.039203	0.986243	790	5
KIRREL	6	0.010217	0.039358	0.986243	791	4
SRSF8	6	0.010229	0.039404	0.986243	792	2
TRIM14	6	0.010229	0.039404	0.986243	793	2
TYK2	6	0.010229	0.039404	0.986243	794	1
TMEM18	6	0.010229	0.039404	0.986243	795	2
BCL2L1	6	0.010255	0.039482	0.986243	796	3
GPX1	6	0.010269	0.039522	0.986243	797	4
hsa-mir-7157	4	0.010331	0.034773	0.986243	798	4
hsa-mir-4264	4	0.010333	0.034777	0.986243	799	3
FOXG1	6	0.010352	0.039814	0.986243	800	2
GTPBP4	6	0.010352	0.039814	0.986243	801	2

(Table Continued)

ID	sgRNA num	score	p-value	FDR	rank	goodsgrna
C5AR2	6	0.010352	0.039814	0.986243	802	4
IL15RA	6	0.010352	0.039814	0.986243	803	4
LPAR4	6	0.010352	0.039814	0.986243	804	3
SYTL3	6	0.010352	0.039814	0.986243	805	3
TIPIN	6	0.010355	0.039826	0.986243	806	3
OR2T8	6	0.010366	0.039863	0.986243	807	4
hsa-mir-548u	4	0.010368	0.034887	0.986243	808	1
POU4F2	6	0.010432	0.040095	0.986243	809	4
MBD3L4	1	0.010434	0.010383	0.858382	810	1
SLC26A10	6	0.010437	0.040118	0.986243	811	4
RCN2	6	0.010439	0.040124	0.986243	812	3
hsa-mir-373	4	0.010449	0.035138	0.986243	813	3
NLRP1	6	0.010455	0.040182	0.986243	814	3
OR4K2	6	0.010455	0.040182	0.986243	815	3
SLC6A2	6	0.010484	0.04029	0.986243	816	5
GDPD5	5	0.010499	0.035842	0.986243	817	3
QARS	5	0.010499	0.035842	0.986243	818	3
OR2H2	6	0.010535	0.040459	0.986243	819	3
PLAG1	6	0.010563	0.040553	0.986243	820	3
NUP155	6	0.010582	0.040621	0.986243	821	2
RNASE6	6	0.010582	0.040621	0.986243	822	3
METTL15	6	0.010591	0.040655	0.986243	823	5
USP25	6	0.010591	0.040655	0.986243	824	5
LIPC	6	0.010591	0.040656	0.986243	825	4
COG2	6	0.010606	0.040698	0.986243	826	2
STX19	6	0.010606	0.040698	0.986243	827	2
KRCC1	6	0.010606	0.040699	0.986243	828	4
B4GALT6	6	0.010682	0.040955	0.986243	829	4
MTM1	6	0.010685	0.040969	0.986243	830	4
CACNA2D2	6	0.010685	0.040969	0.986243	831	4
hsa-mir-548ae-1	4	0.010719	0.035927	0.986243	832	2
RLN1	6	0.010731	0.041132	0.986243	833	3
LAIR1	6	0.010731	0.041132	0.986243	834	3
TBC1D3H	1	0.010754	0.010689	0.858729	835	1
TRAF3IP1	6	0.010764	0.041234	0.986243	836	3
MYO1B	6	0.010764	0.041234	0.986243	837	3
CSMD1	6	0.010764	0.041234	0.986243	838	4
OR7D4	6	0.010813	0.041394	0.986243	839	5
PYY	6	0.010827	0.041436	0.986243	840	4
SPAG4	6	0.010831	0.041453	0.986243	841	3
EIF2S3	6	0.010857	0.041537	0.986243	842	3
PDE4DIP	6	0.010869	0.041586	0.986243	843	5
TMEM181	6	0.010878	0.041613	0.986243	844	5
ELAVL1	6	0.010907	0.041705	0.986243	845	1
ARHGAP1	6	0.01092	0.041754	0.986243	846	5

(Table Continued)

ID	sgRNA num	score	p-value	FDR	rank	goodsgrna
FRMD4A	6	0.01092	0.041754	0.986243	847	5
PRICKLE3	6	0.010926	0.041779	0.986243	848	4
NLRP14	6	0.010931	0.041788	0.986243	849	5
SPDYE2	4	0.010988	0.036536	0.986243	850	3
TMEM39B	5	0.010994	0.037303	0.986243	851	2
TMBIM4	6	0.011013	0.042072	0.986243	852	5
NLRP9	6	0.011014	0.042073	0.986243	853	4
DEPDC4	6	0.011014	0.042073	0.986243	854	4
ZNF263	6	0.011014	0.042073	0.986243	855	4
ZNF502	6	0.011061	0.042243	0.986243	856	3
CHD1	6	0.011088	0.042335	0.986243	857	5
NSUN6	6	0.011088	0.042335	0.986243	858	5
C5orf24	6	0.011088	0.042335	0.986243	859	5
ZNF620	6	0.011088	0.042335	0.986243	860	5
TMEM167A	6	0.011147	0.042532	0.986243	861	2
RIPK1	6	0.011147	0.042532	0.986243	862	2
C15orf61	6	0.011147	0.042532	0.986243	863	4
SNW1	6	0.011147	0.042532	0.986243	864	3
MRTO4	6	0.011147	0.042532	0.986243	865	3
LRRC3C	6	0.011147	0.042532	0.986243	866	4
CREB3L2	6	0.011147	0.042532	0.986243	867	2
PSMA6	6	0.011147	0.042532	0.986243	868	2
MACROD2	6	0.011147	0.042532	0.986243	869	3
CRYGD	6	0.011228	0.042806	0.986243	870	4
PRDM7	6	0.011258	0.04292	0.986243	871	2
LEFTY1	6	0.011258	0.04292	0.986243	872	4
ABHD14B	6	0.011258	0.04292	0.986243	873	3
CDV3	6	0.011258	0.04292	0.986243	874	1
ELF2	6	0.011258	0.04292	0.986243	875	2
LTB4R	6	0.011258	0.04292	0.986243	876	2
TESC	6	0.011313	0.04311	0.986243	877	4
UCP2	6	0.011419	0.043476	0.986243	878	5
DYSF	6	0.011419	0.043476	0.986243	879	5
METTL21B	6	0.011419	0.043476	0.986243	880	5
GLIS2	6	0.011419	0.043476	0.986243	881	5
CHSY1	6	0.011419	0.043476	0.986243	882	5
NANOS1	5	0.011439	0.0386	0.986243	883	2
KIF3A	6	0.011457	0.043587	0.986243	884	4
GPR45	6	0.011457	0.043587	0.986243	885	5
PDE1C	6	0.011457	0.043587	0.986243	886	4
BEX4	6	0.011482	0.043669	0.986243	887	4
NPM1	5	0.011565	0.038959	0.986243	888	1
ABCA13	6	0.011569	0.043956	0.986243	889	4
RPL21	4	0.011572	0.037837	0.986243	890	2
BLZF1	5	0.011573	0.038986	0.986243	891	4

(Table Continued)

ID	sgRNA num	score	p-value	FDR	rank	goodsgrna
VNN1	6	0.011605	0.044084	0.986243	892	5
NR2E3	6	0.011609	0.044098	0.986243	893	1
hsa-mir-2052	2	0.011648	0.022039	0.967727	894	1
C1orf141	6	0.011659	0.044268	0.986243	895	3
SPNS3	6	0.011699	0.044389	0.986243	896	4
AFF4	6	0.011709	0.044421	0.986243	897	3
TXNDC8	6	0.011751	0.044569	0.986243	898	2
KLHL42	6	0.011754	0.044579	0.986243	899	4
FAM118B	6	0.011759	0.044593	0.986243	900	2
PRPS1L1	6	0.01176	0.044596	0.986243	901	3
ACO1	6	0.011825	0.044803	0.986243	902	5
TXNIP	6	0.011834	0.044835	0.986243	903	3
BLOC1S2	6	0.011835	0.044837	0.986243	904	4
hsa-mir-6778	4	0.011839	0.03843	0.986243	905	3
PYCRL	6	0.011863	0.044936	0.986243	906	2
POLR2A	6	0.011898	0.045054	0.986243	907	5
GRK4	6	0.011898	0.045054	0.986243	908	5
SLAMF1	6	0.011909	0.045079	0.986243	909	2
SMCO4	6	0.011944	0.045199	0.986243	910	3
WDR45	5	0.011962	0.040109	0.986243	911	2
ARHGAP21	6	0.011971	0.045289	0.986243	912	4
ORC2	5	0.011983	0.040162	0.986243	913	3
DNPEP	6	0.011986	0.045348	0.986243	914	5
TMEM247	6	0.011986	0.045348	0.986243	915	5
SYCE2	6	0.011986	0.045348	0.986243	916	5
FAM19A2	6	0.011998	0.045386	0.986243	917	3
CEACAM4	6	0.012047	0.045553	0.986243	918	2
CNBP	6	0.012048	0.045556	0.986243	919	4
THRB	6	0.012067	0.045619	0.986243	920	3
GYPA	6	0.012074	0.045643	0.986243	921	5
TGM1	6	0.012074	0.045643	0.986243	922	5
RPS10-NUDT3	2	0.012075	0.022822	0.986243	923	1
HSD3B1	6	0.012143	0.045881	0.986243	924	3
ATP5G3	6	0.012207	0.046095	0.986243	925	4
TCIRG1	6	0.012219	0.046139	0.986243	926	4
GCGR	6	0.012235	0.04619	0.986243	927	2
SLC7A13	6	0.012235	0.04619	0.986243	928	3
GLRA1	6	0.012235	0.04619	0.986243	929	1
INTS7	6	0.012235	0.04619	0.986243	930	1
GALM	6	0.012235	0.04619	0.986243	931	3
LRCH4	6	0.012235	0.04619	0.986243	932	3
C2orf71	6	0.012235	0.04619	0.986243	933	4
SGTB	6	0.012235	0.04619	0.986243	934	3
OR10K1	6	0.012235	0.046192	0.986243	935	5
BMP3	6	0.012249	0.046238	0.986243	936	4

(Table Continued)

ID	sgRNA num	score	p-value	FDR	rank	goodsgrna
OR5K2	6	0.012263	0.046285	0.986243	937	3
TRIM23	6	0.01239	0.04673	0.986243	938	2
EBP	6	0.012438	0.046896	0.986243	939	5
FAM189A2	6	0.012471	0.04701	0.986243	940	3
ATP5E	4	0.012508	0.039926	0.986243	941	1
hsa-mir-6718	4	0.012508	0.039926	0.986243	942	2
CYP4Z1	6	0.01251	0.047149	0.986243	943	3
KCNAB3	6	0.012515	0.047169	0.986243	944	3
BOD1	6	0.012515	0.047169	0.986243	945	3
TP53BP1	6	0.01254	0.047257	0.986243	946	4
RNF138	6	0.01254	0.047257	0.986243	947	3
CHIC2	6	0.01254	0.047257	0.986243	948	3
NDC80	6	0.01254	0.047257	0.986243	949	3
CAND1	6	0.012544	0.047274	0.986243	950	4
DCUN1D3	6	0.012587	0.047419	0.986243	951	4
CCDC63	6	0.012599	0.047459	0.986243	952	3
PHOSPHO2-KLHL23	2	0.01262	0.02382	0.986243	953	1
TRIM6	6	0.012652	0.047636	0.986243	954	4
RXFP3	6	0.012661	0.047665	0.986243	955	2
S1PR3	6	0.012661	0.047671	0.986243	956	5
SYN2	6	0.012661	0.047671	0.986243	957	5
TSNAX	6	0.012661	0.047671	0.986243	958	5
CPB1	6	0.012661	0.047671	0.986243	959	5
ZNF814	6	0.012661	0.047671	0.986243	960	5
CYP27B1	6	0.012677	0.047719	0.986243	961	2
FECH	6	0.012751	0.047981	0.986243	962	3
SYNPR	6	0.012761	0.048015	0.986243	963	1
KRT20	6	0.012785	0.048091	0.986243	964	5
KCNA2	6	0.012785	0.048092	0.986243	965	3
hsa-mir-758	4	0.012796	0.040571	0.986243	966	3
LRG1	6	0.012802	0.04815	0.986243	967	4
CEP128	6	0.012806	0.048162	0.986243	968	3
CCNT1	6	0.012806	0.048162	0.986243	969	5
FUT9	6	0.012811	0.048178	0.986243	970	2
MAST2	6	0.012823	0.048222	0.986243	971	3
RPL3	6	0.012823	0.048224	0.986243	972	4
CCDC102B	6	0.012823	0.048224	0.986243	973	4
CCDC38	6	0.012861	0.048373	0.986243	974	2
MICALL1	6	0.012909	0.048537	0.986243	975	3
ENG	6	0.012911	0.048541	0.986243	976	1
HSPA6	6	0.012949	0.048671	0.986243	977	3
GSG2	6	0.012954	0.048694	0.986243	978	4
10-Mar	6	0.013002	0.048851	0.986243	979	5
TNFSF8	6	0.013002	0.048851	0.986243	980	5

(Table Continued)

ID	sgRNA num	score	p-value	FDR	rank	goodsgrna
OR2B6	6	0.013011	0.048876	0.986243	981	4
CLK3	6	0.013014	0.048889	0.986243	982	3
TFAP2D	6	0.013041	0.048986	0.986243	983	4
CCDC106	6	0.013041	0.048986	0.986243	984	4
SNRNP70	6	0.013042	0.048988	0.986243	985	3
HLCS	6	0.013042	0.048988	0.986243	986	3
MIA3	6	0.013121	0.04925	0.986243	987	2
ANHX	6	0.013126	0.04927	0.986243	988	4
RASA2	6	0.013137	0.049307	0.986243	989	4
C14orf119	6	0.013137	0.049307	0.986243	990	4
TUBB2A	6	0.013157	0.049374	0.986243	991	4
RNF19B	6	0.01321	0.049547	0.986243	992	4
TLL1	6	0.013215	0.04956	0.986243	993	5
MYO6	6	0.013257	0.049694	0.986243	994	5
GTF2H2D	4	0.013264	0.041612	0.986243	995	3
hsa-mir-3132	4	0.013264	0.041612	0.986243	996	2
KRTAP2-4	1	0.013272	0.013196	0.882609	997	1
C3orf18	6	0.013299	0.04983	0.986243	998	4
RASGRP2	6	0.0133	0.049832	0.986243	999	4
GHDC	6	0.0133	0.049832	0.986243	1000	3

Table A3. Top disrupted genes positively selected by BrafV600E in P1F/hTERT fibroblasts

ID	Gene	Control count	Treatment count	Fold increase	P-value	FDR
HGLibB_34499	OR8K1	20.006	358420.0	17915.6	0	0
HGLibA_34377	OR6B2	21.15	280810.0	13277.1	0	0
HGLibA_24230	KCNH8	28.581	258610.0	9048.3	0	0
HGLibB_54812	ZBTB40	29.152	256450.0	8797.0	0	0
HGLibB_36356	PHKA1	46.872	352980.0	7530.7	0	0
HGLibA_56463	ZNF653	60.591	320420.0	5288.2	0	0
HGLibB_53483	VAV1	19.435	48456.0	2493.2	0	0
HGLibB_14605	EGFL7	14.862	25862	1740.1	0	0
HGLibA_28248	MAPK1	22.293	32815	1472.0	0	0
HGLibA_50336	TMEM256	9.7174	13933	1433.8	0	0
HGLibB_21193	HEYL	8.5742	7962.3	928.6	0	0
HGLibA_13748	DOCK5	37.726	31326	830.4	0	0
HGLibA_03488	ATG4A	14.29	8269.6	578.7	0	0
HGLibB_32914	NUDT17	66.307	31993	482.5	0	0
HGLibA_60798	hsa-mir-4670	17.148	8165.8	476.2	0	0
HGLibB_54802	ZBTB37	41.728	18243	437.2	0	0
HGLibA_33184	NYAP2	63.449	24873	392.0	0	0
HGLibB_29141	MIA	5.7161	2175.2	380.5	0	0

(Table Continued)

ID	Gene	Control count	Treatment count	Fold increase	P-value	FDR
HGLibB_13849	DPP3	46.3	15214	328.6	0	0
HGLibB_54618	YIPF6	27.437	6657.2	242.6	0	0
HGLibA_50822	TNFSF4	33.153	7204	217.3	0	0
HGLibA_19978	GPR179	47.444	9530.8	200.9	0	0
HGLibA_43537	SERPINB10	14.862	2913.5	196.0	0	0
HGLibA_43378	SEMG1	13.719	2670.1	194.6	0	0
HGLibB_22055	HRC	17.148	3192.9	186.2	0	0
HGLibA_54282	WFIKKN2	18.863	3101.1	164.4	0	0
HGLibB_05615	C18orf54	13.719	1983.6	144.6	0	0
HGLibA_16709	FAM72B	9.1458	1305.1	142.7	0	0
HGLibA_47644	STX3	9.1458	1297.1	141.8	0	0
HGLibA_42184	RPS6KL1	32.582	4537.9	139.3	0	0
HGLibA_12679	DDX24	5.1445	670.51	130.3	0	0
HGLibA_58228	hsa-mir-2114	23.436	2913.5	124.3	0	0
HGLibB_43692	SFRP5	15.433	1604.4	104.0	0	0
HGLibB_41495	RNF151	32.01	3316.6	103.6	0	0
HGLibA_09932	CLEC12B	33.153	3097.1	93.4	0	0
HGLibB_08815	CDKN1A	38.87	3456.3	88.9	0	0
HGLibA_28154	MAP2K6	38.87	3105.1	79.9	0	0
HGLibB_33896	OR4C12	30.867	2127.3	68.9	0	0
HGLibA_09040	CENPB	21.15	1349	63.8	0	0
HGLibB_02007	ANKRD13D	57.733	3180.9	55.1	0	0
HGLibB_29671	MPDU1	7.4309	319.29	43.0	1.2E-232	6.8E-229
HGLibA_29086	MFSD11	60.591	2410.6	39.8	8.5E-202	4.8E-198
HGLibB_20569	GTPBP1	16.005	451	28.2	4.1E-101	2.26E-97
HGLibA_27392	LRRC56	10.289	287.36	27.9	2.02E-98	1.10E-94
HGLibB_51096	TPP1	5.7161	159.64	27.9	1.82E-95	9.67E-92
HGLibB_44100	SIGLEC9	50.302	1325	26.3	1.12E-87	5.83E-84
HGLibB_54489	XPNPEP2	12.575	327.27	26.0	9.96E-86	5.06E-82
HGLibB_18797	GCNT7	11.432	291.35	25.5	5.59E-82	2.78E-78
HGLibA_12954	DENND4B	9.1458	223.5	24.4	9.31E-75	4.54E-71
HGLibA_36794	PKD1L3	46.872	1065.6	22.7	4.14E-65	1.98E-61
HGLibB_09657	CHTOP	16.577	359.2	21.7	2.25E-59	1.05E-55
HGLibB_48913	TEKT1	49.73	1037.7	20.9	1.11E-54	5.12E-51
HGLibA_52537	UBAC2	17.148	347.23	20.2	8.96E-52	4.04E-48
HGLibB_56633	ZNF77	51.445	1005.8	19.6	6.67E-48	2.95E-44

Table A4. Top disrupted genes positively selected by BrafV600E in H4C melanocytes

ID	Gene	Control count	Treatment count	Fold increase	P-value	FDR
HGLibA_20042	GPR4	397.3	1183400.0	2978.3	0	0
HGLibA_12405	DBT	159.1	296950.0	1867.0	0	0
HGLibA_45322	SLC6A20	397.9	341920.0	859.2	0	0
HGLibA_27736	LYPLA1	18.6	6318.7	338.9	0	0
HGLibB_34499	OR8K1	26.2	3847.0	146.7	0	0
HGLibA_54371	WNT4	30.9	4196.0	135.9	0	0
HGLibB_54812	ZBTB40	21.6	2729.2	126.6	0	0
HGLibB_36356	PHKA1	36.1	3850.5	106.6	0	0
HGLibA_50402	TMEM43	41.4	4351.2	105.2	0	0
HGLibA_34377	OR6B2	38.5	3071.2	79.9	0	0
HGLibB_47707	SULT4A1	13.4	1008.5	75.3	0	0
HGLibA_24230	KCNH8	40.2	2873.8	71.5	0	0
HGLibA_56463	ZNF653	48.9	3420.3	69.9	0	0
HGLibA_49861	TMEM107	60.6	3748.2	61.9	0	0
HGLibA_32488	NPM1	52.4	2574.0	49.1	2.5e-318	4.1e-314
HGLibA_08997	CELA3A	30.248	1249.7	41.3	2.3E-226	3.5E-222
HGLibA_50336	TMEM256	4.1	144.6	35.4	3.6E-157	5.1E-153
HGLibB_53483	VAV1	16.9	518.3	30.7	5.2E-123	6.9E-119
HGLibA_60519	hsa-mir-4519	39.0	1177.7	30.2	1.4E-120	1.7E-116
HGLibA_28248	MAPK1	16.9	359.7	21.3	3.1E-60	3.7E-56

VITA

Tengyu Ko received his Bachelor of Science from University of California, Santa Barbara in July 2010. Thereafter, he worked as a research assistant in Anacor Pharmaceuticals in March 2011. Tengyu enrolled in the Comparative Biomedical Sciences graduate program through the Louisiana State University School of Veterinary Medicine in the spring of 2012. Tengyu is currently completing his doctoral degree under the mentorship of Dr. Shisheng Li.